

# Cavity Quantum Electrodynamics with Ultracold Atoms

Dissertation

Tesis doctoral

zur Erlangung des Grades

des Doktors der Naturwissenschaften

del Departament de Física

der Naturwissenschaftlich-Technischen Fakultät II

de la Universitat Autònoma de Barcelona

- Physik und Mechatronik -

der Universität des Saarlandes

von

por

**Hessam HABIBIAN**

Saarbrücken, Barcelona

2013





Universität des Saarlandes  
Theoretische Physik

Betreuerin der Doktorarbeit:  
**Prof. Dr. Giovanna MORIGI**



Universitat Autònoma de Barcelona  
Departament de Física

Director de la Tesis:  
**Prof. Dr. Ramón CORBALÁN YUSTE**

# Cavity Quantum Electrodynamics with Ultracold Atoms

Dissertation  
zur Erlangung des Grades  
des Doktors der Naturwissenschaften  
der Naturwissenschaftlich-Technischen Fakultät II  
- Physik und Mechatronik -  
der Universität des Saarlandes  
von

Tesis doctoral  
del Departament de Física  
de la Universitat Autònoma de Barcelona  
por

**Hessam HABIBIAN**



This thesis is dedicated to my kind-hearted father, open-armed mother,  
and my lovely patient wife Naeimeh Behbood...

پیشگی به پدر و مادر عزیزم و نعیمه مهربانم



## Abstract

In this thesis we investigate the interactions between ultracold atoms confined by a periodic potential and a mode of a high-finesse optical cavity whose wavelength is incommensurate with the potential periodicity. The atoms are driven by a probe laser and can scatter photons into the cavity field. When the von-Laue condition is not satisfied, there is no coherent emission into the cavity mode. We consider this situation and identify conditions for which different nonlinear optical processes can occur. We characterize the properties of the light when the system can either operate as a degenerate parametric amplifier or as a source of antibunched light. Moreover, we show that the stationary entanglement between the light and spin-wave modes of the array can be generated. In the second part we consider the regime in which the zero-point motions of the atoms become relevant in the dynamics of atom-photon interactions. Numerical calculations show that for large parameter regions, cavity backaction forces the atoms into clusters with a local checkerboard density distribution. The clusters are phase-locked to one another so as to maximize the number of intracavity photons.

## Zusammenfassung

Die vorliegende Arbeit befasst sich mit der Wechselwirkung ultrakalter Atome mit der Mode eines optischen Resonators hoher Güte. Die Atome sind dabei in einem periodischen Potenzial gefangen, dessen Periodizität nicht kommensurabel mit der Wellenlänge des Resonators ist. Ein Laser regt die Atome an und sie streuen Photonen in die Resonatormode, wobei die Emission inkohärent ist, falls die Laue-Bedingung nicht erfüllt ist. Dieser Fall wird betrachtet und es werden Bedingungen ermittelt, für welche nichtlineare optische Prozesse auftreten können. Die Eigenschaften des Lichtes werden untersucht, wenn sich das System entweder wie ein parametrischer Verstärker verhält oder wie eine Lichtquelle mit "Antibunching"-Statistik. Weiterhin kann eine stationäre Verschränkung zwischen Licht und Spinwellen der Atome erzeugt werden. Im zweiten Teil wird die Situation betrachtet, in der die Nullpunktsbewegung der Atome für die Atom-Licht-Wechselwirkung relevant ist. Für große Parameterbereiche zeigen numerische Berechnungen, dass die Rückwirkung des Resonators die Formierung eines lokalen Schachbrettmusters in der atomaren Dichteverteilung erzeugt. Die einzelnen Atomgruppe dieses Musters stehen zueinander in fester Phasenbeziehung, was zur Erhöhung der Zahl der Resonatorphotonen führt.



# Contents

---

|                                                                      |           |
|----------------------------------------------------------------------|-----------|
| <b>Introduction</b>                                                  | <b>1</b>  |
| <b>1 Atom-photon interactions inside a cavity: Basics</b>            | <b>5</b>  |
| 1.1 Coherent dynamics of an atom coupled to a cavity field . . .     | 6         |
| 1.1.1 The cavity field . . . . .                                     | 7         |
| 1.1.2 Atom-cavity field interaction: Jaynes-Cumming model            | 7         |
| 1.1.3 An external pump: a laser driving the atoms . . . . .          | 8         |
| 1.2 Dissipative dynamics . . . . .                                   | 9         |
| 1.3 The system of this thesis: an atomic array in a cavity . . . . . | 11        |
| <b>Part I: Pointlike atoms in a periodic array inside a cavity</b>   | <b>15</b> |
| <b>2 Quantum light by an atomic array in a cavity</b>                | <b>17</b> |
| 2.1 Some properties of nonclassical light . . . . .                  | 18        |
| 2.2 Atomic array in a cavity: effective dynamics . . . . .           | 22        |
| 2.2.1 Weak excitation limit . . . . .                                | 23        |
| 2.2.2 Linear response: polaritonic modes . . . . .                   | 26        |
| 2.2.3 Effective Hamiltonian . . . . .                                | 27        |
| 2.2.4 Discussion . . . . .                                           | 29        |
| 2.2.5 Cavity input-output formalism . . . . .                        | 31        |
| 2.3 Results . . . . .                                                | 33        |
| 2.4 Summary and outlook . . . . .                                    | 37        |
| <b>3 Two-mode squeezing by an atomic array in a cavity</b>           | <b>41</b> |
| 3.1 Non-degenerate parametric amplifier and Entanglement . . . .     | 42        |
| 3.2 Parametric amplifier based on an atomic array in a cavity . .    | 43        |
| 3.3 Results: stationary entanglement between matter and light .      | 47        |
| 3.4 Summary and outlook . . . . .                                    | 56        |

---

|                                                                        |            |
|------------------------------------------------------------------------|------------|
| <b>Part II: Quantum ground state of atoms due to cavity backaction</b> | <b>59</b>  |
| <b>4 Quantum ground state of ultracold atoms in a cavity</b>           | <b>61</b>  |
| 4.1 Bose-Hubbard model and disorder . . . . .                          | 62         |
| 4.2 Trapped atoms in a cavity: effective dynamics . . . . .            | 67         |
| 4.2.1 Coherent dynamics . . . . .                                      | 67         |
| 4.2.2 Heisenberg-Langevin equation and weak-excitation limit           | 70         |
| 4.2.3 Adiabatic elimination of the cavity field . . . . .              | 72         |
| 4.2.4 Effective Bose-Hubbard Hamiltonian . . . . .                     | 73         |
| 4.2.5 Discussion . . . . .                                             | 77         |
| 4.3 Results . . . . .                                                  | 78         |
| 4.3.1 One-dimensional lattice . . . . .                                | 79         |
| 4.3.2 Two-dimensional lattice . . . . .                                | 85         |
| 4.4 Experimental Parameters . . . . .                                  | 91         |
| 4.5 Anderson glass . . . . .                                           | 95         |
| 4.6 Summary and outlook . . . . .                                      | 96         |
| <b>5 Concluding remarks</b>                                            | <b>101</b> |
| <b>Appendices</b>                                                      | <b>103</b> |
| <b>A Derivation of the effective Hamiltonian (2.40)</b>                | <b>105</b> |
| <b>B Positivity</b>                                                    | <b>107</b> |
| <b>C Gaussian dynamics</b>                                             | <b>108</b> |
| <b>D Covariance matrix and logarithmic negativity</b>                  | <b>110</b> |
| <b>E Two-mode squeezing spectrum of the emitted field</b>              | <b>112</b> |
| E.1 Spectral properties of the emitted field . . . . .                 | 112        |
| E.2 Measurement of the squeezing spectrum . . . . .                    | 114        |
| <b>F Wannier function for a periodic potential</b>                     | <b>117</b> |
| <b>Bibliography</b>                                                    | <b>135</b> |

# Introduction

---

Ultracold atoms in cavity quantum electrodynamics (CQED) setups offer possibilities to investigate basic processes in the interaction of atoms and electromagnetic fields [1–3]. For example, Rabi oscillations with a single photon are observed in a so-called strong coupling regime in which atom and cavity can exchange a single photon many times before the photon is lost from the cavity by dissipative processes. A high-finesse cavity mode interacting with ultracold atoms may enhance Bragg scattering of light into one spatial direction, and increase the collection efficiency and thereby suppress a diffusion related to photon scattering [3,4]. In this thesis, we focus on various physical phenomena emerging from scattering of light into a high-finesse cavity mode, in particular, we study quantum properties of a light emitted outside the cavity, an stationary entanglement between the scattered light and a collective excitation mode of the atoms, and quantum ground state properties of the medium when the light scattering into the cavity is enhanced.

Bragg diffraction of light by ultracold atoms in optical lattices may reveal the microscopic crystalline structures of the medium [5,6]. For a regular array of the atoms, at the solid angles for which the von-Laue condition is not satisfied [5], the light is scattered inelastically [7–10]. It has been shown that in this case the scattered light in far field can exhibit vacuum squeezing [10]. The nonlinear response of the atomic medium can be enhanced when the atoms of the array strongly interact with a mode of a high-finesse cavity. In this case, the nonlinearity of the light can be controlled by the angle between laser and the cavity fields wave-vectors and by the intra-atomic distance. When the geometry of the setup is such that the von-Laue condition is not satisfied, photons can only be inelastically scattered into the cavity mode. The smaller system size for which coherent scattering is suppressed, is found

for two atoms inside the resonator. The properties of the light at the cavity output for this specific case have been studied in Refs. [11, 12]. To the best of our knowledge, however, the scaling of the dynamics with the number of atoms  $N$  is still largely unexplored in this regime. In Chapter 2 of this thesis, we characterize the coherence properties of the light at the cavity output when the light is scattered from a laser into the resonator by a periodic array of atoms and the geometry of the system is such that coherent scattering is suppressed. For the phase-matching conditions, at which in free space the light is in a squeezed-vacuum state [10], we find that inside a resonator and at large  $N$  the system behaves as an optical parametric oscillator, which in certain regimes can operate above threshold [13]. For a small number of atoms  $N$ , on the contrary, the medium can act as a source of antibunched light. In this case it can either behave as single-photon or, for the saturation parameters here considered, two-photon “gateway” [14]. The latter behaviour is found for a specific phase-matching condition. We identify the parameter regimes which allow one to control the specific nonlinear optical response of the medium.

Following the famous gedanken experiment by Einstein, Podolsky, and Rosen (EPR) in 1935 [15] on the completeness of quantum mechanics, it has been realized by Schrödinger [16, 17] that the EPR paradox was closely related to the concept of entanglement. A realization of the EPR pair by means of a non-degenerate down-conversion scheme has been studied both theoretically and experimentally [18–21]. These schemes generate entangled pairs by means of a two-mode squeezed light. Recent experiments have been focused on the generation of entanglement by the quantum interference between light and atomic ensembles [22] which can be used as a resource for the quantum teleportation [23]. Moreover it has been shown that collective spin mode of an ensemble of atoms inside an optical cavity can be squeezed [24–27] and hence can be a resource for generating entangled states. Our system of atomic array in a high-finesse cavity, can be used as an alternative source for generating entanglement for applications in quantum communication. In Chapter 3 of the thesis, we discuss that by controlling the system parameters, a collective spin-wave mode of the atomic array and the cavity mode can be two-mode squeezed. We obtain the stationary state entanglement between the two modes and we evaluate the two-mode squeezing spectrum for the output fields.

So far, we described the cases for which the mechanical effects of the scattered light on the atomic state are negligible. Domokos and Ritsch proposed in Ref. [28] a model of dynamical self-generated optical lattice by cold atoms inside a cavity. They realized that two-level atoms interacting with a single-mode cavity and a pump laser oriented transverse to the cavity axis, can be self-organized such that the scattering into the cavity mode is enhanced [29, 30]. Self-organization has been observed in the experiment for cold [31, 32] and ultracold [33–36] atoms in a cavity. At ultralow temperatures the system dynamics can undergo the Dicke quantum phase transition [37] and the self-organized medium is a supersolid [33, 35, 38, 39], while for larger laser intensities incompressible Mott insulator phases are expected [40]. The emergent crystallinity has been proposed for Bose-Einstein condensate interacting with multimode cavities [41, 42]. It has been discussed that this kind of system can be reduced to a spin chain model with frustration and a quantum phase transition from a ferromagnet to a spin-glass phase can be realized [43], as for a multimode Dicke model [44]. Multimode cavities interacting with Bose-Einstein condensate may be also mapped to a bosonic model which exhibits phase transition from a superfluid phase to a Bose-glass or a random-singlet glass phases [43]. All of these interesting phenomena are due to the backaction of the cavity field on the atomic medium, which is usually negligible in free-space. In Chapter 4 of this thesis, we consider a single-mode cavity interacting with bosonic ultracold atoms and a transverse pump laser, and we discuss that the quantum fluctuation emerging from a cavity backaction can lead to a Bose-glass insulating phase for the trapped medium. The formation of this Bose-glass phase is such that the coherent scattering into the cavity mode is enhanced, which is significantly different from the glassy phases realized by bichromatic lattices in free-space in the absence of a cavity [45–49]. We propose how to measure non-destructively the Bose-glass phase at the cavity output.

At the end of the thesis, overall concluding remarks are drawn.



# Atom-photon interactions inside a cavity: Basics

---

CQED investigates the interaction of light and atoms and molecules in the regime where a single photon already significantly modifies the radiative properties of the scattering particles. These conditions are achieved by a high-finesse resonator, which act as an effective trap for photons thereby increasing the interaction strength of a single photon with a single atom to the point. The technology of experiments with optical and microwave cavities has reached a level of control, that has led to the observation of predictions at the core of quantum mechanics as well as the realization of basic elements of quantum information processing [2, 50–52]. These results follow theoretical models, which have been developed few decades ago and which provide a reliable theoretical framework for the description of the dynamics of these systems [3, 53, 54].

The purpose of this chapter is to provide a brief overview of the basic concepts and equations of atom-photon dynamics inside a high-finesse optical cavity. The equations here derived constitute the bases of the theoretical models used throughout this thesis. In the last section of this chapter we then introduce the system whose dynamics are analyzed in the rest of this thesis: an array of atoms with a dipolar transition which is strongly coupled to a high-finesse cavity mode. We give the corresponding equation of motions which are the starting points of the studies persuaded in the following chapters.

## 1.1 Coherent dynamics of an atom coupled to a cavity field

In this section we introduce the Hamiltonian which governs the coupled dynamics of a single atom and a single cavity mode. The cavity is a high-finesse optical resonator, where a mode interacts quasi-resonantly with the optical transition of an atom. The atom scatters radiation in the visible region and is typically an alkali-metal atom, thus it possesses a single valence electron. In the situations we consider the atom interacts with light at a well-defined frequency and polarization, such that the frequency is quasi-resonant with a dipolar transition involving two electronic states, a ground state and an excited state. In this regime the relevant internal atomic degrees of freedom are these two levels, which form a pseudo-spin with a ground state and an excited state denoted by  $|1\rangle$  and  $|2\rangle$ , respectively. The Hamiltonian for the internal degrees of freedom of the atom is thus reduced to the form

$$\hat{H}_{at} = \hbar \omega_0 \hat{\sigma}^\dagger \hat{\sigma}, \quad (1.1)$$

where  $\omega_0$  is the atomic transition frequency, while  $\hat{\sigma} = |1\rangle\langle 2|$  and  $\hat{\sigma}^\dagger = |2\rangle\langle 1|$  are the lowering and raising operators, respectively. The electric dipole operator is defined by  $\hat{\mathbf{d}} = e\hat{\mathbf{r}}_e$  where  $e$  is the electron charge and  $\hat{\mathbf{r}}_e$  is the position operator of the valence electron with respect to the center of mass of the atom. In the reduced Hilbert space composed by  $\{|1\rangle, |2\rangle\}$  the dipole operator can be cast in the form

$$\hat{\mathbf{d}} = \mathbf{d}_{21} \left( \hat{\sigma}^\dagger + \hat{\sigma} \right), \quad (1.2)$$

where the matrix element  $\mathbf{d}_{21} = \langle 2|\hat{\mathbf{d}}|1\rangle$  is taken to be real (without loss of generality). We now include the external atomic degrees of freedom of the atom and denote by  $\hat{\mathbf{r}}$  and  $\hat{\mathbf{p}}$  the position and the canonically conjugated momentum of the atomic center of mass. For non-relativistic velocities, external and internal degrees of freedom are decoupled in absence of external fields and the Hamiltonian for the external degrees of freedom reads

$$\hat{H}_{ext} = \frac{\hat{\mathbf{p}}^2}{2m} + V(\hat{\mathbf{r}}), \quad (1.3)$$

where  $m$  is the mass and  $V(\hat{\mathbf{r}})$  is a potential which will be specified later on.

### 1.1.1 The cavity field

We consider an optical cavity constituted by two reflecting mirrors separated by the linear distance  $L$ . The boundary conditions at the mirrors of the cavity impose a discrete spectrum of field modes along the cavity axis, such that the mode frequencies are equi-spaced and at distance  $\Delta\omega = 2\pi c/L$ , with  $c$  the speed of light in the vacuum. Very good optical cavities as in [33, 55] can realize  $\Delta\omega = 2\pi \times 10$  THz, so that an atomic transition at frequency  $\omega_0$  can be close to the frequency of one cavity mode, say at frequency  $\omega_c$ , and very far-detuned from other modes. In this limit one can talk of a “single-mode” cavity. We denote by  $\hat{a}$  and  $\hat{a}^\dagger$  the annihilation and creation operators of a cavity photon with energy  $\hbar\omega_c$ , with  $[\hat{a}, \hat{a}^\dagger] = 1$ . The Hamiltonian for the cavity mode in second quantization reads

$$\hat{H}_C = \hbar\omega_c \left( \hat{a}^\dagger \hat{a} + \frac{1}{2} \right), \quad (1.4)$$

where it here includes the zero-point energy of the cavity mode. In this limit the cavity electric field can be reduced to the component due to the resonant cavity mode, and it reads

$$\hat{\mathbf{E}}(\mathbf{r}) = \sqrt{\frac{\hbar\omega_c}{2\varepsilon_0 V_0}} v(\mathbf{r}) \mathbf{e} \left( \hat{a} + \hat{a}^\dagger \right), \quad (1.5)$$

where  $\mathbf{e}$  is the polarization of the cavity mode,  $\varepsilon_0$  is the vacuum permittivity, the function  $v(\mathbf{r})$  is the mode function at position  $\mathbf{r}$ , and  $V_0 = \int d\mathbf{r} |v(\mathbf{r})|^2$  is the quantization volume.

### 1.1.2 Atom-cavity field interaction: Jaynes-Cumming model

Let us now assume that the dipolar transition  $|1\rangle \rightarrow |2\rangle$  at a position  $\hat{\mathbf{r}}$  couples quasi-resonantly with the mode  $\omega_c$  of the resonator. In the electric-dipole approximation the interaction Hamiltonian can be cast in the form

$$\hat{H}_{int} = -\hat{\mathbf{d}} \cdot \hat{\mathbf{E}}(\hat{\mathbf{r}}). \quad (1.6)$$

Under the assumption that only one cavity mode interacts resonantly with the atomic transition, we use Eqs. (1.2) and (1.5) in Eq. (1.6) and obtain

$$\hat{H}_{int} = \hbar g(\hat{\mathbf{r}}) \left( \hat{\sigma}^\dagger \hat{a} + \hat{a}^\dagger \hat{\sigma} \right) \quad (1.7)$$

where we applied the rotating-wave approximation [56]. Here  $g(\hat{\mathbf{r}}) = gv(\hat{\mathbf{r}})$  with

$$g = \sqrt{\frac{\omega_c}{2\hbar\epsilon_0 V_0}} |\mathbf{d}_{21} \cdot \mathbf{e}|, \quad (1.8)$$

the so-called vacuum Rabi frequency [57, 58]. This expression shows that strong coupling between a single photon and a single atom can be realized by means of small mode volumes.

The Hamiltonian governing the coupled dynamics of atom and cavity mode now reads

$$\hat{H} = \hat{H}_{ext} + \hat{H}_{JC},$$

where

$$\hat{H}_{JC} = \hbar\omega_0 \hat{\sigma}^\dagger \hat{\sigma} + \hbar\omega_c \hat{a}^\dagger \hat{a} + \hbar g(\hat{\mathbf{r}}) (\hat{\sigma}^\dagger \hat{a} + \hat{a}^\dagger \hat{\sigma}) \quad (1.9)$$

and is known in the literature as Jaynes-Cumming Hamiltonian [59].

The dynamics of the closed system composed by atom and cavity mode is described by Schrödinger equation

$$i\hbar \frac{\partial |\Psi(t)\rangle}{\partial t} = \hat{H} |\Psi(t)\rangle, \quad (1.10)$$

where  $|\Psi(t)\rangle$  is the quantum state of the system at time  $t$ .

### 1.1.3 An external pump: a laser driving the atoms

Energy is usually pumped in the atom-cavity system by injecting photons into the cavity field via the mirrors, which corresponds to a pump on the cavity, or by driving the atomic transition via an external field: in this case the atom scatters photon into the cavity mode. The latter situation is the one we consider in the rest of this thesis. The external field is here assumed to be a laser, which is described by a classical field at frequency  $\omega_p$  and wave vector  $\mathbf{k}_p$ . The Hamiltonian describing the coupling between laser and atom takes the form

$$\hat{H}_L = i\hbar\Omega \left( \hat{\sigma}^\dagger e^{i(\mathbf{k}_p \cdot \hat{\mathbf{r}} - \omega_p t)} - \hat{\sigma} e^{-i(\mathbf{k}_p \cdot \hat{\mathbf{r}} - \omega_p t)} \right) \quad (1.11)$$

where  $\Omega$  is the Rabi frequency, determining the strength of the coupling between classical field and atomic transition, and the total Hamiltonian now reads

$$\hat{H}_{tot} = \hat{H}_{ext} + \hat{H}_{JC} + \hat{H}_L. \quad (1.12)$$

The explicit time dependence in the Hamiltonian can be removed by writing  $\hat{H}_{tot}$  in the frame rotating at frequency  $\omega_p$  (which corresponds to an interaction picture with respect to  $\hat{H}_0 = \hbar\omega_p (\hat{\sigma}^\dagger \hat{\sigma} + \hat{a}^\dagger \hat{a})$ ). In this rotating frame  $\hat{H}_{tot} \rightarrow \hat{\hat{H}}_{tot}$  with

$$\begin{aligned} \hat{\hat{H}}_{tot} = & \hat{H}_{ext} + \hbar\omega_z \hat{\sigma}^\dagger \hat{\sigma} + \hbar\delta_c \hat{a}^\dagger \hat{a} + \hbar g(\hat{\mathbf{r}}) (\hat{\sigma}^\dagger \hat{a} + \hat{a}^\dagger \hat{\sigma}) \\ & + i\hbar\Omega (\hat{\sigma}^\dagger e^{i\mathbf{k}_p \cdot \hat{\mathbf{r}}} - \hat{\sigma} e^{-i\mathbf{k}_p \cdot \hat{\mathbf{r}}}), \end{aligned} \quad (1.13)$$

where  $\omega_z = \omega_0 - \omega_p$  and  $\delta_c = \omega_c - \omega_p$  are the detuning of the laser with respect to the atomic transition frequency and the cavity mode frequency, respectively.

## 1.2 Dissipative dynamics

So far we have considered a coherent dynamics. The physical processes considered in this thesis include also radiative decay of the atomic excited state and cavity losses, so that photons are emitted outside the cavity, as sketched in Fig. 1.1. The inclusion of these processes is usually sufficient to provide a realistic description. In quantum optics, noise and dissipation can be often described by means of a master equation for the density matrix  $\hat{\rho}$  of the atomic internal and external degrees of freedom and the cavity mode. The master equation is based on the Born-Markov approximation and reads [60, 61]

$$\frac{\partial \hat{\rho}}{\partial t} = -\frac{i}{\hbar} [\hat{H}_{tot}, \hat{\rho}] + \mathcal{L} \hat{\rho}, \quad (1.14)$$

where  $\mathcal{L}$  is Lindbladian describing noise and dissipation. In the rest of this thesis we will consider that noise and dissipation are due to the radiative instability of the excited state which decays with a rate  $\gamma$ , and a cavity loss at rate  $\kappa$ . Then,  $\mathcal{L} = \mathcal{L}_\kappa + \mathcal{L}_\gamma$ , where the superoperators  $\mathcal{L}_\kappa$  and  $\mathcal{L}_\gamma$  are the Liouvillians accounting for the effect of the reservoir for the cavity and the atom, respectively. They read [60, 61]

$$\mathcal{L}_\kappa \hat{\rho} = \kappa \left( 2\hat{a} \hat{\rho} \hat{a}^\dagger - \hat{a}^\dagger \hat{a} \hat{\rho} - \hat{\rho} \hat{a}^\dagger \hat{a} \right), \quad (1.15)$$

$$\mathcal{L}_\gamma \hat{\rho} = \frac{\gamma}{2} \left( 2\hat{\sigma} \hat{\rho} \hat{\sigma}^\dagger - \hat{\sigma}^\dagger \hat{\sigma} \hat{\rho} - \hat{\rho} \hat{\sigma}^\dagger \hat{\sigma} \right). \quad (1.16)$$

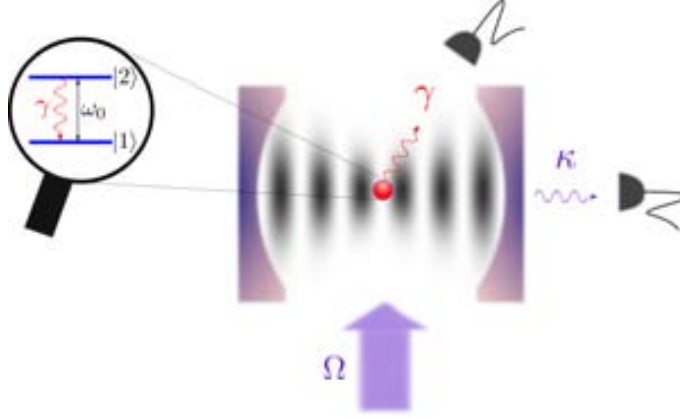


Figure 1.1: Schematic picture of an atom inside a Fabry-Pérot cavity, which is driven by a transverse laser field at Rabi frequency  $\Omega$ . The wiggled lines symbolize cavity decay at rate  $\kappa$  and spontaneous emission at rate  $\gamma$ , with which photons are emitted outside of the system. The inset shows a sketch of the internal degrees of freedom of the atom, where ground and excited state of the atoms are denoted by  $|1\rangle$  and  $|2\rangle$ , respectively, while  $\omega_0$  is the atomic transition frequency. Here we assume that one of the cavity mirrors (left mirror) has zero transmittivity.

Note that in Eq. (1.16) we have ignored the recoil effect due to the emission of the photon into a free-space. The form can be found for instance in Ref. [61]. This effect will be neglected in this thesis since the parameters will be so chosen, that the main source of dissipation occurs via cavity decay.

It is useful to consider the corresponding Heisenberg-Langevin equations, which provide the equivalent description to the master equation but for the system operators [13, 61]. They read

$$\frac{d\hat{a}(t)}{dt} = -\frac{i}{\hbar}[\hat{a}(t), \hat{H}_{\text{tot}}] - \kappa \hat{a}(t) + \sqrt{2\kappa} \hat{a}_{in}(t), \quad (1.17)$$

$$\frac{d\hat{\sigma}(t)}{dt} = -\frac{i}{\hbar}[\hat{\sigma}(t), \hat{H}_{\text{tot}}] - \frac{\gamma}{2} \hat{\sigma}(t) + \sqrt{\gamma} \hat{\sigma}_{in}(t), \quad (1.18)$$

where  $\hat{\sigma}_{in} = -\hat{\sigma}_z \hat{b}_{in}$ , and  $\hat{a}_{in}$  and  $\hat{b}_{in}$  denote the input fields with mean values  $\langle \hat{a}_{in} \rangle = \langle \hat{b}_{in} \rangle = 0$ , and

$$[\hat{a}_{in}(t), \hat{a}_{in}^\dagger(t')] = \delta(t - t'), \quad (1.19)$$

$$[\hat{b}_{in}(t), \hat{b}_{in}^\dagger(t')] = \delta(t - t'). \quad (1.20)$$

The output fields can be written in terms of the input fields and the system operators, so that one can obtain

$$\hat{a}_{out}(t) = \sqrt{\kappa} \hat{a}(t) - \hat{a}_{in}(t), \quad (1.21)$$

$$\hat{\sigma}_{out}(t) = \sqrt{\frac{\gamma}{2}} \hat{\sigma}(t) - \hat{\sigma}_{in}(t), \quad (1.22)$$

for the cavity and the spin output fields, respectively. The Eqs. (1.21),(1.22) will be used later on to evaluate the correlation functions of the output fields.

Noise and dissipation tend to wash away cavity quantum electrodynamics effects: if the loss rates are too large, the dissipative dynamics dominates over the coherent part. The so-called strong coupling regime, in which the dynamics of an atom is significantly modified at the single-photon level, can be reached provided that the so-called cooperativity parameter

$$C_s = \frac{g(\hat{\mathbf{r}})^2}{\kappa\gamma} \quad (1.23)$$

is larger than unity [62]. This parameter is found in the equation of motion for the cavity field, when one formally integrate the atomic degrees of freedom and expresses them in terms of the cavity variable, and scales the nonlinearity due to the atom-photon coupling. In the strong coupling regime in which  $C_s \gg 1$ , to provide an example, nonlinear dynamics such as optical bistability are observed [13, 61, 63].

### **1.3 The system of this thesis: an atomic array in a cavity**

The physical system we consider throughout this thesis is composed by  $N$  identical atoms which are regularly distributed along the cavity axis. The focus of our investigation is to characterize the cavity field as a function of the spatial periodicity of the atomic array in the strong coupling regime. In the second part of the thesis we then analyze how the atomic state is modified by the cavity field when the atoms scatter photon into the cavity mode.

We denote by  $z$  the cavity axis. The atoms are located about at the

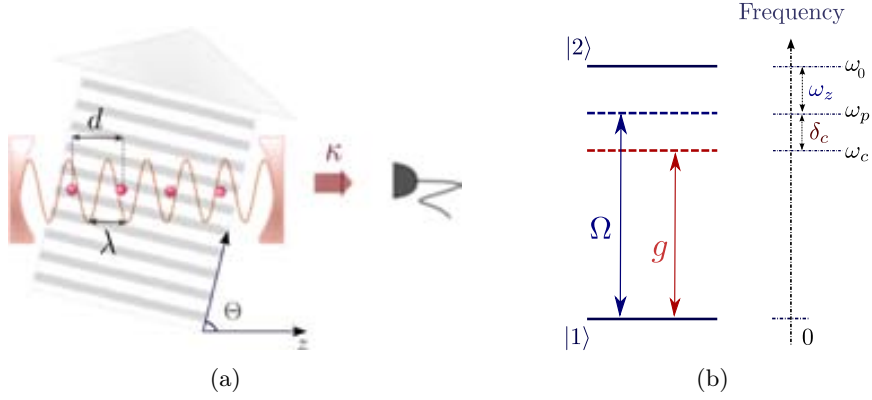


Figure 1.2: (a) A periodic array of atoms, with interparticle distance  $d$ , is confined along the axis of a standing-wave optical cavity at frequency  $\omega_c$  and is transversally driven by a laser, whose wave vector forms the angle  $\Theta$  with the cavity axis. The atomic internal transition and the relevant frequency scales are given in (b), with  $|1\rangle$  and  $|2\rangle$  ground and excited state of an optical transition with frequency  $\omega_0$  and natural linewidth  $\gamma$ . The frequencies  $\omega_z = \omega_0 - \omega_p$  and  $\delta_c = \omega_c - \omega_p$  denote the detunings between the laser frequency  $\omega_p$  and the atomic and cavity frequency, respectively. The other parameters are the laser Rabi frequency  $\Omega$ , the atom-cavity coupling strength  $g$ , and the decay rate  $\kappa$  of the optical cavity.

positions  $z_j = jd$  where  $j = 1, \dots, N$  and  $d$  is the interparticle distance<sup>1</sup>. An optical dipole transition of the confined atoms interacts with the mode of a standing wave cavity, whose wave vector  $k$  is parallel to the atomic array, as illustrated in Fig. 1.2. Moreover, the atoms are transversally driven by a laser and scatter photons into the cavity mode. Cavity and laser modes couple to the atomic dipolar transition at frequency  $\omega_0$  with ground and excited states  $|1\rangle$  and  $|2\rangle$ .

The state of the system, composed by the internal and external degrees of freedom of the  $N$  atoms and by the cavity mode, is described by the density matrix  $\hat{\rho}$ , whose dynamics is governed by the master equation

$$\frac{\partial \hat{\rho}}{\partial t} = -\frac{i}{\hbar} [\mathcal{H}, \hat{\rho}] + \mathcal{L}_\kappa \hat{\rho} + \sum_{j=1}^N \mathcal{L}_{\gamma,j} \hat{\rho}, \quad (1.24)$$

where  $\mathcal{L}_{\gamma,j}$  describes spontaneous decay of the atom  $j$ . The Hamiltonian

<sup>1</sup>This configuration can be achieved by means of an optical lattice trapping the atoms at the minima of the corresponding standing wave, see e.g. [64].

governing the coherent dynamics reads

$$\begin{aligned}
\mathcal{H} = & \sum_i \left( \frac{\hat{p}_i^2}{2m} + V(\hat{\mathbf{r}}_i) \right) + \hbar\omega_c \hat{a}^\dagger \hat{a} + \hbar\omega_0 \sum_{j=1}^N S_j^z \\
& + \hbar g \sum_{j=1}^N \cos(kz_j + \varphi) (S_j^\dagger \hat{a} + \hat{a}^\dagger S_j) \\
& + i\hbar\Omega \sum_{j=1}^N (S_j^\dagger e^{-i\omega_p t} e^{i(k_p z_j \cos \Theta - \phi_L)} - \text{H.c.}), \quad (1.25)
\end{aligned}$$

where  $\hat{p}_i$  is the momentum of  $i$ -th atom which feels a potential  $V(\hat{\mathbf{r}}_i)$  at its position  $\hat{\mathbf{r}}$ . The operators  $S_j = |1\rangle_j \langle 2|$  and  $S_j^\dagger$  indicate the lowering and raising operators for the atom at the position  $z_j$ , and  $S_j^z = \frac{1}{2}(|2\rangle_j \langle 2| - |1\rangle_j \langle 1|)$  is the  $z$  component of the pseudo-spin operator. In Eq. (1.25) we have introduced the angle  $\varphi$ , which is the phase offset of the standing wave at the atomic positions, the phase of the laser  $\phi_L$ , and the angle  $\Theta$  between the laser and the cavity wave vector. For simplicity we will set  $k = k_p$ : The difference between the laser and cavity wave numbers can in fact be neglected for quasi-resonant radiation.

Equation (1.24) is the starting point of the theoretical studies presented in this thesis.



|        |
|--------|
| PART I |
|--------|

Pointlike atoms in a periodic array  
inside a cavity



---

## Quantum light by an atomic array in a cavity

---

Nonclassical light, namely, radiation with properties which have no classical analogue, can be observed in the resonance fluorescence from a single atom [65, 66]. It is due to the quantum nature of the scatterer, such as the discrete spectrum of the electronic bound states of the scattering atom. When the number of scatterers is increased, the quantum properties, such as antibunching, are usually suppressed [67]. The situation can be different when the atoms form a regular array [7–10]. A recent work predicted that when the light is scattered at the solid angles which satisfy the von-Laue condition, the light in the far field is in a squeezed coherent state, while for a large number of atoms it can exhibit vacuum squeezing at scattering angles, for which the elastic component of the scattered light is suppressed [10].

When the atoms of the array are strongly coupled with the mode of a high-finesse resonator, emission into the cavity mode is in general enhanced. The properties of the light at the cavity output will depend on the phase-matching conditions, determined by the angle between laser and cavity wave vector and by the periodicity of the atomic array. The coherence properties of the light at the cavity output may however be significantly different from the ones predicted in free space. An interesting example is found when the geometry of the setup is such that the atoms coherently scatter light into the cavity mode. In this case the intracavity field intensity becomes independent of the number of atoms  $N$  as  $N$  increases, while inelastic scattering is suppressed over the whole solid angle in leading order in  $1/N$  [68]. These dynamics have been confirmed by experimental observations [31, 32, 69], and clearly differ from the behaviour in free space [10].

In this chapter we characterize the coherence properties of the light at the cavity output when the light is scattered from a laser into the resonator by an array of atoms and the geometry of the system is such that coherent scattering is suppressed: In this regime the light is inelastically scattered, while the coherent component is suppressed. Our starting point is the master equation in Eq. (1.24) and the Heisenberg-Langevin equations in Eqs. (1.17) and (1.18). From this model we derive some coherence properties of the light emitted at the cavity output, and show that for some parameter regimes an array of two-level atoms behave as nonlinear optical medium, whose response can be switched: We will show that the medium can generate antibunched or squeezed light on demand. For sake of completeness, in the next section, Sec. 2.1, we first review some basic properties of nonclassical light which are relevant for our study.

## 2.1 Some properties of nonclassical light

The quantum state of the light can be determined by full tomography [70]. Nevertheless, some salient properties can be accessed by measuring moments of the distribution, such as the first and the second order correlation functions (clearly, the knowledge of all moments allows one to reconstruct the density matrix of the field). For instance, the  $n$ -th order correlation function measured at a detector at position  $\mathbf{r}$  determines the correlations of detection events at times  $t_1, \dots, t_n$  for a photon field described by operator  $\hat{a}(\mathbf{r}, t)$  and reads

$$g^{(n)}(\mathbf{r}; t_1, \dots, t_n) = \frac{\langle \hat{a}^\dagger(\mathbf{r}; t_1) \cdots \hat{a}^\dagger(\mathbf{r}; t_n) \hat{a}(\mathbf{r}; t_n) \cdots \hat{a}(\mathbf{r}; t_1) \rangle}{\left[ \langle \hat{a}^\dagger(\mathbf{r}; t_1) \hat{a}(\mathbf{r}; t_1) \rangle \cdots \langle \hat{a}^\dagger(\mathbf{r}; t_n) \hat{a}(\mathbf{r}; t_n) \rangle \right]}, \quad (2.1)$$

where the average  $\langle \cdot \rangle$  is taken over the density matrix of the field at time  $t = 0$ , which is the state to characterize. The times of the operators in (2.1) can be all different, as is the case for the first-order correlation function,  $g^{(1)}(\mathbf{r}; t)$ . In our treatment we are particularly interested in the second-order correlation function,  $g^{(2)}(\mathbf{r}; t, t + \tau)$ , which measures the joint photocount probability of detecting a photon at time  $t$  and another photon at time  $t + \tau$ . This correlation function is particularly interesting as one can identify features which cannot be reproduced by means of the classical theory of radiation. The classical theory, in fact, predicts that the second-order correlation

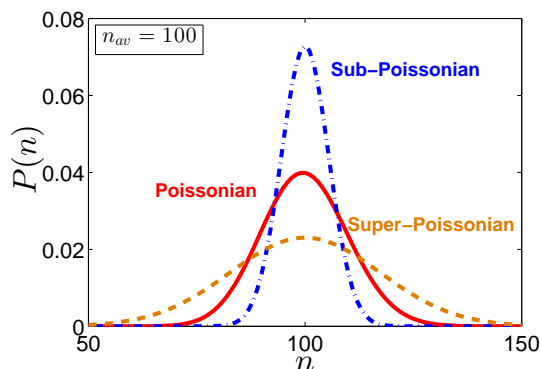


Figure 2.1: Plots of the probability  $P$  of finding  $n$  photons at a detector for a coherent light with Poissonian (red solid curve), anti-bunched light with sub-Poissonian (blue dotted-dashed curve), and bunched light with super-Poissonian (brown dashed curve) statistics. The average photon number  $n_{\text{av}} = 100$ .

function at zero-time delay must always be larger than unity,  $g^{(2)}(t, t) \geq 1$ , while in quantum theory one finds states, for which  $g^{(2)}(t, t) < 1$ . Some statistical properties of the photon distributions can be inferred depending on the value of the second-order correlation function at zero-time delay. When  $g^{(2)}(t, t) = 1$ , the light is coherent. For a fully coherent light beam the probability  $P(n)$  of measuring  $n$  photons with average mean-photon number  $n_{\text{av}}$  follows the Poissonian distribution

$$P(n) = \frac{n_{\text{av}}^n}{n!} e^{-n_{\text{av}}} \quad (2.2)$$

for  $n = 0, 1, 2, \dots$ . When  $g^{(2)}(t, t) > 1$  the light is bunched with super-Poissonian statistics, namely, the variance is larger than the mean number of photons  $n_{\text{av}}$  [13, 71]. On the other hand, for  $g^{(2)}(t, t) < 1$ , which is usually denoted by antibunching, the light possesses sub-Poissonian statistics, with the variance smaller than  $n_{\text{av}}$  [13, 71]. The different behaviors are illustrated in Fig. 2.1 for  $n_{\text{av}} = 100$ . Antibunching of light has been observed in the resonance fluorescence of a single atom or ion, the first experiment has been reported in Ref. [72], and is a characteristic of single emitters.

In this thesis we will identify the conditions when antibunched light is generated by an array of atoms which scatter light inelastically into the cavity. Another situation we will analyze is when the array generates squeezed light [13]. This is usually generated by nonlinear devices such as optical para-

metric amplifiers [73]. Here, a nonlinear medium is pumped by a classical field of a frequency  $\omega_{\text{pump}}$ , which is converted into pairs of identical photons of frequency  $\omega_{\text{ph}} = \omega_{\text{pump}}/2$ . The dynamics of such process is governed by the Hamiltonian [13, 73]

$$\mathcal{H} = \hbar\omega_{\text{ph}}\hat{a}^\dagger\hat{a} - i\hbar\frac{\alpha}{2}\left(\hat{a}^2e^{i\omega_{\text{pump}}t} - \hat{a}^{\dagger 2}e^{-i\omega_{\text{pump}}t}\right) \quad (2.3)$$

where  $\alpha$  is a real parameter. The Heisenberg equations of motion lead to the solution

$$\hat{a}(t) = \hat{a}(0)\cosh(\alpha t) + \hat{a}(0)^\dagger\sinh(\alpha t), \quad (2.4)$$

with  $\hat{a}(t)^\dagger$  its adjoint. After introducing the quadratures

$$\hat{x}_1 = \hat{a} + \hat{a}^\dagger, \quad (2.5)$$

$$\hat{x}_2 = -i\left(\hat{a} - \hat{a}^\dagger\right), \quad (2.6)$$

one finds that

$$\hat{x}_1(t) = e^{\alpha t}\hat{x}_1(0), \quad (2.7)$$

$$\hat{x}_2(t) = e^{-\alpha t}\hat{x}_2(0). \quad (2.8)$$

In order to satisfy the requirement of the minimum-uncertainty relation  $V(\hat{x}_1)V(\hat{x}_2) = 1$ , with  $V(\hat{x}_i) = \langle\hat{x}_i^2\rangle - \langle\hat{x}_i\rangle^2$  being the variance, the noise in one quadrature is less and on the other quadrature is greater than the standard quantum limit, namely, the quadrature of the coherent state. The amount of the squeezing of one quadrature, or noise reduction, depends thus on  $\alpha$ , which is proportional to the strength of nonlinearity and the pump amplitude, and on the interaction time.

Noise and dissipation introduce a threshold in the process. When the nonlinear medium is inside a cavity, the interaction time is determined by the cavity linewidth  $\kappa$ . The Heisenberg-Langevin equation of motion now take the form

$$\frac{d\hat{\mathbf{a}}}{dt} = A\hat{\mathbf{a}} + \sqrt{2\kappa}\hat{\mathbf{a}}_{in} \quad (2.9)$$

for  $\hat{\mathbf{a}} = (\hat{a}, \hat{a}^\dagger)^T$  and  $\hat{\mathbf{a}}_{in} = (\hat{a}_{in}, \hat{a}_{in}^\dagger)^T$ , where

$$A = \begin{pmatrix} \kappa & -\alpha \\ -\alpha & \kappa \end{pmatrix}. \quad (2.10)$$

From Eq. (2.9) the solution of  $\hat{\mathbf{a}}(t)$  reaches the steady state when  $\alpha$  is below a threshold value defined by  $\alpha_{th} = \kappa$ . We will focus on situations in which the nonlinear medium operates below threshold and evaluate the squeezing spectrum at steady state. The squeezing spectrum is determined by the expression [13]

$$S_i^{out}(\omega) = \int dt \langle \hat{x}_i^{out}(t), \hat{x}_i^{out}(0) \rangle e^{-i\omega t}, \quad (2.11)$$

where  $\hat{x}_1^{out} = \hat{a}_{out} + \hat{a}_{out}^\dagger$  and  $\hat{x}_2^{out} = -i(\hat{a}_{out} - \hat{a}_{out}^\dagger)$ , in which  $\langle \hat{A}, \hat{B} \rangle = \langle \hat{A}\hat{B} \rangle - \langle \hat{A} \rangle \langle \hat{B} \rangle$ . The emitted light at a frequency  $\omega$  (in rotating frame of the pump laser) is squeezed when  $S_i^{out}(\omega) < 1$ . The spectrums for the two quadratures at the threshold ( $\alpha = \kappa$ ) are reduced to

$$S_1^{out}(\omega) = 1 + \left( \frac{2\kappa}{\omega} \right)^2, \quad (2.12)$$

$$S_2^{out}(\omega) = 1 - \frac{4\kappa^2}{4\kappa^2 + \omega^2}. \quad (2.13)$$

Figure 2.2 displays the squeezing spectrum of  $S_2^{out}(\omega)$  at the threshold, for which the noise is maximally reduced at the resonant frequency with the pump laser, i.e., when  $\omega = 0$ .

Before analyzing the nonlinear optical response of an atomic array inside an optical resonator, we shortly review the basics of nonlinear optics. In linear optics, the polarization of a medium induced by an electric field depends linearly upon the field amplitude, but in fact, this is just an approximation. In reality the optical response of a medium is a nonlinear function of the electric field amplitude [73], and for lossless and dispersionless materials, the polarization can be written as [73]

$$\hat{\mathcal{P}}(t) = \chi^{(1)} \hat{\mathbf{E}}(t) + \chi^{(2)} \hat{\mathbf{E}}(t)^2 + \chi^{(3)} \hat{\mathbf{E}}(t)^3 + \dots \quad (2.14)$$

where  $\chi^{(j)}$  is the electric susceptibility of  $j$ th order. This response originates from the microscopic response of the individual molecules forming the

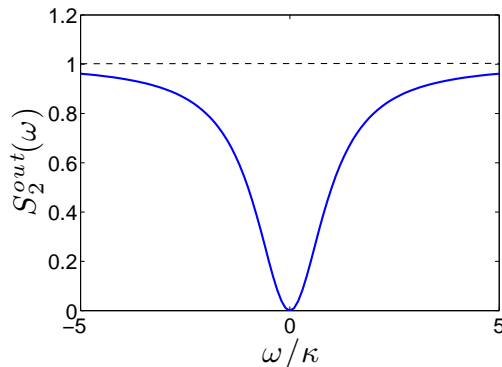


Figure 2.2: The squeezing spectrum  $S_2^{out}(\omega)$  at the cavity output related to the quadrature  $\hat{x}_2^{out} = -i(\hat{a}_{out} + \hat{a}_{out}^\dagger)$  is plotted at the threshold, i.e. when  $\alpha = \kappa$ , in units of the cavity decay rate  $\kappa$ . The spectrum is obtained from the Eq. (2.13). The dashed line shows the (classical) shot-noise limit for which  $S^{out}(\omega) = 1$ .

medium, which undergo multi-photon processes. In nonlinear optical crystals the different orders of the susceptibilities are controlled through the properties of the material, which either enhance or suppress the light emitted by each single component. An optical parametric amplifier is thus realized in a medium where the response given by  $\chi^{(2)}$  is dominant, whereby for a Kerr medium the  $\chi^{(3)}$  susceptibility is dominant [13, 73].

In the following we will show that an array of two-level atoms in a cavity can behave as a nonlinear medium. In the regime in which the relevant atomic transition is a two-level, dipolar transition, we will show that the nonlinear optical processes giving rise to different collective responses are due to excitations of atomic Dicke states, which are enhanced or suppressed by the geometry of the setup, here controlled by the interparticle distance in relation with the wave-length of the resonator.

## 2.2 Atomic array in a cavity: effective dynamics

We now turn to the physical system, whose nonlinear optical properties we intend to characterize. We consider the light scattered by an atomic array inside a resonator which is transversally pumped by a laser. Our starting point is Hamiltonian (1.25) in the limit in which quantum fluctuations about the spatial points where the atoms are localized can be neglected.

In this section we will introduce and discuss the approximations, which allow us to solve the dynamics obtained by the Hamiltonian (1.25) and determine the properties of the cavity field. In order to do so, we consider the low saturation limit and resort to the Holstein-Primakoff representation for the spin operators. This allows us to determine an effective Hamiltonian, with which we can predict the state of the cavity field.

### 2.2.1 Weak excitation limit

We now consider the low saturation limit for the spins of the atomic array and resort to the Holstein-Primakoff representation for the spin operators entering in Eq. (1.25), according to the relation <sup>1</sup> [74]

$$\begin{aligned} S_j^\dagger &= b_j^\dagger (1 - b_j^\dagger b_j)^{1/2}, \\ S_j &= (1 - b_j^\dagger b_j)^{1/2} b_j, \\ S_j^z &= b_j^\dagger b_j - \frac{1}{2}, \end{aligned} \tag{2.15}$$

where  $b_j$  ( $b_j^\dagger$ ) is the bosonic operator annihilating (creating) an excitation of the atom at  $z_j$ , such that  $[b_j, b_{j'}^\dagger] = \delta_{jj'}$ . In the limit in which the atomic dipoles are driven below saturation, we treat saturation effects in the lowest non-vanishing order of a perturbative expansion, whose small parameter is the total excited-state population of the atoms, denoted by  $\mathcal{N}_{\text{tot}}$ . We denote the detuning of the laser from the atomic transition by

$$\omega_z = \omega_0 - \omega_p, \tag{2.16}$$

and by  $\gamma$  the natural linewidth. In the low saturation limit,  $|\omega_z + i\gamma/2| \gg \sqrt{N}\Omega$ , then  $\mathcal{N}_{\text{tot}} \ll N$  and we can expand the operators on the right-hand side of the equations (2.15) in second order in the small parameter  $\langle b_j^\dagger b_j \rangle \ll 1$ , obtaining

$$\begin{aligned} S_j^\dagger &\approx b_j^\dagger - \frac{1}{2} b_j^\dagger b_j^\dagger b_j, \\ S_j &\approx b_j - \frac{1}{2} b_j^\dagger b_j b_j. \end{aligned} \tag{2.17}$$

---

<sup>1</sup>From now on, we drop the hat symbol  $\hat{\phantom{x}}$  for operators.

For  $N \gg 1$  the dynamics is expected to be irrelevantly affected by the assumptions on the boundaries. Therefore, we take periodic boundary conditions on the lattice, such that  $z_{N+1} = z_1$ . The atomic excitations are studied in the Fourier transformed variable  $q$ , quasi-momentum of the lattice, which is defined in the Brillouin zone (BZ)  $q \in (-G_0/2, G_0/2]$  with  $G_0 = 2\pi/d$  the primitive reciprocal lattice vector. Correspondingly, we introduce the operators  $b_q$  and  $b_q^\dagger$ , defined as

$$b_q = \frac{1}{\sqrt{N}} \sum_{j=1}^N b_j e^{-iqjd}, \quad (2.18)$$

$$b_q^\dagger = \frac{1}{\sqrt{N}} \sum_{j=1}^N b_j^\dagger e^{iqjd}, \quad (2.19)$$

which annihilate and create, respectively, an excitation of the spin wave at quasimomentum  $q$  and fulfilling the commutation relation  $[b_q, b_{q'}^\dagger] = \delta_{q,q'}$ . After rewriting the Hamiltonian in Eq. (1.25) in terms of spin-wave operators, we find

$$\mathcal{H} \approx -\frac{N\hbar\omega_z}{2} + H_{\text{pump}} + \mathcal{H}^{(2)} + \mathcal{H}^{(4)}, \quad (2.20)$$

where the first term on the Right-Hand Side (RHS) is a constant and will be discarded from now on, while

$$H_{\text{pump}} = i\hbar\Omega\sqrt{N} \left( b_{Q'}^\dagger e^{-i(\omega_p t + \phi_L)} - b_{Q'} e^{i(\omega_p t + \phi_L)} \right) \quad (2.21)$$

is the linear term describing the coupling with the laser. Term

$$\begin{aligned} \mathcal{H}^{(2)} = & \hbar\omega_c a^\dagger a + \hbar\omega_0 \sum_{q \in \text{BZ}} b_q^\dagger b_q \\ & + \frac{\hbar g \sqrt{N}}{2} \left[ (b_Q^\dagger e^{i\varphi} + b_{-Q}^\dagger e^{-i\varphi}) a + \text{H.c.} \right] \end{aligned} \quad (2.22)$$

determines the system dynamics when the linear pump is set to zero and the dipoles are approximated by harmonic oscillators (analog of the classical

model of the elastically bound electron), while

$$\begin{aligned} \mathcal{H}^{(4)} = & -\frac{\hbar g}{4\sqrt{N}} \sum_{q_1, q_2 \in \text{BZ}} (b_{q_1}^\dagger b_{q_2}^\dagger b_{q_1+q_2-Q} a e^{i\varphi} \\ & + b_{q_1}^\dagger b_{q_2}^\dagger b_{q_1+q_2+Q} a e^{-i\varphi} + \text{H.c.}) \\ & - i \frac{\hbar \Omega}{2\sqrt{N}} \sum_{q_1, q_2 \in \text{BZ}} (b_{q_1}^\dagger b_{q_2}^\dagger b_{q_1+q_2-Q'} e^{-i(\omega_p t + \phi_L)} - \text{H.c.}) \end{aligned} \quad (2.23)$$

accounts for the lowest-order corrections due to saturation. In Eqs. (2.22) and (2.23) we have denoted by  $\pm Q$  and  $Q'$  the quasimomenta of the spin waves which couple to the cavity and laser mode, respectively, and which fulfill the phase matching conditions

$$Q = k + G, \quad (2.24)$$

$$Q' = k \cos \Theta + G', \quad (2.25)$$

with reciprocal vectors  $G, G'$  such that  $Q, Q' \in \text{BZ}$ . The atoms scatter coherently into the cavity mode when the von-Laue condition is satisfied, namely one of the two relations is fulfilled:

$$2k \sin^2(\Theta/2) = nG_0, \quad (2.26)$$

$$2k \cos^2(\Theta/2) = n'G_0, \quad (2.27)$$

with  $n, n'$  integer numbers. In free space, the von-Laue condition corresponds to Eq. (2.26): for these angles one finds squeezed-coherent states in the far field [10]. When the scattered mode for which the von-Laue condition is fulfilled corresponds to a cavity mode, superradiant scattering enhances this behaviour, until the number of atoms  $N$  is sufficiently large such that the cooperativity exceeds unity. In this limit one observes saturation of the intracavity field intensity, which reaches an asymptotic value whose amplitude is independent of  $N$  as  $N$  is further increased. In the limit  $N \gg 1$  the light at the cavity output is in a coherent state, while inelastic scattering is suppressed at leading order in  $1/N$  [68].

When the von-Laue condition is not satisfied, classical mechanics predicts that there is no scattering into the cavity mode. These modes of the electromagnetic fields are solely populated by inelastic scattering processes.

Moreover, in free space, when

$$2k \sin^2(\Theta/2) = (2n + 1)G_0/2, \quad (2.28)$$

then the inelastically scattered light is in a vacuum-squeezed state [10]. Inside a standing-wave resonator, on the other hand, the mode is in a vacuum-squeezed state provided that either Eq. (2.28) or an additional relation,

$$2k \cos^2(\Theta/2) = (2n + 1)G_0/2, \quad (2.29)$$

is satisfied.

In the following we will study the field at the cavity output as determined by the dynamics of Hamiltonian (2.20) when  $Q' \neq \pm Q$ , namely, when the scattering processes which pump the cavity are solely inelastic. We remark that throughout this treatment we do not make specific assumptions about the ratio between the array periodicity  $d$  and the light wavelength  $\lambda$  (and therefore also consider the situation in which  $\lambda \neq 2d$ . This situation has been experimentally realized for instance in Refs. [64, 69, 75–77]).

### 2.2.2 Linear response: polaritonic modes

We first solve the dynamics governed by Hamiltonian  $\mathcal{H}^{(2)}$  in Eq. (2.22). In the diagonal form the quadratic part can be rewritten as

$$\mathcal{H}^{(2)} = \sum_{j=1}^2 \hbar\omega_j \gamma_j^\dagger \gamma_j + \sum_{q \neq Q_s, q \in BZ} \hbar\omega_0 b_q^\dagger b_q, \quad (2.30)$$

where  $Q_s$  labels the spin wave which couples with the cavity mode, such that

$$b_{Q_s} = b_Q \text{ if } Q = 0, G_0/2, \quad (2.31)$$

$$b_{Q_s} = \frac{b_Q e^{-i\varphi} + b_{-Q} e^{i\varphi}}{\sqrt{2}} \text{ otherwise.} \quad (2.32)$$

The resulting polaritonic eigenmodes are

$$\gamma_1 = -a \cos X + b_{Q_s} \sin X, \quad (2.33)$$

$$\gamma_2 = a \sin X + b_{Q_s} \cos X, \quad (2.34)$$

with respective eigenfrequencies

$$\omega_{1,2} = \frac{1}{2} (\omega_c + \omega_0 \mp \delta\omega), \quad (2.35)$$

$$\delta\omega = \sqrt{(\omega_0 - \omega_c)^2 + 4\tilde{g}^2 N}, \quad (2.36)$$

and

$$\tan X = \tilde{g}\sqrt{N}/(\omega_0 - \omega_1), \quad (2.37)$$

which defines the mixing angle  $X$ . The parameter  $\tilde{g}$  is proportional to the coupling strength. In particular,  $\tilde{g} = g \cos \varphi$  when  $Q = 0, G_0/2$  and the cavity mode couples with the spin wave  $b_{Q_s} = b_Q$ , otherwise  $\tilde{g} = g/\sqrt{2}$  and the spin wave is given in Eq. (2.32).

Hamiltonian (2.21) describes the coupling of the pump with the spin wave  $Q'$ . When  $Q' \neq \pm Q$ , photons are pumped into the cavity via inelastic processes, which in our model are accounted for by the Hamiltonian term in Eq. (2.23). On the other hand, when the dynamics is considered up to the quadratic term (hence, inelastic processes are neglected), only the mode  $Q'$  is pumped and the Heisenberg equation of motion for  $b_{Q'}$  reads

$$\dot{b}_{Q'} = -i\omega_z b_{Q'} - \frac{\gamma}{2} b_{Q'} + \Omega\sqrt{N}e^{-i\phi_L} + \sqrt{\gamma}b_{q,\text{in}}(t), \quad (2.38)$$

that has been written in the reference frame rotating at the laser frequency  $\omega_p$ . Here,  $\gamma$  is the spontaneous decay rate and  $b_{q,\text{in}}(t)$  is the corresponding Langevin force operator, such that  $\langle b_{q,\text{in}}(t) \rangle = 0$  and  $\langle b_{q,\text{in}}(t)b_{q,\text{in}}^\dagger(t') \rangle = \delta(t-t')$  [13]. The general solution reduces, in the limit in which  $|\omega_z| \gg \gamma$ , to the form

$$b_{Q'} \simeq -i\frac{\Omega\sqrt{N}}{\omega_z}e^{-i\phi_L} \quad (2.39)$$

which is consistent with the expansion to lowest order in Eq. (2.17) provided that  $\Omega^2 N \ll \omega_z^2$ . In the reference frame rotating at the laser frequency the explicit frequency dependence of the Hamiltonian terms is dropped, and  $\omega_1 \rightarrow \omega_1 - \omega_p$ ,  $\omega_2 \rightarrow \omega_2 - \omega_p$ ,  $\omega_0 \rightarrow \omega_z$ , and  $\omega_c \rightarrow \omega_c - \omega_p \equiv \delta_c$ .

### 2.2.3 Effective Hamiltonian

Under the assumptions discussed so far, we derive from Hamiltonian (2.20) an effective Hamiltonian for the polariton  $\gamma_1$ . The effective Hamiltonian is obtained by adiabatically eliminating the coupling with the other polaritons,

according to the procedure sketched in Appendix A, and reads

$$\begin{aligned} \mathcal{H}_{\text{eff}} = & \hbar\delta\omega_1\gamma_1^\dagger\gamma_1 \\ & + \frac{\hbar}{2}(\alpha\gamma_1^{\dagger 2}e^{2i\phi_L} + \alpha^*\gamma_1^2e^{-2i\phi_L}) + \hbar\chi\gamma_1^\dagger\gamma_1^\dagger\gamma_1\gamma_1 \\ & + i\hbar(\nu\gamma_1^{\dagger 2}\gamma_1e^{i\phi_L} - \nu^*\gamma_1^\dagger\gamma_1^2e^{-i\phi_L}), \end{aligned} \quad (2.40)$$

where <sup>2</sup>

$$\delta\omega_1 = \omega_1 - \omega_p + \frac{2\Omega^2}{\omega_z} \left( \tilde{S}^2 + \frac{\tilde{g}\sqrt{N}}{\omega_z} \tilde{S}\tilde{C} \right), \quad (2.41)$$

$$\alpha = -\frac{\Omega^2}{\omega_z} \left( \tilde{S}^2 + \frac{\tilde{g}\sqrt{N}}{\omega_z} \tilde{S}\tilde{C} \right) \left( \delta_{Q',G/2} + \mathcal{C}_\alpha^{k \neq G/2} \right), \quad (2.42)$$

$$\chi = \frac{\tilde{g}}{\sqrt{N}} \tilde{S}^3 \tilde{C} \left[ 1 + \mathcal{C}_\chi^{k \neq G/2} \right], \quad (2.43)$$

$$\nu = -\frac{\Omega}{4\sqrt{N}} \left( \tilde{S}^3 + \frac{3\tilde{g}\sqrt{N}}{\omega_z} \tilde{S}^2 \tilde{C} \right) \mathcal{C}_\nu^{k \neq G/2}, \quad (2.44)$$

with  $\tilde{S} = \sin X$  and  $\tilde{C} = \cos X$ . The terms  $\mathcal{C}_j^{k \neq G/2}$  do not vanish when  $k \neq G/2$ , and their explicit form is

$$\begin{aligned} \mathcal{C}_\chi^{k \neq G/2} &= \left( \frac{1}{2} + \frac{1}{2} \delta_{Q, \pm G_0/4} \cos(4\varphi) \right) (1 - \delta_{k,G/2}), \\ \mathcal{C}_\alpha^{k \neq G/2} &= \frac{1}{2} (\delta_{Q', Q+G/2} e^{-2i\varphi} + \delta_{Q', -Q+G/2} e^{2i\varphi}) (1 - \delta_{k,G/2}), \\ \mathcal{C}_\nu^{k \neq G/2} &= \frac{1}{\sqrt{2}} (\delta_{Q', 3Q} e^{-3i\varphi} + \delta_{Q', -3Q} e^{3i\varphi}) (1 - \delta_{k,G/2}). \end{aligned}$$

The coefficients have been evaluated under the requirement  $Q' \neq \pm Q$ .

We now comment on the condition  $\Omega^2 N \ll \omega_z^2$ , on which the validity of Eq. (2.39) is based. When this is not fulfilled, such that  $|\langle b_{Q'} \rangle| \sim 1$ , Eq. (2.38) must contain further non-anharmonic terms from the expansion of Eq. (2.15) and which account for the saturation effects in  $b_{Q'}$ . Since this spin mode is weakly coupled to the other modes, which are initially empty, we expect that the polaritons  $\gamma_1$  and  $\gamma_2$  will remain weakly populated and the structure of their effective Hamiltonian will qualitatively not change.

---

<sup>2</sup>To be precise, the frequency  $\omega_z$  in the denominator of the various coefficients should be replaced by  $(\omega_z^2 + \gamma^2/4)/\omega_z$ , which reduces to  $\omega_z$  in the limit  $|\omega_z| \gg \gamma/2$  and which we are going to introduce later on. The coefficients do not include the cavity decay rate in the denominator, under the assumption that it is much smaller than  $\omega_z$ .

We also note that in the resonant case, when  $\omega_z = 0$ , the form of Hamiltonian in Eq. (2.40) remains unchanged, while in the coefficients  $\delta\omega_1$ ,  $\alpha$ ,  $\nu$ ,  $\chi$  the following substitution  $\omega_z \rightarrow (\omega_z^2 + \gamma^2/4)/\omega_z$  must be performed. A first consequence is that  $\alpha = 0$ , which implies that there are no processes in this order for which polaritons are created (annihilated) in pairs. A further consequence is that spontaneous decay plays a prominent role in the dynamics. We refer the reader to Sec. 2.2.5 for a discussion of the related dissipative effects.

### 2.2.4 Discussion

Let us now discuss the individual terms on the RHS of Eq. (2.40). For this purpose it is useful to consider multilevel schemes, which allow one to illustrate the relevant nonlinear processes. The multilevel schemes are depicted in Fig. 2.3: state  $|\tilde{n}\rangle$  is the polariton number state with  $\tilde{n}$  excitations. The blue arrows indicate transitions which are coupled by the laser, for which the polariton state is not changed; The red arrows denote transitions which are coupled by the cavity field, for which the polariton state is modified by one excitation.

Using this level scheme, one can explain the dynamical Stark shift  $\delta\omega_1$  of the polariton frequency in Eq. (2.41) as due to higher-order scattering processes, in which laser- and cavity-induced transition creates and then annihilates, in inverse sequential order, a polariton.

The second term on the RHS has coupling strength given in Eq. (2.42), it generates squeezing of the polariton and does not vanish provided that  $Q' = G/2$  or  $Q' = \pm Q + G/2$ . The latter condition is equivalent to the free-space condition (2.28), while the first arises from the fact that the cavity mode couples with the symmetric superposition  $b_{Q_s}$  in Eq. (2.31). The corresponding phase-matched scattering event is a four-photon process, in which two laser photons are absorbed (emitted) and two polaritonic quanta are created (annihilated). For  $Q' = G/2$  and  $Q' \neq \pm Q$  the polaritons are created in pairs with quasi-momentum  $Q$  and  $-Q$  (the relation  $Q = G/2$  corresponds to  $b_{-Q} = b_Q$ ). This specific term is also present when the geometry of the setup is such that von-Laue condition is fulfilled, and at this order is responsible for the squeezing present in the light at the cavity output.

The Kerr-nonlinearity (third term on the RHS) gives rise to an effective interaction between the polaritons and emerges from processes in which

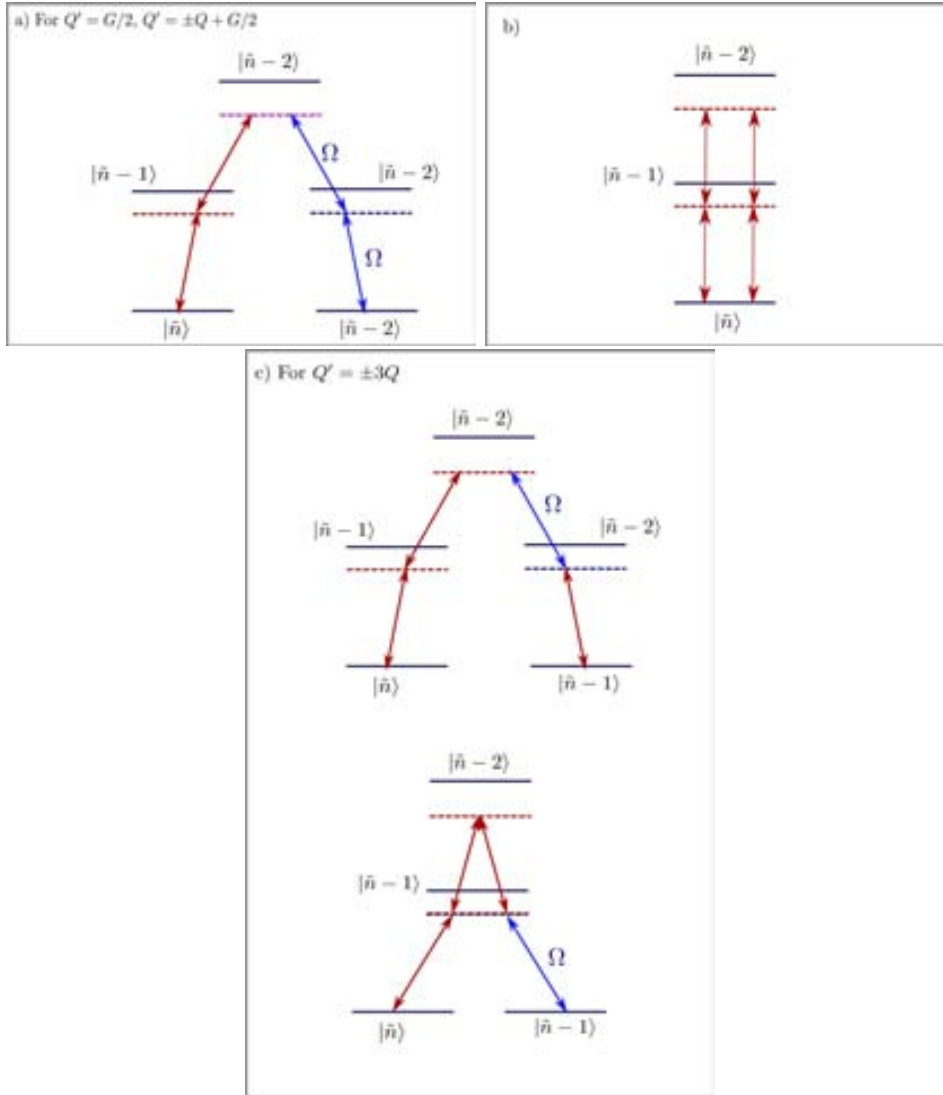


Figure 2.3: Schematic diagram of transitions which fulfill the phase-matching condition till fourth order. State  $|\tilde{n}\rangle$  denote the number state of the polariton mode  $\gamma_1$ . The blue arrows denote the laser-induced couplings and the red arrows denote the creation (annihilation) of polaritons due to the coupling with the cavity field. See text for a detailed discussion.

polaritons are absorbed and emitted in pairs. It is depicted in Fig. 2.2.4 for a generic case. This term is directly proportional to the cavity coupling strength and inversely proportional to  $\sqrt{N}$ . In this order, it is the term that gives rise to anti-bunching.

The last term on the RHS, finally, is a nonlinear pump of the polariton mode, whose strength depends on the number of polaritonic excitations. It is found when the phase-matching condition  $Q' = \pm 3Q + G$  is satisfied, which is equivalent to the relation  $\cos \theta = (3 + n\lambda/d)$  when laser and optical resonator have the same wavelength, as in the case here considered. This relation can be fulfilled for  $n \neq 0$  and specific ratios  $\lambda/d$ . This term vanishes over the vacuum state, and it pumps a polariton at a time with strength proportional to the number of polariton excitations.

In general, photons into the cavity mode are pumped provided that either (i)  $Q' = \pm Q$  or (ii) (for  $Q' \neq \pm Q$ ) one of the two conditions are satisfied:  $Q' = G/2$  or  $Q' = \pm Q + G/2$ . We note that the strength of the Rabi frequency and of the cavity Rabi coupling may allow one to tune the relative weight of the various terms in Hamiltonian (2.40). Their ratio scales differently with the number of atoms in different regimes, which we will discuss below. Moreover, the interparticle distance of the atomic array constitutes an additional control parameter over the nonlinear optical response of the medium. Further phase-matching conditions are found when considering higher-order terms in the expansion of the spin operators in harmonic-oscillator operators from Eq. (2.15). Their role in the dynamics will be relevant, as long as they compete with the dissipative rates, here constituted by the cavity loss rate and spontaneous emission.

### 2.2.5 Cavity input-output formalism

We consider the full system dynamics, including the atomic spontaneous emission and the cavity quantum noise due to the coupling to the external modes of the electromagnetic field via the finite transmittivity of the cavity mirrors. The Heisenberg-Langevin equations for the operator  $b_q$  according to Eq. (1.18) reads

$$\dot{b}_q = \frac{1}{i\hbar}[b_q, \mathcal{H}] - \frac{\gamma}{2}b_q + \sqrt{\gamma}b_{q,\text{in}}(t), \quad (2.45)$$

where  $b_{q,\text{in}}$  is the Langevin operator and fulfills the relations  $\langle b_{q,\text{in}}(t) \rangle = 0$  and  $\langle b_{q,\text{in}}(t)b_{q,\text{in}}^\dagger(t') \rangle = \delta(t-t')$ . Here, the average  $\langle \cdot \rangle$  is taken over the density matrix at time  $t = 0$  of the system composed by the atomic spins and by the electromagnetic field. The output field  $a_{\text{out}}$  at the cavity mirror is given by the relation in Eq. (1.21).

Let us now consider the scattering processes occurring in the system. They can be classified into three types: (i) a laser photon can be scattered into the modes of the external electromagnetic field (emf) by the atoms, without the resonator being pumped in an intermediate time; (ii) a laser photon can be scattered into the cavity mode by the atom and then dissipated by cavity decay; (iii) a laser photon can be scattered into the cavity mode by the atom, then be reabsorbed and emitted into the modes of the external emf. Processes of kind (i) include elastic scattering. They can be the fastest processes, but do not affect the properties of the light at the cavity output. Processes of kind (ii) are the ones which outcouple the intracavity field, but need to be sufficiently slow in order to allow for the build-up of the intracavity field. Processes of kind (iii) are detrimental for the nonlinear optical dynamics we intend to observe, as they introduce additional dissipation (see for instance [78, 79] for an extensive discussion and [11] for a system like the one here considered but composed by two atoms).

Processes (iii), i.e., reabsorption of cavity photons followed by spontaneous emission, can be neglected assuming that the laser and cavity mode are far-off resonance from the atomic transition. In this limit, the cavity is pumped by coherent Raman scattering processes and an effective Heisenberg-Langevin equation for the polariton  $\gamma_1$  can be derived assuming that its effective linewidth  $\kappa_1 = \kappa \cos^2 X + (\gamma/2) \sin^2 X$  fulfilling the inequality  $\kappa_1 \ll \delta\omega$  (that corresponds to the condition for which the vacuum Rabi splitting is visible in the spectrum of transmission [58, 75–77, 80, 81]). We find

$$\dot{\gamma}_1 = \frac{1}{i\hbar}[\gamma_1, \mathcal{H}_{\text{eff}}] - \kappa_1 \gamma_1 + \sqrt{2\kappa} \tilde{C} a_{\text{in}}(t) + \sqrt{\gamma} \tilde{S} b_{q,\text{in}}(t), \quad (2.46)$$

which determines the dissipative dynamics of the polariton. The field at the cavity output is determined using the solution of the Heisenberg Langevin equation (2.46) with Eqs. (2.33)-(2.34) in Eq. (1.21). In some calculations, when appropriate we solved the corresponding master equation for the density matrix of the polaritonic modes  $\gamma_1$  and  $\gamma_2$ .

Some remarks are in order at this point. Nonlinear-optical effects in an atomic ensemble, which is resonantly pumped by laser fields, have been studied for instance [82], where the nonlinearity is at the single atom level and is generated by appropriately driving a four-level atomic transitions [83–85].

It is important to note, moreover, that Eq. (2.46) is valid as long as the loss mechanisms occur on a rate which is of the same order, if not smaller, than the inelastic processes. This leads to the requirement that the atom-cavity system be in the strong-coupling regime.

## 2.3 Results

We now study the properties of the light at the cavity output as a function of various parameters, assuming that  $Q' = G/2$  and that the relations  $Q' \neq \pm Q$  and  $Q' \neq \pm 3Q + G$  hold. Under these conditions the effective Hamiltonian in Eq. (2.40) contains solely the squeezing and the Kerr-nonlinearity terms, while  $\nu = 0$ . Moreover, we assume the condition  $\kappa_1 \simeq \kappa > \gamma$ .

The possible regimes which may be encountered can be classified according to whether the ratio

$$\varepsilon = |\alpha/\chi|$$

is larger or smaller than unity. In the first case the medium response is essentially the one of a parametric amplifier. In the second case the Kerr nonlinearity dominates, and polaritons can only be pumped in pairs provided that the emission of two polaritons is a resonant process.

Let us now focus on the regime in which the system acts as a parametric amplifier, namely,  $\varepsilon \gg 1$ . In this case one finds that the number of photons at the cavity output at time  $t$  is

$$\langle a_{out}^\dagger a_{out} \rangle_t \simeq 2\kappa \tilde{C}^2 \langle \gamma_1^\dagger \gamma_1 \rangle_t,$$

with

$$\begin{aligned} \langle \gamma_1^\dagger \gamma_1 \rangle_t &= \frac{1}{2} \frac{\alpha^2}{\kappa_1^2 - \alpha^2} + e^{-2\kappa_1 t} \sinh^2(\alpha t) \\ &+ \frac{e^{-2\kappa_1 t}}{2} \left( 1 - \kappa_1 \frac{\kappa_1 \cosh(2\alpha t) + \alpha \sinh(2\alpha t)}{\kappa_1^2 - \alpha^2} \right). \end{aligned} \quad (2.47)$$

Depending on whether  $\alpha > \kappa_1$  or  $\alpha < \kappa_1$ , one finds that the dynamics of the

intracavity polariton corresponds to a parametric oscillator above or below threshold, respectively. In the following we focus on the case below threshold and evaluate the spectrum of squeezing. We first observe that the quadrature  $x^{(\theta)} = \gamma_1 e^{-i\theta} + \gamma_1^\dagger e^{i\theta}$  has minimum variance for  $\theta = \pi/4$  and reads [11]

$$\langle \Delta x^{(\frac{\pi}{4})^2} \rangle_{st} = \frac{\kappa_1}{\kappa_1 + |\alpha|}, \quad (2.48)$$

where the subscript  $st$  refers to the expectation value taken over the steady-state density matrix. The squeezing spectrum of the maximally squeezed quadrature is

$$S_{out}(\omega) = 1 + \int_{-\infty}^{+\infty} \langle : x_{out}^{(\frac{\pi}{4})}(t+\tau), x_{out}^{(\frac{\pi}{4})}(t) : \rangle_{st} e^{-i\omega\tau} d\tau \quad (2.49)$$

$$= 1 - \frac{4\kappa\tilde{C}^2|\alpha|}{(\kappa_1 + |\alpha|)^2 + \omega^2}, \quad (2.50)$$

where  $\langle : \cdot : \rangle_{st}$  indicates the expectation value for the normally-ordered operators over the steady state, with

$$x_{out}^{(\theta)} = a_{out} e^{-i\theta} + a_{out}^\dagger e^{i\theta}.$$

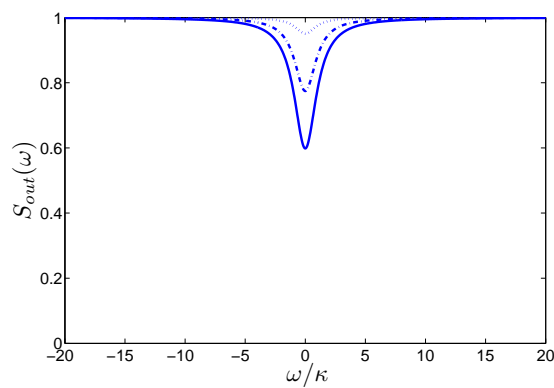
We now discuss the parameter regime in which these dynamics can be encountered. The relation  $\varepsilon \gg 1$  is found provided that  $\Omega \gg g$ . When  $|\omega_z| \gg \Omega\sqrt{N}$ , in this limit  $|\alpha| \simeq \Omega^2 g^2 N / \omega_z^3$ , and squeezing can be observed only for very small values of  $\kappa$ . Far less demanding parameter regimes can be accessed when relaxing the condition on the laser Rabi frequency, and assuming that  $\Omega\sqrt{N} \sim |\omega_z|$ . In this case squeezing in the light at the cavity output can be found provided that  $\Omega \gg \kappa$  when  $g\sqrt{N} \sim |\omega_z|$ <sup>3</sup>.

Figures 2.4(a) and (b) display the spectrum of squeezing when the system operates as a parametric amplifier below threshold. Here, one observes that squeezing increases with  $N$ . Comparison between Fig. 2.4(a) and 2.4 (b) shows that squeezing increases also as the single-atom cooperativity increases (provided the corresponding phase-matching conditions are satisfied and the laser Rabi frequency  $\Omega \gg g$ ). These results agree and extend the findings in Ref. [11], which were obtained for an array consisting of 2 atoms.

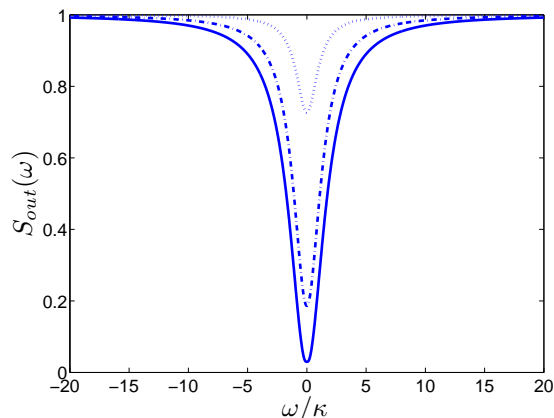
Let us now focus on the regime when  $\varepsilon \ll 1$ . Here, the polaritons may be

---

<sup>3</sup>In this limit, the dependence on the number of atoms is contained in the mixing angle  $X$ , Eq. (2.37), and is such that  $\tan X \rightarrow 1$  as  $N$  is increased.



(a)



(b)

Figure 2.4: Squeezing spectrum for the maximum squeezed quadrature when  $k = G/2$ ,  $Q' = G/2$  and  $Q' \neq Q$  for  $\varphi, \phi_L = 0$ . The parameters are  $\Omega = 200\kappa$ ,  $\omega_z = 10^3\kappa$  and  $N = 10, 50, 100$  atoms (from top to bottom) for (a)  $g = 4\kappa$  and (b)  $g = 10\kappa$ . The detuning  $\delta_c$  is chosen such that  $\delta\omega_1$  is zero. The curves are evaluated from Eq. (2.49) by numerically calculating the density matrix of the polariton field for a dissipative dynamics, whose coherent term is governed by the effective Hamiltonian in Eq. (2.40). The value  $g = 4\kappa$  is consistent with the experimental data of Ref. [86, 87].

only emitted in pairs into the resonator. In order to characterize the occurrence of these dynamics we evaluate the second-order correlation function at zero-time delay in the cavity output defined by [13]

$$g^{(2)}(0) = \frac{\langle a_{\text{out}}^\dagger a_{\text{out}}^\dagger a_{\text{out}} a_{\text{out}} \rangle_{st}}{\langle a_{\text{out}}^\dagger a_{\text{out}} \rangle_{st}^2}. \quad (2.51)$$

Function  $g^{(2)}(0)$  quantifies the probability to measure two photon at the cavity output at the same time. Therefore, sub-Poissonian (super-Poissonian) statistics are here connected to the value of  $g^{(2)}(0)$  smaller (larger) than one, while for a coherent state  $g^{(2)}(0) = 1$ .

Sub-Poissonian photon statistics at the cavity output can be found as a result of the dynamics of Eq. (2.40). Here, for phase-matching conditions leading to  $\nu = 0$  and  $\alpha \neq 0$ , polaritons can only be created in pairs. When the Kerr-nonlinearity is sufficiently large, however, the condition can be reached in which only two polaritons can be emitted into the cavity, while emission of a larger number is suppressed because of the blockade due to the Kerr-term. This is reminiscent of the two-photon gateway realized in Ref. [14], where injection of two photons inside a cavity, pumped by a laser, was realized by exploiting the anharmonic properties of the spectrum of a cavity mode strongly coupled to an atom. In the case analysed in this Chapter, the anharmonicity arises from collective scattering by the atomic array, when this is transversally driven by a laser. Moreover, we note that the observation of these dynamics requires  $\Omega\sqrt{N} \ll |\omega_z|, g\sqrt{N}$  and  $|\alpha| > \kappa$ , which reduces to the condition  $\Omega^2/\omega_z > \kappa$  when  $g\sqrt{N} \sim \omega_z$ .

Figure 2.5(a) displays  $g^{(2)}(0)$  as a function of the pump frequency  $\omega_p$  for the phase matching conditions giving  $\nu = 0$  and  $\alpha \neq 0$ . Function  $g^{(2)}(0)$  is evaluated by numerically integrating the master equation with cavity decay, where the coherent dynamics is governed by an effective Hamiltonian which accounts for the effect of both polariton modes and is reported in Eq. (A.1) in the Appendix. Antibunching is here observed over an interval of values of  $\omega_p$ , about which the cavity mode occupation has a maximum (blue curve in Fig. 2.5(b)). The maximum corresponds to the value of  $\omega_p$  for which the emission of two polaritons  $\gamma_2$  is resonant. Note that the spin-wave excitation, red curve in Fig. 2.5(b), is still sufficiently small to justify the perturbative expansion at the basis of our theoretical model. Figure 2.5(c) displays the amplitudes  $|\chi|$ , determining the strength of the Kerr-nonlinearity, and  $|\alpha|$ ,

scaling the squeezing dynamics, in units of  $|\delta\omega_1|$  and as a function of  $\omega_p$ . One observes that for the chosen parameters  $|\chi| > |\alpha|$ . Maximum antibunching is here found when the cavity mean photon number is maximum.

It is important to notice that emission of polaritons in pairs is possible when the collective dipole of the atomic array is driven. For fixed values of  $\Omega$  and  $g$ , we expect that this effect is washed away as  $N$  is increased: this behaviour is expected from the scaling of the ratio  $\varepsilon$  with  $N$ . Taking  $k = G/2$  and mixing angles  $X \ll 1$ , for instance, one finds  $\varepsilon \sim \sqrt{N}$ , indicating that the strength of the Kerr nonlinearity decreases relative to the coupling  $\alpha$  as  $N$  grows. This is also consistent with the results reported in Fig. 2.4. In this context, the expected dynamics is reminiscent of the transition from antibunching to bunching observed as a function of the number of atoms in atomic ensembles coupled with CQED setups [67].

For the results here presented we have assumed the spontaneous emission rate to be smaller than  $\kappa$ . In general, the predicted nonlinear effects can be observed in cavities with a large single-atom cooperativity and in the so-called good cavity regime [80]. The required parameter regimes for observing squeezing have been realized in recent experiments [86, 87]. The parameters required in order to observe a two-photon gateway are rather demanding for the regime in which the atoms are driven well below saturation. Nevertheless, a reliable quantitative prediction with an arbitrary number of atoms would require a numerical treatment going beyond the Holstein-Primakoff expansion here employed.

## 2.4 Summary and outlook

An array of two-level atoms coupling with the mode of a high-finesse resonator and driven transversally by a laser can operate as controllable nonlinear medium. The different orders of the nonlinear responses correspond to different nonlinear processes exciting collective modes of the array. Depending on the phase-matching condition and on the strength of the driving laser field a nonlinear process can prevail over others, determining the dominant nonlinear response. These dynamics are enhanced for large single-atom cooperativities. We have focussed on the situation in which the scattering into the resonator is inelastic, and found that at lowest order in the saturation parameter the light at the cavity output can be either squeezed or

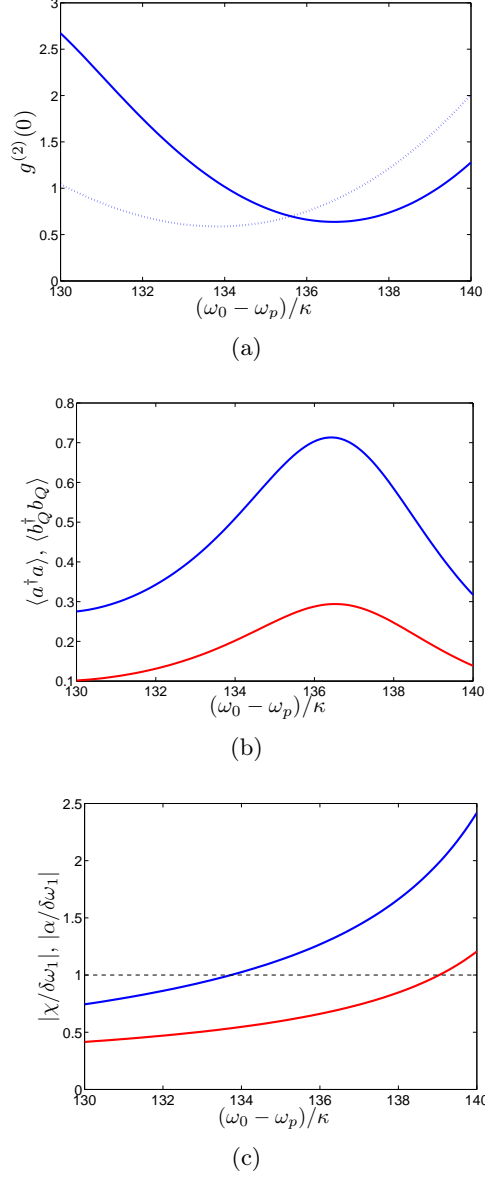


Figure 2.5: (a) Second order correlation function at zero-time delay  $g^{(2)}(0)$  versus  $\omega_p$  (in units of  $\kappa$ ) when the cavity is solely pumped by inelastic processes (here,  $k = G/2$ ,  $Q' \neq Q, 3Q$  and  $Q' = G'/2$  for  $\varphi, \phi_L = 0$ ). The correlation function is evaluated numerically solving the master equation for the polaritons in presence of cavity decay, with the coherent dynamics given by Hamiltonian (A.1) (solid line) and by Hamiltonian (2.40) (dashed line). (b) Corresponding average number of intracavity photons  $\langle a^\dagger a \rangle$  (blue line) and spin wave occupation  $\langle b_Q^\dagger b_Q \rangle$  (red line). (c) Ratios  $|\chi/\delta\omega_1|$  (blue line) and  $|\alpha/\delta\omega_1|$  (red line) versus  $\omega_p$ . The parameters are  $g = 80\kappa$ ,  $\Omega = 30\kappa$ ,  $\omega_z - \delta_c = 70\kappa$ , and  $N = 2$  atoms. At the minimum of  $g^{(2)}(0)$ ,  $\omega_z \simeq 137\kappa$  and  $\delta_c \simeq 67\kappa$ .

antibunched. In the latter case, it can either operate as single-photon or two-photon gateway, depending on the phase-matching conditions. Our analysis permits one to identify the parameter regimes, in which a nonlinear-optical behaviour can prevail over others, thereby controlling the medium response.

In view of recent experiments coupling ultracold atoms with optical resonators [31–33, 55, 68, 69, 75–77, 81, 86–91], these findings show that the coherence properties at the cavity output can be used for monitoring the spatial atomic distribution inside the resonator. A related question is how the properties of the emitted light depend on whether the atomic distribution is bi- or multi-periodic [92]. In this case, depending on the characteristic reciprocal wave vectors one expects a different nonlinear response at different pump frequency and possibly also wave mixing. When the interparticle distance is uniformly distributed, then coherent scattering will be suppressed. Nevertheless, the atoms will pump inelastically photons into the cavity mode. While in free space the resonance fluorescence is expected to be the incoherent sum of the resonance fluorescence from each atom, inside a resonator one must consider the backaction due to the strong coupling with the common cavity mode.

A further outlook is to consider these dynamics in order to create entanglement between cavity mode and spin-wave modes. Such entanglement can be a resource for quantum communication. A protocol for entangling cavity and spins based on this setup is discussed in Chapter 3 of this thesis.

Finally, in this Chapter we neglected the atomic kinetic energy, assuming that the spatial fluctuations of the atomic center of mass at the potential minima are much smaller than the typical length scales determining the coupling with radiation [11]. It is important to consider, that when the mechanical effects of the scattered light on the atoms is taken into account, conditions could be found where selforganized atomic patterns are observed [28, 33, 38, 40–42, 55, 89, 90, 93, 94]. In Chapter 4 we will analyze the quantum ground state of the atomic array in lowest order in the saturation parameter when quantum fluctuations about the equilibrium position are not negligible. In this case we will show that quantum fluctuations support the formation of an intracavity field, which itself modifies the quantum state of the atoms.



---

## Two-mode squeezing by an atomic array in a cavity

---

In the latest decade hot atomic ensembles in cells have been the physical system, with which milestone experiments have been performed [22]. The key element of this remarkable progress has been the detailed knowledge of atom-photon interactions, which permitted the engineering of the dynamics leading to the demonstration of the building blocks of a quantum network. These and analogous dynamics are being explored for atoms in optical resonators with the objectives of exploiting the strong atom-photon coupling in order to realize efficient quantum interfaces [24–26, 95–103] and high-precision optical clocks [104, 105].

One important requirement for a quantum interface is a controlled non-linear dynamics capable of generating entanglement [22, 106–108]. With this objective in mind, in this chapter, we analyze the dynamics of an atomic array coupled with the mode of a high-finesse optical cavity, as in Chapter 2, and identify parameter regimes for which a collective spin excitation is entangled with the cavity field at steady state. We will show that this entanglement is found at the stationary state of the system, and is robust against noise and dissipation due to cavity decay.

We first start this chapter by giving a sketchy review of a coherent non-linear dynamics generating entanglement between two harmonic oscillators in Sec. 3.1, which is the one of a non-degenerate parametric oscillator [13]. Here, we will also introduce entanglement measure for Gaussian states. This is particular relevant for our study, since starting from Hamiltonian (1.25), we will identify analogous dynamics leading to entanglement between light and a collective spin excitation of the atomic array. We will then character-

ize the final state of the system. The study on the specific physical system, which is the object of this thesis, is performed starting from Sec. 3.2.

### 3.1 Non-degenerate parametric amplifier and Entanglement

In nonlinear optics the non-degenerate parametric amplifier is a device in which a classical pump laser with frequency  $2\omega$  in a nonlinear optical medium generates two photons of frequency  $\omega_A$  and  $\omega_B$  ( $\omega_A \neq \omega_B$ ) where  $2\omega = \omega_A + \omega_B$ . The dynamics of the two oscillators  $A$  and  $B$  is governed by the Hamiltonian [13]

$$\hat{H} = \hbar\omega_A \hat{a}_A^\dagger \hat{a}_A + \hbar\omega_B \hat{a}_B^\dagger \hat{a}_B + i\hbar\eta \left( \hat{a}_A^\dagger \hat{a}_B^\dagger e^{-2i\omega t} - \hat{a}_A \hat{a}_B e^{2i\omega t} \right) \quad (3.1)$$

with  $\eta$  the two-mode squeezing parameter proportional to the amplitude of the pump laser and the second-order susceptibility of the medium (see  $\chi^{(2)}$  in Eq. (2.14)). In (3.1) operators  $\hat{a}_A$  and  $\hat{a}_B$  annihilate a photon of the mode with frequency  $\omega_A$  and  $\omega_B$ , respectively, while  $\hat{a}_A^\dagger$  and  $\hat{a}_B^\dagger$  are the corresponding self-adjoint. In interaction picture the Hamiltonian is reduced to the form  $\hat{H}' = i\hbar\eta(\hat{a}_A^\dagger \hat{a}_B^\dagger - \hat{a}_A \hat{a}_B)$ . The unitary operator determining the system evolution at time  $t$  is  $U_s(t) = \exp \left[ \eta t (\hat{a}_A^\dagger \hat{a}_B^\dagger - \hat{a}_A \hat{a}_B) \right]$  which is the two-mode squeezing operator [13]. In particular,

$$\begin{aligned} \hat{a}_A(t) &= \hat{a}_A(0) \cosh(\eta t) + \hat{a}_B^\dagger(0) \sinh(\eta t), \\ \hat{a}_B(t) &= \hat{a}_B(0) \cosh(\eta t) + \hat{a}_A^\dagger(0) \sinh(\eta t). \end{aligned} \quad (3.2)$$

If the two oscillators are initially in the vacuum state, their initial state reads  $|\Phi(0)\rangle = |0, 0\rangle$ , and the mean occupation number grows with time according to the relation  $\langle \hat{a}_A^\dagger(t) \hat{a}_A(t) \rangle = \langle \hat{a}_B^\dagger(t) \hat{a}_B(t) \rangle = \sinh^2(\eta t)$ . Correspondingly, the state of the oscillators at time  $t$  is given by  $|\Phi(t)\rangle = U_s(t)|0, 0\rangle$  and in the Fock-state basis reads [13]

$$|\Phi(t)\rangle = \frac{1}{\cosh(\eta t)} \sum_{n=0}^{\infty} \left( \tanh(\eta t) \right)^n |n, n\rangle, \quad (3.3)$$

where  $|n, n\rangle = |n\rangle_A |n\rangle_B$  is the state with  $n$  photons in each mode. State  $|\Phi(t)\rangle$  is the two-mode squeezed state and it is an entangled state: In

Ref. [109] it was shown that this is a realization of Einstein-Podolsky-Rosen (EPR) entangled state [15].

To use entanglement as a resource for quantum information processing, one needs to identify a way to quantify it. In this respect the two-mode squeezed state is particularly important in quantum information processing with continuous variables since the degree of two-mode squeezing, here  $\zeta = \eta t$ , can be related to a measure of entanglement [110–113]. One entanglement measure for Gaussian states, which we are going to use in this thesis, is the logarithmic negativity [114]. For a density matrix  $\hat{\rho}$  describing two systems  $A + B$ , the logarithmic negativity is defined as

$$E_N(\hat{\rho}) = \log_2 \|\hat{\rho}^{TA}\| \quad (3.4)$$

where  $\|\cdot\|$  denotes the trace norm and  $\hat{\rho}^{TA}$  is the partial transpose of  $\hat{\rho}$  with respect to the subsystem  $A$ . Further details are provided in Appendix B. In general when the logarithmic negativity  $E_N(\hat{\rho})$  is larger than zero,  $\hat{\rho}$  is entangled. For bipartite Gaussian states, the logarithmic negativity is a measure of entanglement and it provides a necessary and sufficient criterion for entangled states [114, 115]. For non-Gaussian states, on the other hand, there is to date no general measure which quantifies entanglement [113]: In this case, the logarithmic negativity is only a witness. This means that, while for  $E_N > 0$  there is entanglement in the system, for  $E_N = 0$  one cannot make any statement on whether A and B are entangled.

## 3.2 Parametric amplifier based on an atomic array in a cavity

We now turn to the physical system which is the object of this thesis, an array of atoms, whose dipolar transition couples with a mode of a high-finesse resonator. The cavity is a standing wave and is pumped by the photons scattered by the atoms, which are driven by a laser illuminating them from the side. The Hamiltonian of the model is given in Eq. (1.25). As in Chapter 2, we assume that the array is periodic and that the geometry of the setup is fixed so that coherent scattering into the cavity mode is suppressed.

The atomic transitions are driven well below saturation, corresponding

to the choice of parameters  $\Omega \ll |\omega_z + i\gamma/2|$ . We then perform the Holstein-Primakoff transformation for the atomic spins and expand in the bosonic operators up to third order, as in Eqs. (2.17). The procedure follows the same steps as in Chapter 2, and is detailed in Appendix A. Hamiltonian (1.25) is reduced to a form, describing the nonlinear coupling of oscillators with the cavity field, where the nonlinearity are due to saturation effects, and which reads  $\mathcal{H} = \mathcal{H}^{(2)} + \mathcal{H}^{(4)}$ . Here <sup>1</sup>

$$\begin{aligned} \mathcal{H}^{(2)} = & \hbar\delta_c a^\dagger a + \hbar\omega_z (b_Q^\dagger b_Q + b_{Q'}^\dagger b_{Q'}) \\ & + \hbar\tilde{g}\sqrt{N}(b_Q^\dagger a + \text{H.c.}) + i\hbar\Omega\sqrt{N}(b_{Q'}^\dagger - \text{H.c.}), \end{aligned} \quad (3.5)$$

with  $\tilde{g} = g \cos(\varphi)$ , accounts for the atom-field linear interactions,  $Q$  the laser wave vector,  $Q' \neq Q$ , and

$$\begin{aligned} \mathcal{H}^{(4)} = & \frac{-\hbar\tilde{g}}{2\sqrt{N}} \left( b_{Q'}^\dagger b_{Q'}^\dagger b_Q \delta_{Q',G/2} + 2b_{Q'}^\dagger b_Q^\dagger b_{Q'} + b_Q^\dagger b_Q^\dagger b_Q \right) a \\ & - i \frac{\hbar\Omega}{2\sqrt{N}} \left( 2b_{Q'}^\dagger b_Q^\dagger b_Q + b_Q^\dagger b_Q^\dagger b_{Q'} \delta_{Q',G/2} \right) + \text{H.c.}, \end{aligned} \quad (3.6)$$

describes the lowest order inelastic processes. This form holds when  $Q = G/2$  with  $G$  some reciprocal lattice vector. Consistently with the low-saturation limit, we make use of the approximation  $b_{Q'} \approx -i\Omega\sqrt{N}e^{-i\phi_L}/\omega_z$  in  $\mathcal{H}$  and derive the effective Hamiltonian

$$\begin{aligned} \mathcal{H}_{\text{eff}} = & \hbar\delta_c a^\dagger a + \hbar\delta_b b_Q^\dagger b_Q + \hbar\alpha_{\text{BS}}(a^\dagger b_Q + \text{H.c.}) \\ & + \hbar\chi \left( b_Q^\dagger b_Q^\dagger b_Q a + \text{H.c.} \right) \\ & + \hbar(\alpha_{Q,a} a^\dagger b_Q^\dagger + \text{H.c.}) + \hbar(\alpha_Q b_Q^{\dagger 2} + \text{H.c.}), \end{aligned} \quad (3.7)$$

---

<sup>1</sup>From here on, we drop the hat symbol  $\hat{\cdot}$  for operators.

with the parameters

$$\begin{aligned}
 \delta_b &= \omega_z + \frac{2\Omega^2}{\omega_z}, \\
 \alpha_{\text{BS}} &= \tilde{g}\sqrt{N} \left( 1 - \frac{\Omega^2}{\omega_z^2} \right), \\
 \chi &= \frac{\tilde{g}}{2\sqrt{N}}, \\
 \alpha_{Q,a} &= \tilde{g}\sqrt{N} \frac{\Omega^2}{2\omega_z^2} \delta_{Q',G'/2}, \\
 \alpha_Q &= -\frac{\Omega^2}{2\omega_z} \delta_{Q',G'/2}.
 \end{aligned} \tag{3.8}$$

The parameter  $\delta_b$  accounts for the spin resonance frequency which is modified by the dynamical Stark shift due to the interaction with the laser light. The third term in Eq. (3.7) describes the linear interaction between spins and cavity and its strength,  $\alpha_{\text{BS}}$ , is modified by the nonlinear interaction with the spin mode  $Q'$ .

The remaining three terms in Eq. (3.7), accounts for the inelastic processes. The fourth term, whose coefficient is  $\chi$  (see Eq. (3.8)) describes four-wave mixing processes involving cavity field and the spin wave mode  $Q$ . Its strength is inversely proportional to  $\sqrt{N}$ , hence its effect is negligible for sufficiently large number of atoms. The last two terms with coefficients  $\alpha_{Q,a}$  and  $\alpha_Q$ , describe squeezing of the spins and of the cavity field. These two terms are present only when the phase-matching condition  $Q' = G'/2$ , with  $G'$  reciprocal lattice vector, is satisfied. Together with the assumption  $Q \neq Q'$  and  $Q = G/2$ , these relations imply that either  $Q'$  is at the edge of the Brillouin zone and  $Q$  at the center, or, vice-versa  $Q'$  is at the center and  $Q$  at the edge.

When  $\delta_c \sim 0$ , such that the cavity mode is resonant with the driving field, the last two terms of (3.7) are responsible for the squeezing of the cavity light as discussed in Chapter 2. Here we are interested in parameters regime for which the light is strongly entangled with the spins. This is obtained when

$$\delta_c \sim -\delta_b. \tag{3.9}$$

Under this condition, in fact, the Hamiltonian term proportional to  $\alpha_{Q,a}$

in Eq. (3.7) is resonant. This term describes the correlated emission and absorption of excitations of spin-wave and cavity modes, which are typical of non-degenerate parametric oscillations.

Dissipation processes for the dynamics of the cavity field coupled with the spin-wave mode  $Q$  include two channels: (i) through the cavity mirrors described by the cavity line-width  $\kappa$  and (ii) through the coupling of the spin-wave mode  $Q$  to the external electromagnetic fields determined by the atomic transition line-width  $\Gamma$ . Therefore the master equation (1.14) describing the system dynamics takes the form

$$\dot{\rho} = -\frac{i}{\hbar}[\mathcal{H}_{\text{eff}}, \rho] + \mathcal{L}\rho \quad (3.10)$$

where

$$\mathcal{L}\rho = \kappa(2a\rho a^\dagger - a^\dagger a\rho - \rho a^\dagger a) + \Gamma(2b_Q\rho b_Q^\dagger - b_Q^\dagger b_Q\rho - \rho b_Q^\dagger b_Q). \quad (3.11)$$

Here we consider the situation in which the detuning of the pump laser fields from the atomic transition is much larger than the atomic line-width, i.e.,  $|\omega_z| \gg \Gamma$ .

Let us now discuss the validity of the low-saturation assumption, on which the effective Hamiltonian we derived is based. This can be checked by estimating the atomic excited state population  $\langle S_j^\dagger S_j \rangle \sim \langle b_j^\dagger b_j \rangle$  which has to be much smaller than unity. Since the mode  $Q'$  is not coupled to the cavity and is only weakly coupled, non-resonantly, to the other modes, then the populations of the other modes remain always very small. The only spin mode that can be relevantly populated is the mode  $Q$ . This mode, in fact, can be driven resonantly by the nonlinear processes involving also the cavity.

Therefore the condition over the atomic excited state population can be written as

$$\begin{aligned} \langle b_j^\dagger b_j \rangle &\simeq \frac{1}{N} \sum_q \langle b_q^\dagger b_q \rangle \simeq \frac{1}{N} [\langle b_{Q'}^\dagger b_{Q'} \rangle + \langle b_Q^\dagger b_Q \rangle] \\ &\simeq \frac{\Omega^2}{\omega_z^2} + \frac{\langle b_Q^\dagger b_Q \rangle}{N} \ll 1. \end{aligned} \quad (3.12)$$

Here we have neglected the populations of the spin modes different from  $Q$  and  $Q'$ , and also the correlations between spin modes.

### 3.3. Results: stationary entanglement between matter and light<sup>47</sup>

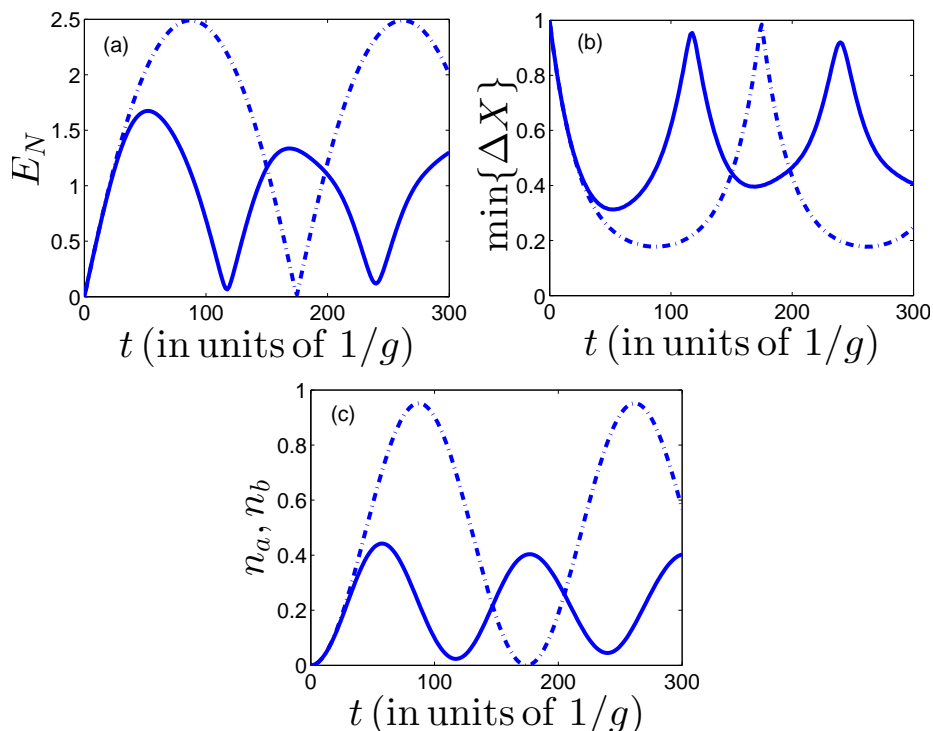


Figure 3.1: (a) Logarithmic negativity  $E_N$  in (3.4) is evaluated as a function of time  $t$  (in units of  $1/g$ ), in the absence of dissipations. The solid lines are evaluated numerically by solving the Schrödinger equation of motion using the Hamiltonian (3.7), according to the App. D, whereby the dash-dotted lines are the corresponding results for  $\chi = 0$ . The corresponding plots for the minimum variance of a composite quadrature  $\min\{\Delta X(\theta_a, \theta_b)\}$  (see Eq. (3.13)) with respect to the angles  $\theta_a$  and  $\theta_b$ , are shown in panel (b). The value of  $\Delta X = 1$  corresponds to the shot-noise limit. The curves in (c) display the field modes population  $n_a = \langle a^\dagger a \rangle$  and  $n_b = \langle b_Q^\dagger b_Q \rangle$  as a function of time in which the two curves for  $n_a$  and  $n_b$  are superimposed. The parameters are  $\omega_z = 100g, \Omega = 5g, N = 50, \delta_c = -100.55g$  and the decay rates  $\kappa$  and  $\Gamma$  are set to zero. Here  $\delta_b = 100.5g$ . The oscillatory behaviour for the curves is due to non-resonance condition  $\delta_c \neq -\delta_b$  (see App. C). The initial state is the vacuum for both modes.

### 3.3 Results: stationary entanglement between matter and light

In this section we study the system dynamics and we identify the regimes in which light and collective atomic modes are efficiently squeezed. We charac-

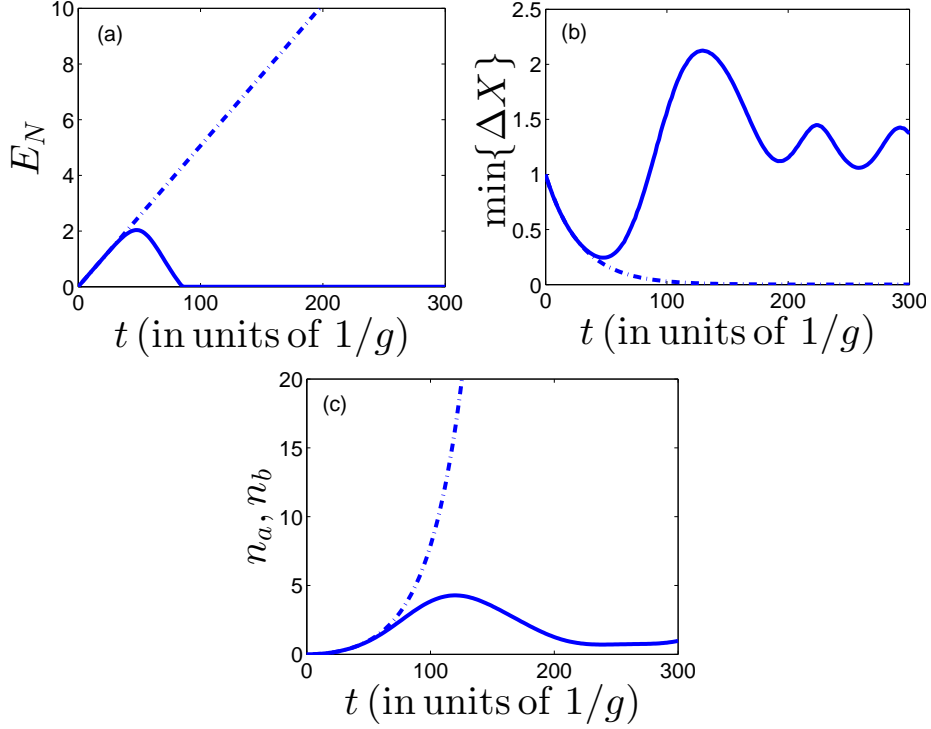


Figure 3.2: The same plots as in Fig. 3.1 with  $\delta_c = -\delta_b = -100.5g$ .

terize the system in terms of the population of the modes, the logarithmic negativity, which measure the entanglement between the two modes (see Appendix D), and the minimum of the variance

$$\Delta X(\theta_a, \theta_b) = \langle X(\theta_a, \theta_b)^2 \rangle - \langle X(\theta_a, \theta_b) \rangle^2, \quad (3.13)$$

with respect to the quadrature angles  $\theta_a$  and  $\theta_b$ , where

$$X(\theta_a, \theta_b) = \frac{1}{\sqrt{2}} \left( a e^{i\theta_a} + a^\dagger e^{-i\theta_a} + b_Q e^{i\theta_b} + b_Q^\dagger e^{-i\theta_b} \right), \quad (3.14)$$

are generic composite quadratures. According to these definitions the shot-noise level is set to  $\Delta X(\theta_a, \theta_b) = 1$ . When  $\Delta X(\theta_a, \theta_b) < 1$  the system is two-mode squeezed [13, 20].

Entanglement and two-mode squeezing are two related features. In fact, in case the Hamiltonian is symmetric under the exchange of the two modes, the quadrature variance  $\Delta X$  can be used to construct entanglement measures [113]. In our case, however the dynamics of the two modes  $a$  and  $b_Q$

### 3.3. Results: stationary entanglement between matter and light<sup>49</sup>

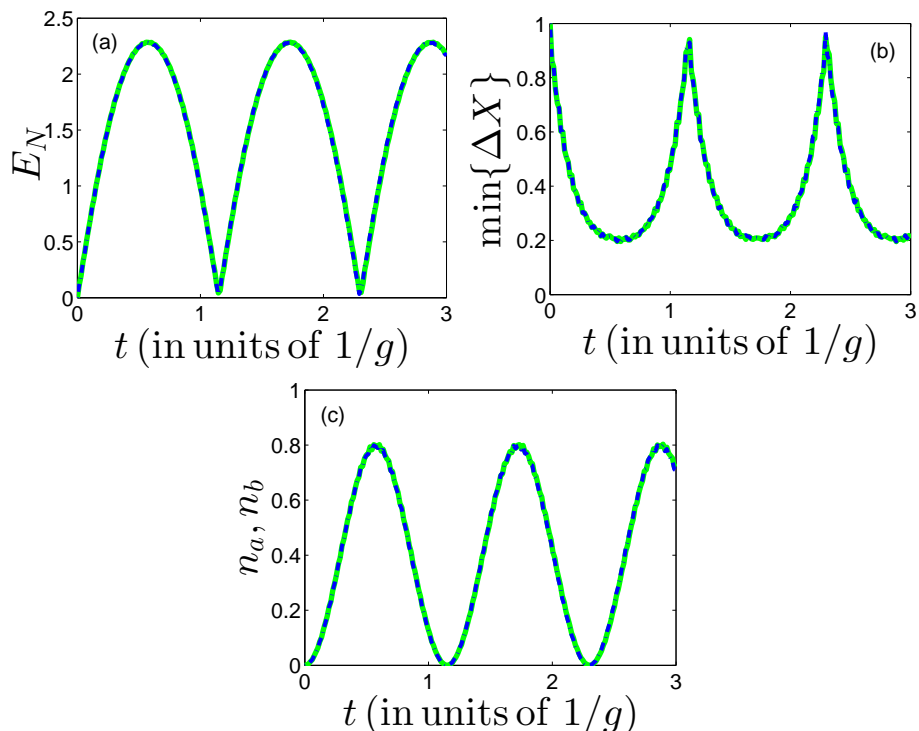


Figure 3.3: The same plots as in Fig. 3.1 with  $\omega_z = 100g, \Omega = 30g, N = 1000, \delta_c = -125g$  and the decay rates  $\kappa$  and  $\gamma$  are set to zero. The corresponding  $\delta_b = 118g$ . Here, due to a large value of  $N$ , the non-quadratic term in (3.7) due to four-wave mixing is negligible.

described by the Hamiltonian (3.7) are not symmetric under the exchange of the modes, and the squeezing is only a sufficient condition for entanglement. For this reason we resort to the logarithmic negativity to detect the entanglement shared by atoms and light.

We first consider the Hamiltonian evolution with no dissipation. The results describe correctly the system dynamics for sufficiently short times such that the effects of dissipation are negligible. We also identify the parameters regime in which the non-quadratic term in the Hamiltonian is negligible.

For a sufficiently large number of atoms  $N$  and small number of excitations, the term proportional to  $\chi$  in Eq. (3.7) is negligible. In this case, the Hamiltonian is quadratic in the field operators. The system dynamics can be determined by studying the normal modes. These can be found diagonalizing the matrix of coefficient of the Heisenberg equations for the field modes (see App. C). When the corresponding eigenvalues are purely imagi-

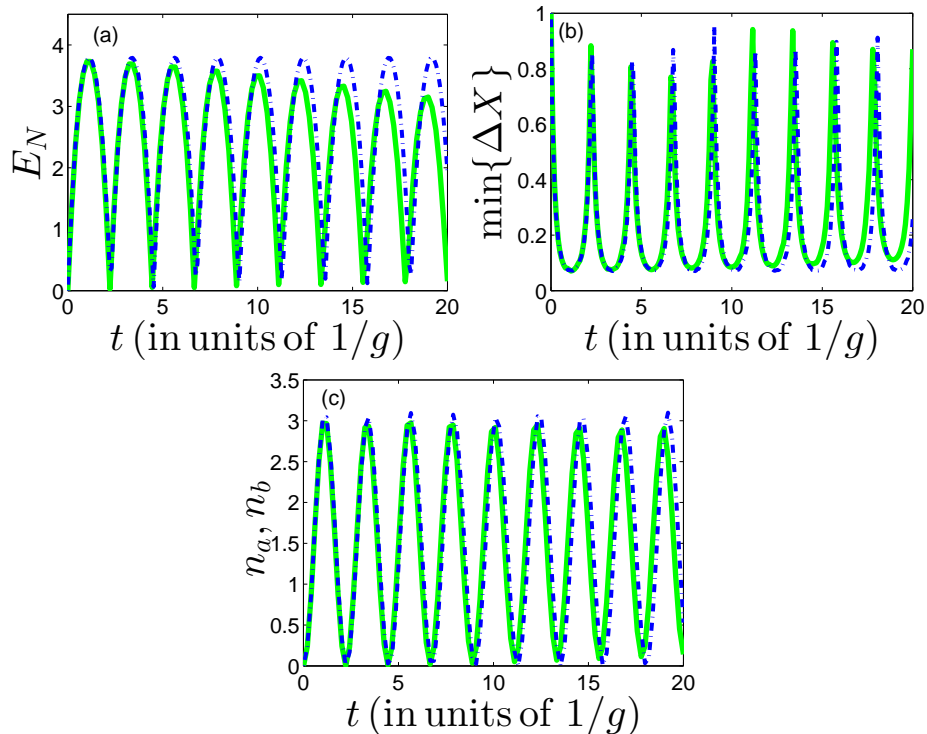


Figure 3.4: The same plots as in Fig. 3.3, but with  $\delta_c = -123.3g$ . The populations of the two-modes get larger with respect to Fig. 3.3 and hence for larger time, the effect of the four-wave mixing gets relevant in the dynamics.

nary the populations of the two modes oscillate in time and remain always finite. If on the other hand the eigenvalues are complex with a finite real part then the population of spin and cavity modes increases with time. This second regime is accessed when  $\delta_c = -\delta_a$  (see App. C). In this case, when the population become sufficiently large then the four wave mixing term, whose strength is  $\chi$ , become relevant. It leads to a shift of the resonance condition, hence to a reduction of the absorption of laser photons. Correspondingly the populations of the spin modes and of the cavity field remain finite.

In Figs. 3.1 and 3.2 we consider parameters regime for which the non-quadratic term in (3.7) has a significant effect in the dynamics. In Fig. 3.1 the detuning  $\delta_b$  is not resonant with  $-\delta_c$ , whereby for Fig. 3.2 we choose  $\delta_b = -\delta_c$ . Panels (a) display the logarithmic negativity (3.4) as a function of time which is evaluated by the Schrödinger equation using the Hamiltonian (3.7). The logarithmic negativity is calculated in terms of the covariance matrix as discussed in App. D. In Fig. 3.1(a), for which  $\delta_c \neq -\delta_b$ , the eigen-

### 3.3. Results: stationary entanglement between matter and light<sup>51</sup>

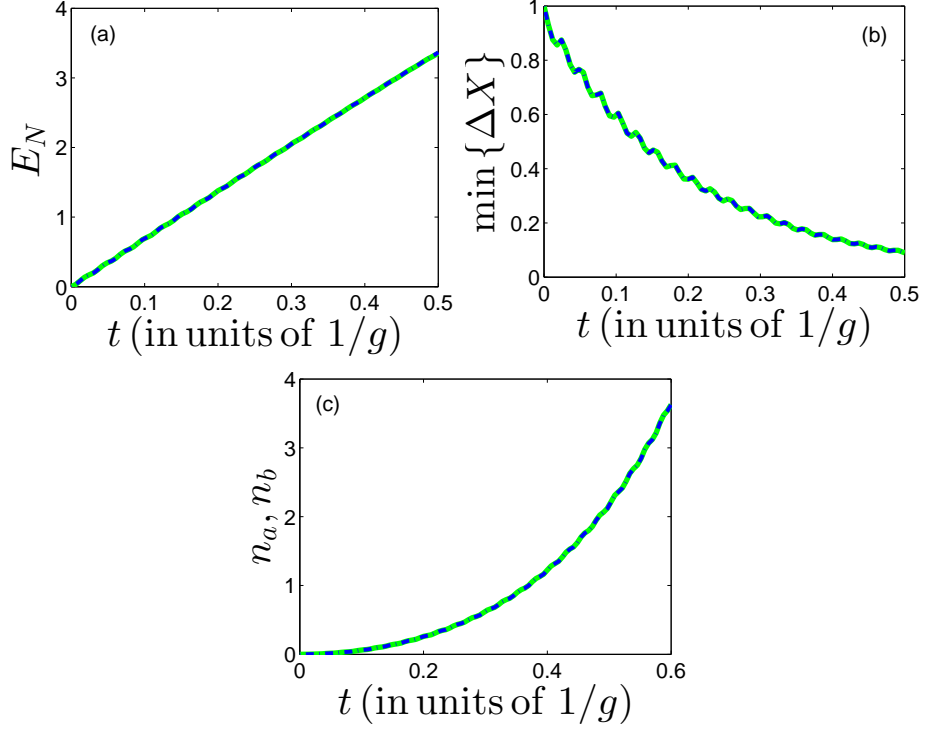


Figure 3.5: The same plots as in Fig. 3.3 with  $\delta_c = -120g$ . The populations increase in a smaller time-scale than Fig. 3.4.

values of the Hamiltonian (3.7) are imaginary (see App. C) and therefore the logarithmic negativity oscillates as a function of time. The similar oscillating behaviors are observed in Figs. 3.1(b),(c). Panel (b) displays the minimum variance of composite quadratures defined in (3.13) with respect to the angles  $\theta_a$  and  $\theta_b$ . We see in (b) that a squeezed composite quadrature with  $\Delta X < 1$  is found, when the two modes are entangled, i.e.,  $E_N > 0$ . The populations of the cavity and the spin-wave modes are shown in (c): As time  $t$  goes, the populations of the two modes increase, and therefore the effect of the non-quadratic term becomes relevant. In these figures the initial state is the vacuum for both modes. In Figs. 3.1 the oscillations of the populations and correspondingly of the entanglement and of the squeezing increase in intensity when the four-wave mixing (non-quadratic) term is neglected, meaning that photons are more efficiently pumped into the system. In Fig. 3.2, the populations increase under the effect of the quadratic Hamiltonian (dash-dotted lines). However, the non-quadratic term is responsible for the reduction of the populations and correspondingly of the two-mode

squeezing (solid lines). In particular, in this limit, at large times the spin-wave and the cavity modes, under the effect of coherent dynamics, result to be not entangled.

The system parameters can be chosen such that the effect of non-quadratic term is not relevant in the dynamics. In Figs. 3.3, 3.4 and 3.5, for the parameters and the time interval that we are able to simulate <sup>2</sup>, the effect of the non-quadratic term is negligible. We show in Figs. 3.3 and 3.5 that for a chosen parameters, there is no discrepancy for the curves with and without the non-quadratic term of the Hamiltonian (3.7). In the oscillating regime, in Fig. 3.4, when the population is not very small and the time is large then a small discrepancy between the results with and without the non-quadratic term is observed. When the non-quadratic term is negligible (see Fig. 3.5) we observe almost perfect suppression of the quadrature fluctuation for large times.

We include now the decay rates in the dynamics and consider the parameters regime in which the four-wave mixing term in Eq. (3.7) is negligible. The dynamics is therefore Gaussian and we can evaluate the results according to Appendix C. Including dissipation, the system dynamics, is characterized by two regimes determined by the relative strength of coherent and incoherent processes. At sufficiently large decay rates, the system admits a steady state. Below threshold values for the decay rates, no steady state is reached. Here we are interested in the steady state of the system. Similar to a non-degenerate parametric oscillator, when the decay rates approach the threshold values, the variance of a composite quadrature is reduced of  $\sim 50\%$  below the shot-noise limit, and correspondingly, the two-mode squeezing spectrum of the emitted field (i.e. the field lost by the cavity and the field scattered by the atoms out of the cavity) shows almost perfect suppression of the quadrature fluctuation at the central frequency [18, 19]. We obtain the steady-state solution by the master equation (3.10) in Figs. 3.6-3.9 when the dissipations are included. Figs. 3.6 and 3.7 display the steady-state solution as a function of the decay rates  $\kappa$  and  $\Gamma$  above the steady-state threshold. The vertical dotted lines indicate the threshold values for the decay rates which separate the two regimes. At smaller values of the decay rates, the system admits no steady state. In Fig. 3.6 maximum values of the population of

---

<sup>2</sup>At larger time the populations in Fig. 3.5 become to large and out of our numerical capabilities.

### 3.3. Results: stationary entanglement between matter and light<sup>53</sup>

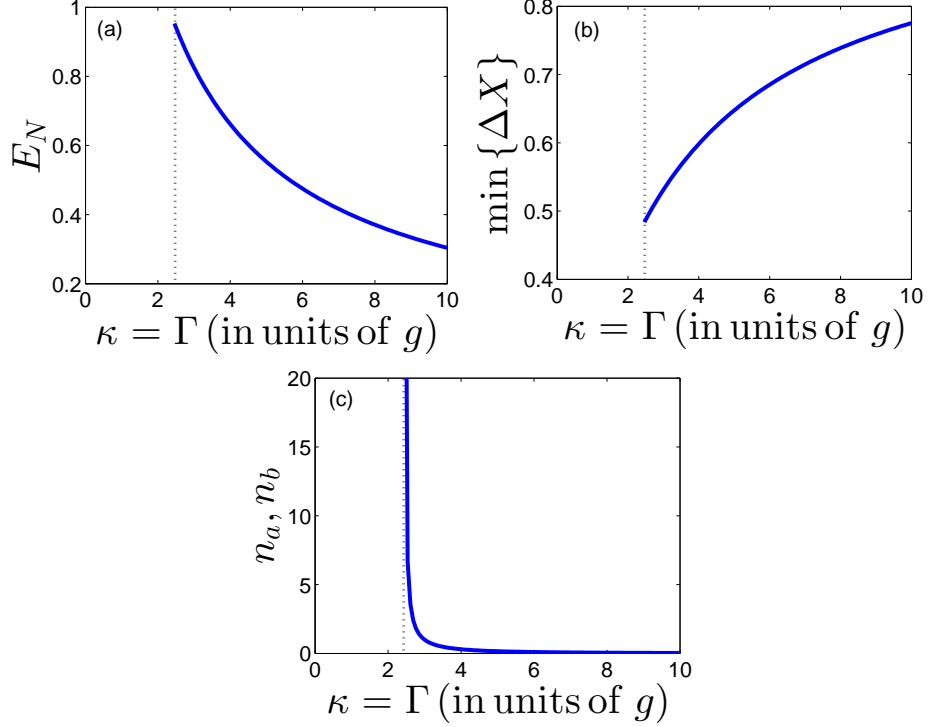


Figure 3.6: (a) Logarithmic negativity  $E_N$  is plotted at the steady state as a function of the decay rates  $\kappa = \Gamma$  in units of  $g$ . In (b) the minimum variance of a composite quadrature  $\min\{\Delta X(\theta_a, \theta_b)\}$  (see Eq. (3.13)) with respect to the angles  $\theta_a$  and  $\theta_b$  at the steady states is evaluated, whereby in (c) the corresponding populations of the field modes  $n_a = \langle a^\dagger a \rangle$  and  $n_b = \langle b_Q^\dagger b_Q \rangle$  (the two curves are superimposed) are shown as a function the decay rates  $\kappa = \Gamma$  (in units of  $g$ ). Note that here the two decay rates are varied together. The dotted lines determine the threshold for the steady state. The results are evaluated using the master equation (3.10) with  $\chi = 0$ . The parameters are  $\omega_z = 100g, \Omega = 30g, N = 1000, \delta_c = -\delta_b = -118g$ .

the two modes (plots (c)), and corresponding maximum entanglement (plot (a)) and squeezing (plots (b)) are obtained at the threshold. The minimum variance is  $\min\{\Delta X(\theta_a, \theta_b)\}$  is slightly smaller than 0.5 (in the case of a non-degenerate parametric oscillator at the threshold it is exactly 0.5). This discrepancy is due to the spin-mode squeezing amplitude  $\alpha_Q$  in the Hamiltonian (3.7). In Fig. 3.6  $\kappa = \Gamma$  and the two decay rates are varied together. On the other hand in Fig. 3.7  $\kappa$  is kept fixed. In this case maximum squeezing and entanglement is not obtained at the threshold. In general optimum two-mode squeezing is obtained when the two decay rates are equal. Fig. 3.8

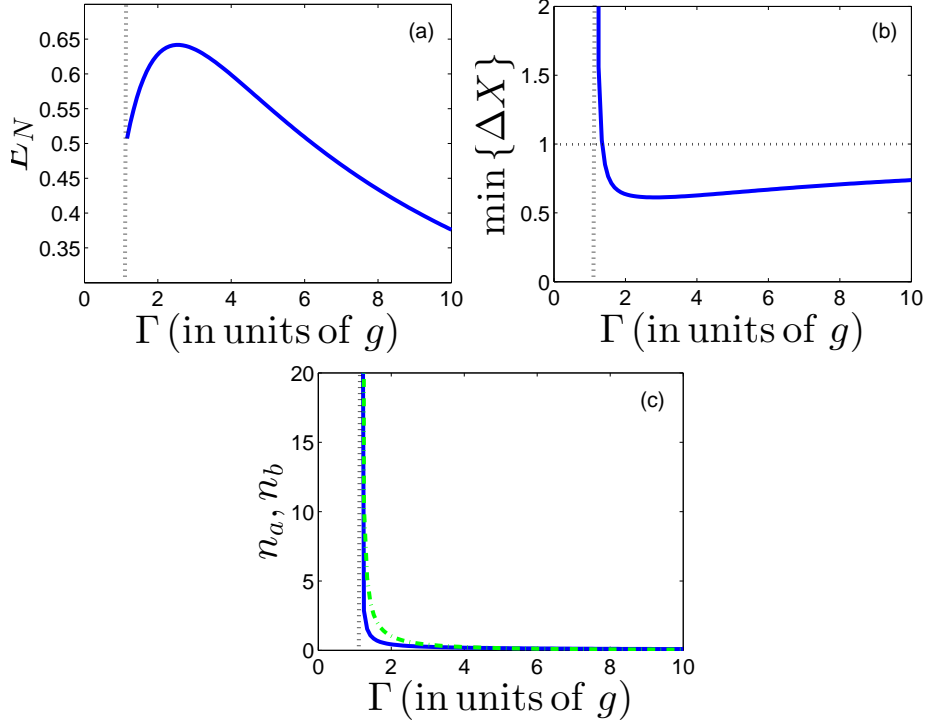


Figure 3.7: The same plots as in Fig. 3.6 with  $\kappa = 5g$ . In (c) the populations for the two modes are not equal and the two curves are not superimposed: the dark blue lines represent  $n_a$  and the light green lines represent  $n_b$ . Note that here, close the threshold value, the two-modes are entangled but the composite quadrature is not squeezed.

shows that maximum populations and entanglement, is obtained when the resonance condition  $\delta_c = -\delta_b$  is satisfied. At last, in Fig. 3.9 one observes that the two mode squeezing increases with the number of atoms  $N$ . The parameters used for this results are similar to that of recent CQED experiments. In particular  $g, \kappa$ , and  $\Gamma$  in Fig. 3.9 correspond to that discussed in [24–26]:  $(g, \kappa, \Gamma)/2\pi \simeq (0.4, 1, 3)$  MHz.

The field emitted by the cavity and the field scattered by the atoms out of the cavity are entangled as well. The squeezing spectrum for composite output fields read

$$S(\theta_a, \theta_b, \omega) = \lim_{\delta_\omega \rightarrow 0} \int_{-\omega - \delta_\omega/2}^{-\omega + \delta_\omega/2} d\omega' \widetilde{\Delta X}^{(\theta_a, \theta_b)}(\omega, \omega'), \quad (3.15)$$

### 3.3. Results: stationary entanglement between matter and light<sup>55</sup>

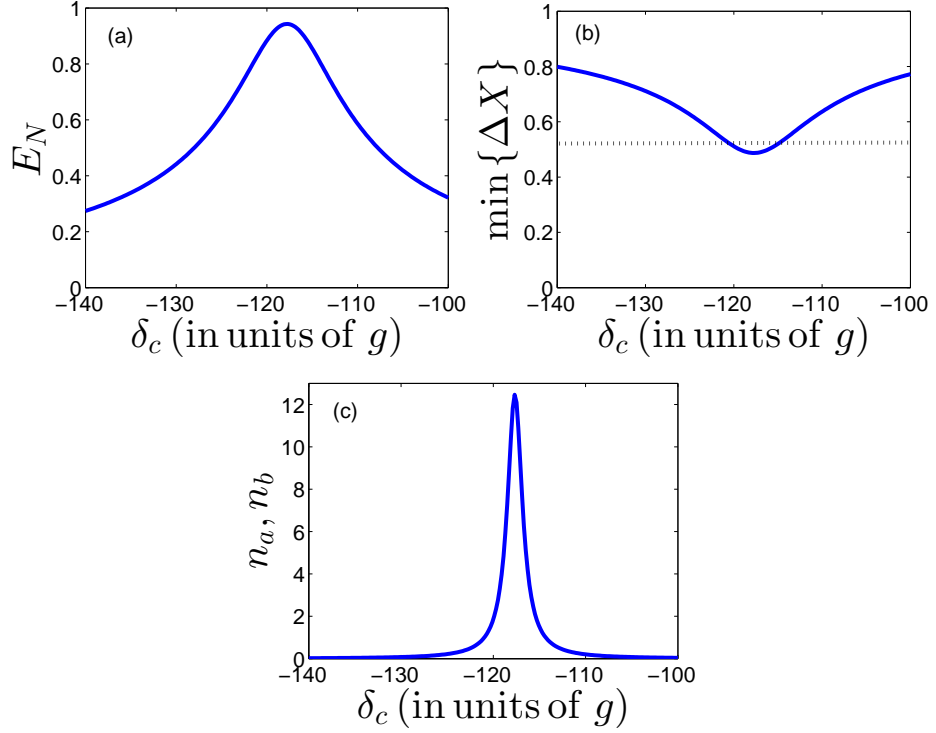


Figure 3.8: The same plots as in Fig. 3.6, as a function of  $\delta_c$  (in units of  $g$ ) for  $\kappa = \Gamma = 2.5g$ . In panel (b), the minimum variance shows more than 50% reduction of the noise, which is due to the single-mode squeezing amplitude  $\alpha_Q$  in (3.7).

where  $\widetilde{\Delta X}^{(\theta_a, \theta_b)}(\omega, \omega')$  are the Fourier transform of the variance of composite quadratures (3.14) and are derived rigorously in App. E. It is shown in Fig. 3.10 that maximum entanglement and almost perfect suppression of the fluctuations are expected at zero frequency, for the parameters of Fig. 3.8. These predictions can be tested in experiments by homodyne detections (see App. E) [20]. When the detection efficiency is not unit, the squeezing and the entanglement of the detected modes are reduced as described by the dashed and dot-dashed lines of Fig. 3.10. In case of asymmetric detection efficiency (dot-dashed lines of Fig. 3.10) the detected fields are not symmetric and the corresponding squeezing is not maximum at the central frequency. Nevertheless the amount of entanglement as measured by the logarithmic negativity is always maximum at the  $\omega = 0$ .

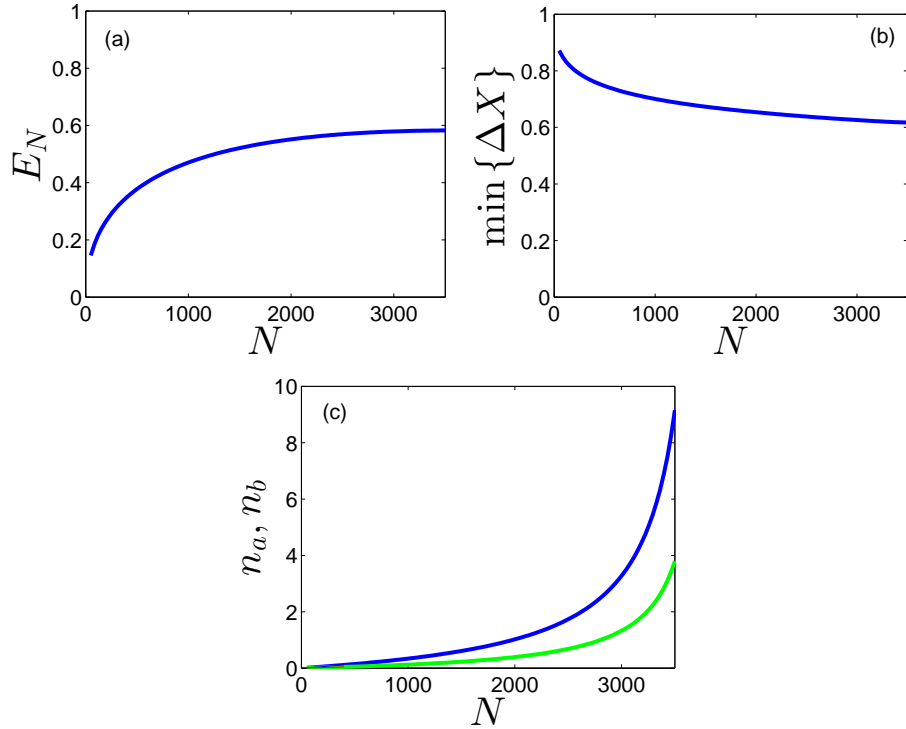


Figure 3.9: The same plots as in Fig. 3.6, as a function of the number of atoms  $N$  for  $\kappa = 2.5g$  and  $\Gamma = 7.5g$ . In (c) the dark blue lines represent  $n_a$  and the light green lines represent  $n_b$ .

### 3.4 Summary and outlook

In this Chapter we have studied the dynamics of an array of atoms inside an optical cavity transversally driven by a laser field and we have identified the regimes in which an atomic spin wave mode and the cavity field mode are efficiently two-mode squeezed.

Two-photon scattering processes in which one laser photons is absorbed or emitted by the collective atomic spin, and the other one is scattered into the cavity or form the cavity field, can be selected resonantly when the laser field drives the system at the intermediate frequency between cavity and atomic transition frequencies. In this regime the system behaves as a non-degenerate parametric oscillator, where the roles of signal and idler are played by the cavity mode and by the spin-wave mode of the atomic array. In this way EPR-like correlations are created between atom and light. Spin-light entanglement can be obtained either at the steady state, or in a

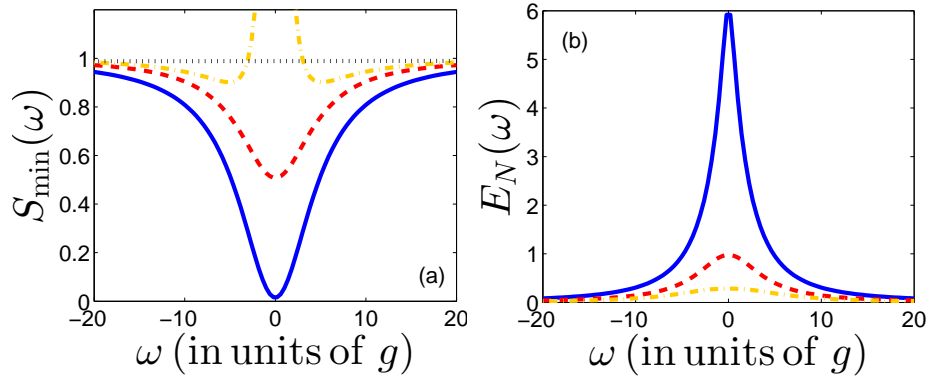


Figure 3.10: (a) Two-mode squeezing spectrum of the emitted fields is evaluated for maximally squeezed composite quadratures  $\widetilde{\Delta X}^{(\theta_a, \theta_b)}$  in Eq (3.15) with respect to the angles  $\theta_a$  and  $\theta_b$  (for details see App. E). (b) Corresponding logarithmic negativity  $E_N(\omega)$  as a function of the frequency of the emitted field, is plotted (see App. E). Different curves correspond to the results for the fraction of modes which are detected when the detection efficiencies  $\eta_a$  and  $\eta_b$  (see App. E) are set to:  $\eta_a = \eta_b = 1$  for the blue solid lines,  $\eta_a = \eta_b = 0.5$  for the red dashed lines and  $\eta_a = 1, \eta_b = 0.1$  for the yellow dot-dashed lines. The parameters are  $\kappa = \Gamma = 2.5g$ ,  $\omega_z = 100g$  and  $\delta_c = -\delta_b = -118g$  and  $\Omega = 30g$ ,  $N = 1000$ ;  $\theta_a$  and  $\theta_b$  are set to the values which mainimizes the squeezing spectrum at each frequency  $\omega$ .  $\Delta_a$  and  $\Delta_b$  (see App. E) are set to the frequencies of the normal modes:  $\Delta_a = -\Delta_b = -121.3g$ .

transient regime. We note that steady state entanglement involving collective atomic spins have been discussed and experimentally demonstrated in Refs. [108, 116]. In Ref. [108] it is shown that for an infinite optical depth of the atomic sample, complete suppression of the collective spin fluctuations can be achieved. For reasonable optical depth ( $\sim 30$ ) the expected optimal suppression is  $\sim 50\%$  below the fluctuations of a coherent spin state. These dynamics, although of different nature is comparable with the steady state reduction of quadrature fluctuation that we have demonstrated in our system.

Finally we note that the atom-cavity system has a potential application to generate an atomic spin-squeezed state at the steady state using a so-called quantum bath engineering [27]. This system can be more robust against noise as compared to existing methods [22] that produce short-lived spin-squeezed states, which can be destroyed due to dissipation or decoherence.

|         |
|---------|
| PART II |
|---------|

Quantum ground state of  
atoms due to cavity backaction



---

# Quantum ground state of ultracold atoms in a cavity

---

Bragg diffraction is a manifestation of the wave-properties of light and a powerful probe of the microscopic structure of a medium: Bragg peaks are intrinsically related to the existence of spatial order of the scatterers composing a medium and provide a criterion for the existence of long-range order [6]. Bragg diffraction of light by atoms in optical lattices has been measured for various geometries and settings, from gratings of laser-cooled atoms [69, 117–120] to ultracold bosons in the Mott-Insulator (MI) phase [121]. In most of these setups the backaction of light on the atomic medium, due to the mechanical effects of atom-photon interactions, is usually negligible, while photon recoil can give rise to visible effects in the spectrum of the diffracted light [92]. Recent work proposed to use high-finesse optical resonators to enhance light scattering into one spatial direction, increasing the collection efficiency and thereby suppressing diffusion related to photon scattering [4]. As it is discussed in Chapter 2, for appropriate geometries, properties of the medium’s quantum state can be revealed by measuring the light at the cavity output [4, 92]. These proposals assume that backaction of the cavity field on the atoms can be discarded. Such an assumption is, however, not valid in the regime considered in Refs. [28, 30–35, 39, 55]: Here, the strong coupling between cavity and atoms can induce the formation of stable Bragg gratings in cold [28, 31, 32] and ultracold atomic gases [30, 33–35, 39, 55] that coherently scatter light from a transverse laser into the cavity mode. When the intensity of the pump exceeds a certain threshold, the atoms organize themselves such that the collective scattering into the cavity is enhanced [29–33]. At ultralow temperatures the self-organized medium is a

supersolid [33, 39], while for larger pump intensities incompressible phases are expected [40].

In Chapter 2, 3 we have studied the dynamics of ultracold atoms in an array interacting with a mode of an optical cavity, when the geometry is such that the photons are pumped into the cavity via incoherent processes. In this Chapter we include the atomic motion and we study the quantum ground state properties of the medium inside the cavity. More specifically, we focus on a regime in which the effect of cavity backaction on the atomic state provides coherent emission into the cavity. We show that the cavity backaction provides an effective long-range interaction between the atoms and can substantially modify the quantum ground state.

In Section 4.1 we give some basics of the Bose-Hubbard model, which will be the starting points of our physical model. In particular, we will review the basics of the MI to superfluid (SF) phase transition, which we will partly recover in our analysis. Starting from Sec. 4.2, we obtain the effective dynamics of trapped atoms inside an optical cavity in presence of cavity backaction, which can be described by the Bose-Hubbard Hamiltonian, and we discuss the quantum ground state properties of this system.

## 4.1 Bose-Hubbard model and disorder

Let us consider ultracold bosonic atoms which are trapped by a two-dimensional optical lattice as shown in Fig. 4.1. The two-dimensional optical lattice is generated by counterpropagating laser fields along two orthogonal directions in a two-dimensional plane. A conceptually simple model that gives an approximate physical description for ultracold bosonic atoms trapped by an optical lattice, and interacting via  $s$ -wave scattering, is the Bose-Hubbard model [122, 123] and is described by the Hamiltonian

$$\mathcal{H} = \frac{U}{2} \sum_i \hat{n}_i(\hat{n}_i - 1) - \sum_i \mu_i \hat{n}_i - t \sum_{\langle i,j \rangle} (\hat{b}_i^\dagger \hat{b}_j + \text{H.c.}) \quad (4.1)$$

in which  $U > 0$  is a repulsive onsite interacting strength between the bosonic particles, and  $\hat{n}_i = \hat{b}_i^\dagger \hat{b}_i$  is the bosonic number operator where  $\hat{b}_i$  ( $\hat{b}_i^\dagger$ ) annihilates (creates) a boson at lattice site  $i$ . The onsite energy  $\mu_i = \mu + \delta\mu_i$  in which  $\mu$  is a chemical potential and  $\delta\mu_i$  is an energy offset of each lattice site. The tunneling rate  $t$  in (4.1), which is determined by the atomic ki-

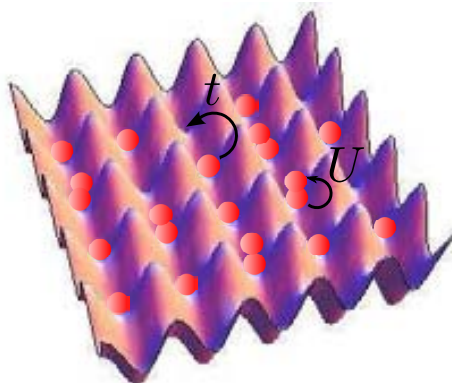


Figure 4.1: Ultracold atoms in a two-dimensional optical lattice which is generated by two counterpropagating laser strongly confined in the third dimension.

netic energy, has been considered only over the neighbor lattice sites  $i$  and  $j$  (denoted by  $\langle i, j \rangle$ ). In fact due to the tight-binding approximation, tunnelings to next-nearest neighbors can be neglected [124]. For ultracold atoms trapped by an optical lattice, the tunneling rate can be tuned by the lattice potential depth: The deeper the lattice potential, the smaller the tunneling rate's is [123, 124].

The quantum ground state properties of the Bose-Hubbard Hamiltonian (4.1) have been first studied by Fisher *et al.* in Ref. [125] using mean-field approach, and have been discussed in other seminal works in the literature (for a review, see [124]). In the spatial homogeneous case when there is no energy offset between different lattice sites, i.e.,  $\mu_i = \mu, \forall i$ , and in the limit of zero tunneling  $t/U \rightarrow 0$ , the ground state of the Bose-Hubbard Hamiltonian at commensurate atomic densities  $\bar{n} = 0, 1, 2, \dots$  are MI states [124]

$$|\Psi_{\text{MI}}(\bar{n})\rangle = \prod_{i=1}^K \frac{(\hat{b}_i^\dagger)^{\bar{n}}}{\sqrt{\bar{n}!}} |0\rangle \quad (4.2)$$

for a lattice with  $K$  sites, where  $|0\rangle$  denotes the vacuum state. The MI state is gapped, meaning that adding or removing a particle to this state costs energy. The compressibility defined by  $\chi = \frac{\partial \bar{n}}{\partial \mu}$ , vanishes for the MI state. As the tunneling  $t$  increases, the atoms start to delocalize over several lattice sites and the system encounters a phase transition from MI to SF

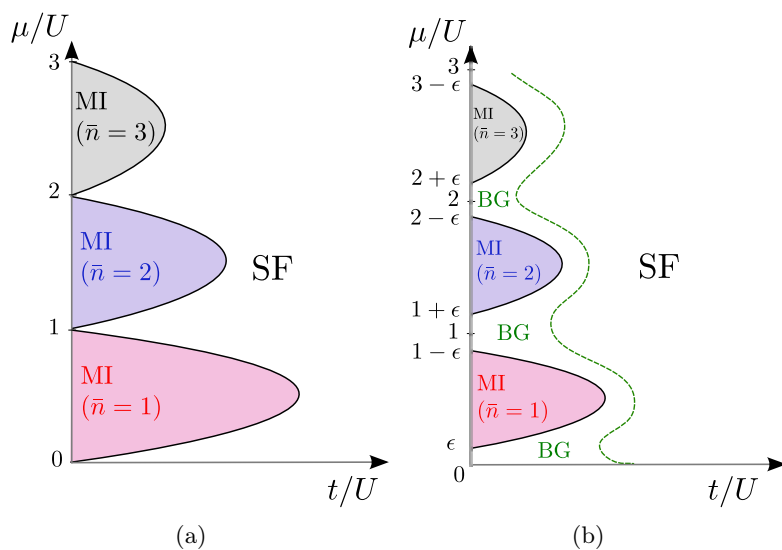


Figure 4.2: Qualitative phase diagram for (a) a pure and (b) a disordered system (with a random disorder) described by the Bose-Hubbard Hamiltonian (4.1). In (a) MI lobes with integer densities  $\bar{n} = 1, 2, 3$  for low values of the tunneling and SF for larger values of tunneling are shown, whereby in (b) the MI-SF transition passes through the BG phase. Here  $\epsilon = \max |\mu_i|/U$  which is zero when there is no energy offset at different lattice sites. Solid lines indicate phase transition from MI to compressible phases, and dashed lines separate insulator phases from SF. The phase transition points highly depend on a lattice dimensionality, and a method used to be obtained.

at certain values of  $t/U$  and  $\mu$ . In the limit of vanishing onsite interaction,  $U/t \rightarrow 0$ , the ground state of the Bose-Hubbard Hamiltonian is SF and has a form [124]

$$|\Psi_{\text{SF}}(\bar{n})\rangle = \frac{1}{\bar{\mathcal{N}}} \left( \sum_{i=1}^K \hat{b}_i^\dagger \right)^N |0\rangle \quad (4.3)$$

with the number of atoms  $N$  and the normalization factor  $\bar{\mathcal{N}}$ . The transition to SF is accompanied by a change in the excitation energy spectrum of the system, where in the SF the system becomes gapless and compressible. In the intermediate region between the states introduced in (4.2), (4.3) there is a value of  $t/U$  at any specific  $\mu$ , for which a phase transition occurs, which has been observed in experiments for optical lattices [126, 127]. The superfluidity in two- and three-dimensions is characterized by nonvanishing values of SF density [124], or SF order parameter  $\sum_i \langle \hat{b}_i \rangle / K$ . The diagram of Fig. 4.2 shows the distinct phases in the thermodynamic limit at equilibrium. Depending on the values of  $t$ ,  $U$  and the chemical potential  $\mu$ , the particle density  $\bar{n}$  varies, and the system ground state is either MI or SF. Fig. 4.2(a) displays the phase diagram of the Bose-Hubbard Hamiltonian (4.1) when  $\mu_i = \mu, \forall i$ , as a function of the chemical potential  $\mu$  versus the tunneling  $t$  in units of the onsite interaction  $U$ . One observes that a lobe structure appears for the MI states with integer densities  $\bar{n} = 1, 2, 3, \dots$ . Outside the lobes the system is SF. At  $t \rightarrow 0$  MI with a commensurate density  $\bar{n}$  is found for the values of the chemical potential  $(\bar{n} - 1)U < \mu < \bar{n}U$ . As the tunneling increases, the MI phase with a density  $\bar{n}$  gets smaller until vanishing [128], and the phase becomes SF.

In the spatial inhomogenous case for which there is an energy offset between all lattice sites, that is,  $\delta\mu_i \neq \delta\mu_j$  for any two lattice sites  $i, j$ , the onsite energy of the Bose-Hubbard Hamiltonian is disordered over the lattice. The disorder effects the ground state properties of the atomic system. It has been shown that in presence of disorder, the MI-SF phase transition occurs through a Bose-glass (BG) phase with no long-range coherence [125, 129]. In this case the MI regions in the phase diagram shrink according to the amplitude of the disorder  $\epsilon = \max |\mu_i| / U$  (see Fig. 4.2(b)). The BG phase is an insulating phase with vanishing superfluidity, but compressible and gapless which makes it distinguished from the MI and SF.

Disordered potentials for cold atoms can be produced by different ap-

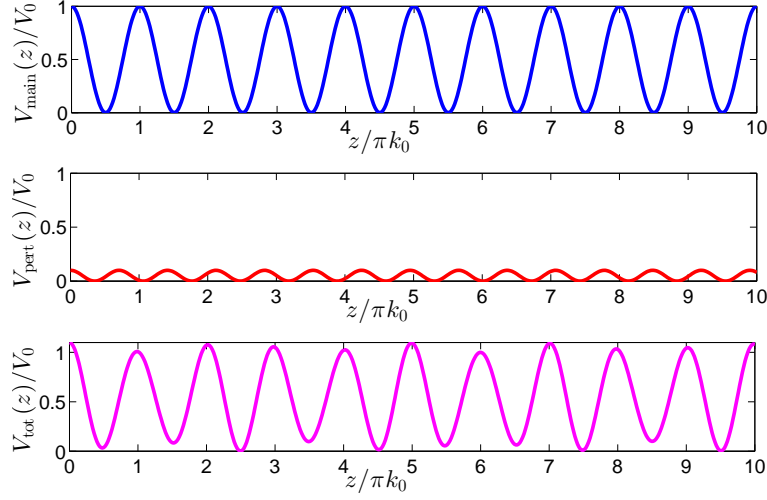


Figure 4.3: The quasi-periodic lattice potential  $V_{\text{tot}}(z) = V_{\text{main}}(z) + V_{\text{pert}}(z)$  which includes a main lattice potential  $V_{\text{main}}(z) = V_0 \cos^2(k_0 z)$  and a perturbative incommensurate lattice with  $V_{\text{pert}}(z) = \frac{V_0}{10} \cos^2(\sqrt{2}k_0 z)$  are plotted. The perturbative potential generates disorder to the main potential.

proaches like speckle patterns [130–132], or bichromatic lattices [45–49]. In this Chapter we discuss the disorder generated by means of incommensurate bichromatic lattices. In the framework of the interacting Bose-Hubbard Hamiltonian (4.1) the phase diagrams obtained by the two different kinds of disorder, i.e., speckle patterns and bichromatic lattices, are qualitatively the same but quantitatively different [48, 49, 133]. As shown in Fig. 4.3 by means of two incommensurate optical lattices in one spatial direction, where one of them is a main lattice and the other one is a perturbation, a quasi-periodic bichromatic optical lattice can be generated. The perturbative lattice potential generates an energy offset  $\delta\mu_i$  to every lattice site of the main optical lattice creating disorder. When the main potential is much deeper than the perturbative potential, the Wannier functions for such a lattice are well-approximated by the ones obtained for the main potential [45, 48]. In the Appendix F we describe how to find the Wannier functions of a periodic potential  $V_{\text{main}}(z)$  shown in Fig. 4.3, which will be used in the following to obtain the parameters of the Bose-Hubbard Hamiltonian.

In the rest of this Chapter we derive the effective Hamiltonian which describes our system dynamics. In particular, we derive the effective Bose-Hubbard Hamiltonian for ultracold atoms trapped by an optical lattice and

interacting with the incommensurate potential of a cavity. The cavity potential is generated by the scattering of light by ultracold atoms into the cavity, and includes the infinitely-ranged cavity potential. We study the BG phase emerging from a disordered Bose-Hubbard Hamiltonian of our system which is here due to the cavity backaction.

## 4.2 Trapped atoms in a cavity: effective dynamics

Following the model introduced in Sec. 1.3, the system we consider is composed by  $N$  ultracold identical atoms of mass  $m$  which obey Bose-Einstein statistics. The atoms are tightly confined by a two-dimensional optical lattice of wave number  $k_0 = 2\pi/\lambda_0$ , with  $\lambda_0$  the wave length, such that the typical length scale is  $d_0 = \lambda_0/2$ . An optical dipole transition of the atoms is driven by a laser and scatters photons into a mode of a high-finesse resonator, according to the geometry shown in Fig. 4.4(a). The resonator field is a standing wave of wave length  $\lambda$  which is incommensurate with the wave length  $\lambda_0$  of the external potential confining the atoms. As discussed in the Chapters 2, 3 when quantum fluctuations can be neglected, i.e., deep in the MI phase of the external potential, the cavity field is in the vacuum. Kinetic energy, on the other hand, induces photon scattering into the cavity field, giving rise to the formation of patterns which maximize scattering into the cavity mode.

In order to provide an appropriate description we consider the Hamiltonian of the system in second quantization, where atomic and field degrees of freedom are described by operators. We derive an effective Hamiltonian for the atomic external degrees of freedom, which can be reduced to a Bose-Hubbard model. This Bose-Hubbard model is the starting point of the numerical investigations in Sec. 4.3.

### 4.2.1 Coherent dynamics

The atoms are prepared in an electronic ground state which we denote by  $|1\rangle$  (see Fig. 4.4(b)). We assume that the atoms are confined on the  $x - z$  plane by an external potential, and motion along the  $y$  axis is frozen out. For an atom at position  $\mathbf{r} = (x, z)$  the external potential reads

$$V_{cl}(\mathbf{r}) = V_0\{\cos^2(k_0z) + \beta \cos^2(k_0x)\}, \quad (4.4)$$

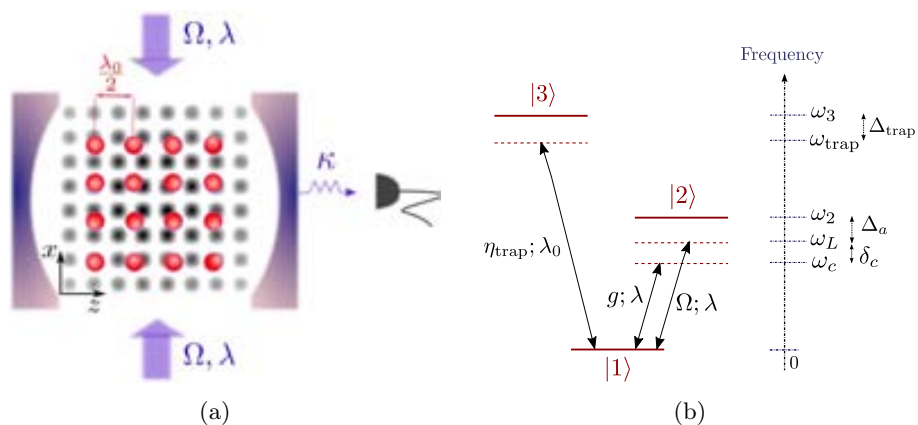


Figure 4.4: (a) Ultracold atoms are tightly confined by an optical lattice of periodicity  $\lambda_0/2$ . They are driven by a weak transverse laser at Rabi frequency  $\Omega$  and strongly coupled to the mode of a standing-wave cavity both at wavelength  $\lambda$ . The level structure of the atoms is shown in panel (b) where the transition between internal levels  $|1\rangle$  and  $|2\rangle$  is driven by the transverse laser which is close to resonance with the cavity mode, while the optical lattice field whose depth is determined by an amplitude  $\eta_{\text{trap}}$  is close to resonance with the atomic transition  $|1\rangle \rightarrow |3\rangle$ . Since  $\lambda$  and  $\lambda_0$  are incommensurate, one would expect no coherent scattering into the cavity mode. The mechanical effects due to multiphoton scattering, however, give rise to an incommensurate quantum potential, which mediates an effective long-range interaction between the atoms and modifies the properties of the quantum ground state. As a result, the intracavity photon number can be large. The corresponding ground state can show features typical of a BG.

where  $V_0$  is the potential depth along the  $z$  direction and  $\beta V_0$  the potential depth along  $x$ . The atoms are at ultralow temperature  $T$  and tightly bound to the potential minima. The quantum gas density also spatially overlaps with the field of an optical resonator: an atomic dipole transition with ground state  $|1\rangle$  and excited state  $|2\rangle$  at frequency  $\omega_0$  couples strongly with a cavity mode at frequency  $\omega_c$ , wave length  $\lambda$ , and wave number  $k = 2\pi/\lambda$  such that the wave vector is along the  $z$  axis. The intracavity field is pumped by the photons that the atoms scatter, when these are driven by a transverse laser at frequency  $\omega_L$  close to  $\omega_c$  such that it has effectively the same wave length  $\lambda$  as the cavity mode. The setup is shown in Fig. 4.4(a).

The coherent dynamics of the cavity field and the atomic internal and external degrees of freedom is governed by Hamiltonian  $\hat{\mathcal{H}}$ , which we decompose into the sum of the Hamiltonian for the cavity, the atoms, and their mutual interaction:

$$\hat{\mathcal{H}} = \hat{\mathcal{H}}_A + \hat{\mathcal{H}}_C + \hat{\mathcal{H}}_{\text{int}}.$$

The Hamiltonian for the cavity mode reads

$$\hat{\mathcal{H}}_C = \hbar\omega_c \hat{a}^\dagger \hat{a}, \quad (4.5)$$

where  $\hat{a}$  and  $\hat{a}^\dagger$  are the annihilation and creation operators of a cavity photon, respectively, and obey the bosonic commutation relation.

The Hamiltonian for the atomic degrees of freedom  $\hat{\mathcal{H}}_A$  (in absence of the resonator) takes the form

$$\begin{aligned} \hat{\mathcal{H}}_A = & \sum_{j=1,2} \int d^2\mathbf{r} \hat{\Psi}_j^\dagger(\mathbf{r}) \hat{H}_j(\mathbf{r}) \hat{\Psi}_j(\mathbf{r}) \\ & + U_{12} \int d^2\mathbf{r} \hat{\Psi}_1^\dagger(\mathbf{r}) \hat{\Psi}_2^\dagger(\mathbf{r}) \hat{\Psi}_2(\mathbf{r}) \hat{\Psi}_1(\mathbf{r}), \end{aligned} \quad (4.6)$$

and is written in terms of the atomic field operator  $\hat{\Psi}_j(\mathbf{r}, t)$ , which destroys an atom in the internal state  $|j = 1, 2\rangle$  at position  $\mathbf{r}$  and time  $t$ , and obeys the commutation relations  $[\hat{\Psi}_i(\mathbf{r}, t), \hat{\Psi}_j^\dagger(\mathbf{r}', t)] = \delta_{ij} \delta(\mathbf{r} - \mathbf{r}')$ . Here,

$$\hat{H}_j(\mathbf{r}) = -\frac{\hbar^2 \nabla^2}{2m} + V_{cl}^{(j)}(\mathbf{r}) + \frac{U_{jj}}{2} \hat{\Psi}_j^\dagger(\mathbf{r}) \hat{\Psi}_j(\mathbf{r}) + \hbar\omega_0 \delta_{j,2}, \quad (4.7)$$

where  $V_{cl}^{(j)}(\mathbf{r})$  is the optical potential of the atoms in state  $j = 1, 2$ , which for the ground state,  $j = 1$ , coincides with  $V_{cl}(\mathbf{r})$  in Eq. (4.4),  $\delta_{j,2}$  is the

Kronecker delta, and  $U_{j,l}$  is the strength of the contact interaction between atoms in states  $j$  and  $l$ , with  $j, l = 1, 2$ .

Finally, the Hamiltonian describing the interaction between the atomic dipoles and the electric fields reads

$$\begin{aligned} \hat{\mathcal{H}}_{\text{int}} = & \hbar g_0 \int d^2\mathbf{r} \cos(kz) \left( \hat{a}^\dagger \hat{\Psi}_1^\dagger(\mathbf{r}) \hat{\Psi}_2(\mathbf{r}) + \text{H.c.} \right) \\ & + \hbar \Omega \int d^2\mathbf{r} \cos(kx) \left( \hat{\Psi}_2^\dagger(\mathbf{r}) \hat{\Psi}_1(\mathbf{r}) e^{-i\omega_L t} + \text{H.c.} \right), \end{aligned} \quad (4.8)$$

where  $g_0$  is the cavity vacuum Rabi frequency, while the term in the second line describes the coherent coupling between the dipolar transition and a standing-wave laser along the  $x$  direction with Rabi frequency  $\Omega$ .

#### 4.2.2 Heisenberg-Langevin equation and weak-excitation limit

Throughout this Chapter we assume that the photon scattering processes are elastic. This regime is based on assuming that the detuning between fields and atoms is much larger than the strength with which they are mutually coupled. The large parameter is the detuning  $\Delta_a = \omega_L - \omega_0$  between the pump and the atomic transition frequency, which is chosen so that  $|\Delta_a| \gg \gamma$ , where  $\gamma$  the radiative linewidth of the excited state, and so that  $|\Delta_a| \gg \Omega, g_0 \sqrt{n_c}$ , namely, the detuning is much larger than the strength of the coupling between the ground and excited state, where,  $n_c = \langle \hat{a}^\dagger \hat{a} \rangle$  is the intracavity photon number. In this regime the population of the excited state is neglected.

Photons are elastically scattered into the resonator when the laser is quasi resonant with the cavity field, which here requires that  $|\Delta_a| \gg |\delta_c|$  with  $\delta_c = \omega_L - \omega_c$ . In this limit the field operator  $\hat{\Psi}_2(\mathbf{r}, t)$  is a function of the cavity field and atomic field operator  $\hat{\Psi}_1(\mathbf{r}, t)$  at the same instant of time according to the relation [40, 93, 94]

$$\hat{\Psi}_2(\mathbf{r}, t) = \frac{g_0}{\Delta_a} \cos(kz) \hat{\Psi}_1(\mathbf{r}, t) \hat{a}(t) + \frac{\Omega}{\Delta_a} \cos(kx) \hat{\Psi}_1(\mathbf{r}, t), \quad (4.9)$$

which is here given to lowest order in the expansion in  $1/|\Delta_a|$ , in the rotating frame of the pump laser. Using Eq. (4.9) in the Heisenberg equation of

motion for the field operator  $\hat{\Psi}_1(\mathbf{r}, t)$  results in the equation

$$\begin{aligned} \dot{\hat{\Psi}}_1 = & -\frac{i}{\hbar}[\hat{\Psi}_1, \hat{\mathcal{H}}_A] \\ & -i\frac{\Omega^2}{\Delta_a}\cos^2(kx)\hat{\Psi}_1 - iU_0\cos^2(kz)\hat{a}^\dagger\hat{\Psi}_1\hat{a} \\ & -iS_0\cos(kz)\cos(kx)\left(\hat{a}^\dagger\hat{\Psi}_1 + \hat{\Psi}_1\hat{a}\right), \end{aligned} \quad (4.10)$$

which determines the dynamics of the system together with the Heisenberg-Langevin equation for the cavity field:

$$\dot{\hat{a}} = -\kappa\hat{a} + i(\delta_c - U_0\hat{\mathcal{Y}})\hat{a} - iS_0\hat{\mathcal{Z}} + \sqrt{2\kappa}\hat{a}_{\text{in}}, \quad (4.11)$$

where  $\kappa$  is the cavity linewidth and  $\hat{a}_{\text{in}}(t)$  is the cavity input noise operator described in Sec. 1.2 and satisfies the relation (1.19). The other parameters are the frequency  $U_0 = g_0^2/\Delta_a$ , which scales the depth of the intracavity potential generated by a single photon, and the frequency  $S_0 = g_0\Omega/\Delta_a$ , which is the Raman scattering amplitude with which a single photon is scattered by a single atom between the cavity and the laser mode [134]. Moreover, in Eq. (4.11) we have introduced the operators

$$\begin{aligned} \hat{\mathcal{Z}} &= \int d^2\mathbf{r} \cos(kz) \cos(kx) \hat{n}(\mathbf{r}), \\ \hat{\mathcal{Y}} &= \int d^2\mathbf{r} \cos^2(kz) \hat{n}(\mathbf{r}), \end{aligned} \quad (4.12)$$

where

$$\hat{n}(\mathbf{r}) = \hat{\Psi}_1^\dagger(\mathbf{r})\hat{\Psi}_1(\mathbf{r}) \quad (4.13)$$

is the atomic density. The operators in Eq. (4.12) count the number of atoms, weighted by the spatial-mode function of the fields and the corresponding intensity. In the limit in which the atoms can be considered point-like, then  $\hat{n}(\mathbf{r}) \approx n_{\text{cl}}(\mathbf{r}) = \sum_j \delta(\mathbf{r} - \mathbf{r}_j)$  and  $\mathcal{Z}_{\text{cl}} = \sum_j \cos(kz_j) \cos(kx_j)$ ,  $\mathcal{Y}_{\text{cl}} = \sum_j \cos^2(kz_j)$ . Hence, when the atoms are randomly distributed in the cavity field potential then  $\mathcal{Z}_{\text{cl}} \rightarrow 0$ , and no photon is elastically scattered into the cavity mode and the cavity field is in the vacuum. This behavior can be also found in the situation we consider in this work, where the atoms are ordered in an array with periodicity which is incommensurate with the periodicity of the pump and cavity standing wave. The focus of this work is

to analyze the effect of cavity backaction on this behaviour.

### 4.2.3 Adiabatic elimination of the cavity field

We now derive an effective Hamiltonian governing the motion of the atoms inside the resonator by eliminating the cavity degrees of freedom from the atomic dynamics. This is performed by assuming that the cavity field follows adiabatically the atomic motion. Formally, this consists in a time-scale separation. We identify the time-scale  $\Delta t$  over which the atomic motion does not significantly evolve while the cavity field has relaxed to a state which depends on the atomic density at the given interval of time. This requires that  $|\delta_c + i\kappa|\Delta t \gg 1$  while  $\kappa_B T \ll \hbar/\Delta t$ , with  $k_B$  Boltzmann constant [40]. Moreover, the coupling strengths between atoms and fields, which determine the time-scale of the evolution due to the mechanical effects of the interaction with the light, are much smaller than  $1/\Delta t$ . In this limit, we identify the "stationary" cavity field operator  $\hat{a}_{\text{st}}$ , which is defined by the equation

$$\int_t^{t+\Delta t} \hat{a}(\tau) d\tau / \Delta t \approx \hat{a}_{\text{st}},$$

such that  $\int_t^{t+\Delta t} \dot{\hat{a}}(\tau) d\tau = 0$ , with  $\dot{\hat{a}}$  given in Eq. (4.11). The "stationary" cavity field is a function of the atomic operators at the same (coarse-grained) time, and in particular takes the form

$$\hat{a}_{\text{st}} = \frac{S_0 \hat{\mathcal{Z}}}{(\delta_c - U_0 \hat{\mathcal{Y}}) + i\kappa} + \frac{i\sqrt{2\kappa} \bar{\hat{a}}_{\text{in}}}{(\delta_c - U_0 \hat{\mathcal{Y}}) + i\kappa}, \quad (4.14)$$

with  $\bar{\hat{a}}_{\text{in}}$  the input noise averaged over  $\Delta t$ . The quantum noise term (second term on the RHS of (4.14)) can be neglected when the mean intracavity photon number is larger than its fluctuations, that corresponds to taking  $|S_0 \langle \hat{\mathcal{Z}} \rangle| \gg \kappa$ . In this limit, similar to the relation (1.21) the field at the cavity output

$$\hat{a}_{\text{out}} = \sqrt{2\kappa} \hat{a}_{\text{st}} - \bar{\hat{a}}_{\text{in}}, \quad (4.15)$$

allows one to monitoring the state of the atoms [4, 13]. Using Eq. (4.14) in place of the field  $\hat{a}$  in Eq. (4.10) leads to an equation of motion for the atomic field operator which depends solely on the atomic variables [40, 93, 94].

#### 4.2.4 Effective Bose-Hubbard Hamiltonian

Denoting the number of lattice sites by  $K$ , a well-defined thermodynamic limit is identified assuming the cavity parameters scale with  $K$  according to the relations  $S_0 = s_0/\sqrt{K}$  and  $U_0 = u_0/K$  [29, 40]. Under the assumption that the atoms are tightly bound by the external periodic potential in Eq. (4.4), we make the single-band approximation and perform the Wannier decomposition of the atomic field operator,

$$\hat{\Psi}_1(\mathbf{r}) = \sum_{i,j} w_{i,j}(\mathbf{r}) \hat{b}_{i,j}, \quad (4.16)$$

with the Wannier function  $w_{i,j}(\mathbf{r})$  centered at a lattice site with coordinate  $(x_i, z_j)$  (with  $x_i = id_0$ ,  $z_j = jd_0$  and  $d_0 = \lambda_0/2$  the lattice periodicity), while  $\hat{b}_{i,j}$  and  $\hat{b}_{i,j}^\dagger$  are the bosonic operators annihilating and creating, respectively, a particle at the corresponding lattice site. The details for evaluation of the Wannier function is given in Appendix F. The decomposition is performed starting from the equation of motion of the atomic field operator, obtained from Eq. (4.10) with the substitution  $\hat{a} \rightarrow \hat{a}_{\text{st}}$ , Eq. (4.14). The details of the procedure are similar to the ones reported in Refs. [40, 93, 94], and are summarized in the following.

We first substitute the cavity field operator (4.14), after neglecting the quantum noise term, into the equation for the quantum field operator in Eq. (4.10). Using the Wannier decomposition, we obtain the equations of motion for operators  $\hat{b}_{l,m}$ , that read

$$\dot{\hat{b}}_{l,m} = \frac{1}{i\hbar} [\hat{b}_{l,m}, \hat{\mathcal{H}}_0 + \hat{\mathcal{H}}_p] - i\hat{\mathcal{C}}_{l,m}, \quad (4.17)$$

where <sup>1</sup>

$$\hat{\mathcal{H}}_0 = \frac{U}{2} \sum_{i,j} \hat{n}_{i,j} (\hat{n}_{i,j} - 1) + (E_0 + V_0 X_0) \hat{N} + (E_1 + V_0 X_1) \hat{B}, \quad (4.18)$$

is the Bose-Hubbard Hamiltonian in the absence of the cavity field and of

---

<sup>1</sup>Note that the Hamiltonian (4.18) is valid for a symmetric tw-dimensional lattice with  $\beta = 1$ , and for a one-dimensional lattice, i.e., when  $\beta \gg 1$ .

the transverse laser, with

$$X_s = \int d^2\mathbf{r} w_{i,j}(\mathbf{r}) [\cos^2(k_0 x) + \beta \cos^2(k_0 z)] w_{i',j'}(\mathbf{r}), \quad (4.19)$$

$$E_s = -\frac{\hbar^2}{2m} \int d^2\mathbf{r} w_{i,j}(\mathbf{r}) \nabla^2 w_{i',j'}(\mathbf{r}), \quad (4.20)$$

such that for  $s = 0$  then  $(i, j) = (i', j')$ , while for  $s = 1$  then  $(i', j')$  is a nearest-neighbour site. The onsite interaction is reduced to

$$U = U_{11} \int d^2\mathbf{r} w_{i,j}(\mathbf{r})^4, \quad (4.21)$$

for which the atoms are in internal ground states. In Eq. (4.18)  $\hat{B} = \hat{B}^x + \hat{B}^z$  is the hopping term, where  $\hat{B}^x = \sum_{i,j} (\hat{b}_{i+1,j}^\dagger \hat{b}_{i,j} + \hat{b}_{i,j}^\dagger \hat{b}_{i+1,j})$  describes tunneling between neighbouring sites of the lattice along  $x$  and  $\hat{B}^z = \sum_{i,j} (\hat{b}_{i,j+1}^\dagger \hat{b}_{i,j} + \hat{b}_{i,j}^\dagger \hat{b}_{i,j+1})$  describes tunneling between neighbouring sites of the lattice along  $z$ . Hamiltonian  $\hat{\mathcal{H}}_p$  contains the terms due to the pumping laser propagating along the  $x$  direction and reads

$$\hat{\mathcal{H}}_p = V_1 \sum_{i,j} J_0^{(i,j)} \hat{n}_{i,j} + V_1 \sum_{i,j} J_1^{(i,j)} \hat{B}_{i,j}^x, \quad (4.22)$$

with  $V_1 = \hbar\Omega^2/\Delta_a$ , where

$$J_0^{(i,j)} = \int d^2\mathbf{r} w_{i,j}(\mathbf{r}) \cos^2(kx) w_{i,j}(\mathbf{r}), \quad (4.23)$$

$$J_1^{(i,j)} = \int d^2\mathbf{r} w_{i,j}(\mathbf{r}) \cos^2(kx) w_{i+1,j}(\mathbf{r}), \quad (4.24)$$

are site-dependent parameters along the  $x$  direction, namely, in the direction of propagation of the transverse field, while it is constant along the  $z$  direction when  $x$  is fixed. Finally, operator  $\hat{\mathcal{C}}_{l,m}$  in Eq. (4.17) is due to the coupling with the cavity field and reads

$$\hat{\mathcal{C}}_{l,m} = S_0 \left( \frac{S_0 \hat{\mathcal{Z}}}{\hat{D}^\dagger} \hat{\mathcal{P}}_{l,m} + \hat{\mathcal{P}}_{l,m} \frac{S_0 \hat{\mathcal{Z}}}{\hat{D}} \right) + U_0 \left( S_0^2 \frac{\hat{\mathcal{Z}}}{\hat{D}^\dagger} \hat{\mathcal{Q}}_{l,m} \frac{\hat{\mathcal{Z}}}{\hat{D}} \right), \quad (4.25)$$

where we have introduced operators  $\hat{D} = (\delta_c - U_0\hat{\mathcal{Y}}) + i\kappa$  and

$$\begin{aligned}\hat{\mathcal{P}}_{l,m} &= [\hat{b}_{l,m}, \hat{\mathcal{Z}}] \\ &\approx Z_{0,0}^{(l,m)}\hat{b}_{l,m} + Z_{0,1}^{(l,m)}\hat{b}_{l,m+1} + Z_{1,0}^{(l,m)}\hat{b}_{l+1,m} \\ &\quad + Z_{1,0}^{(l-1,m)}\hat{b}_{l-1,m} + Z_{0,1}^{(l,m-1)}\hat{b}_{l,m-1}, \\ \hat{\mathcal{Q}}_{l,m} &= [\hat{b}_{l,m}, \hat{\mathcal{Y}}] \\ &\approx Y_0^{(l,m)}\hat{b}_{l,m} + Y_1^{(l,m)}\hat{b}_{l,m+1} + Y_1^{(l,m-1)}\hat{b}_{l,m-1},\end{aligned}\tag{4.26}$$

where

$$\begin{aligned}Y_0^{(i,j)} &= \int d^2\mathbf{r} w_{i,j}(\mathbf{r}) \cos^2(kz) w_{i,j}(\mathbf{r}), \\ Z_{0,0}^{(i,j)} &= \int d^2\mathbf{r} w_{i,j}(\mathbf{r}) \cos(kz) \cos(kx) w_{i,j}(\mathbf{r}),\end{aligned}\tag{4.27}$$

are the overlap integrals due to the cavity optical lattice and the mechanical potential associated with the scattering of cavity photons, respectively. Operator  $\hat{\mathcal{C}}_{l,m}$  cannot be generally cast into the form of the commutator between  $\hat{b}_{l,m}$  and a Hermitian operator. However, in the thermodynamic limit (very large  $K$ ) the term  $\frac{1}{D}$  in (4.25) commutes with  $\hat{b}_{l,m}$  (up to the order of  $1/K$ ), and hence  $\hat{a}_{\text{st}}$  commutes with  $\hat{b}_{l,m}$  when  $U_0/|\delta_c + i\kappa|$  is a small number to allow for an expansion, and one can cast  $\hat{\mathcal{C}}_{l,m} \approx [\hat{b}_{l,m}, \hat{\mathcal{H}}_1/\hbar]$ , where

$$\hat{\mathcal{H}}_1 = \hbar S_0^2 \hat{\mathcal{Z}} \left( \frac{\hat{\delta}_{\text{eff}}}{\hat{\delta}_{\text{eff}}^2 + \kappa^2} \hat{\mathcal{Z}} + \frac{U_0 \hat{\mathcal{Z}}}{\hat{\delta}_{\text{eff}}^2 + \kappa^2} \hat{\mathcal{Y}} \right),\tag{4.28}$$

with  $\hat{\delta}_{\text{eff}} = \delta_c - U_0\hat{\mathcal{Y}}$ . Here the Wannier functions are independent of the cavity mean photon number and therefore the effective Hamiltonian reduces to  $\hat{\mathcal{H}} = \hat{\mathcal{H}}_0 + \hat{\mathcal{H}}_1$ . The effective Hamiltonian  $\hat{\mathcal{H}}$  is reduced to a Bose-Hubbard Hamiltonian which can be cast into the sum of two terms,

$$\hat{\mathcal{H}}_{\text{BH}} = \hat{\mathcal{H}}_0 + \hat{\mathcal{H}}_{\text{BH}}^{(1)},\tag{4.29}$$

where

$$\hat{\mathcal{H}}_{\text{BH}}^{(1)} = \sum_{i,j} \left( \delta\hat{\epsilon}_{i,j} \hat{n}_{i,j} + \delta\hat{t}_{i,j}^x \hat{B}_{i,j}^x + \delta\hat{t}_{i,j}^z \hat{B}_{i,j}^z \right),\tag{4.30}$$

is different from zero when the pump laser is on,  $\Omega > 0$ . Due to the incom-

mensurate wavelength of laser and cavity mode with respect to the lattice spacing, the coefficients of the Hamiltonian  $\hat{\mathcal{H}}_{\text{BH}}^{(1)}$  are site-dependent. The site-dependent onsite energy reads

$$\delta\hat{\epsilon}_{i,j} = V_1 J_0^{(i,j)} + \frac{\hbar s_0^2}{\hat{\delta}_{\text{eff}}^2 + \kappa^2} \hat{\Phi} \left( \hat{\delta}_{\text{eff}} Z_{0,0}^{(i,j)} + u_0 \hat{\Phi} Y_0^{(i,j)} \right), \quad (4.31)$$

while the site-dependent tunneling terms read

$$\begin{aligned} \delta\hat{t}_{i,j}^x &= -2\hbar \frac{s_0^2 \hat{\delta}_{\text{eff}}}{\hat{\delta}_{\text{eff}}^2 + \kappa^2} \hat{\Phi} Z_{1,0}^{(i,j)} - V_1 J_1^{(i,j)}, \\ \delta\hat{t}_{i,j}^z &= \frac{-\hbar s_0^2}{\hat{\delta}_{\text{eff}}^2 + \kappa^2} \hat{\Phi} \left( 2\hat{\delta}_{\text{eff}} Z_{0,1}^{(i,j)} + u_0 \hat{\Phi} Y_1^{(i,j)} \right). \end{aligned} \quad (4.32)$$

Note that the collective operator

$$\hat{\Phi} = \sum_{i,j} Z_{0,0}^{(i,j)} \hat{n}_{i,j} / K, \quad (4.33)$$

appears in the site-dependent parameters which includes a global effect over the whole lattice. In the regime of the parameters we consider (see Sec. 4.2.5) for which  $\max |\langle \delta\hat{\epsilon}_{i,j} \rangle| \sim U$  and  $|V_0| \gg \max |\langle \delta\hat{\epsilon}_{i,j} \rangle|$  (hence the validity of a single-band approximation)  $\delta\hat{t}_{i,j}^x$  and  $\delta\hat{t}_{i,j}^z$  are at least 8 order of magnitude smaller than  $t^{(0)}$ . Therefore the disorder (site-dependent coefficient) is considerable only in the onsite energy  $\delta\hat{\epsilon}_{i,j}$  of the Bose-Hubbard Hamiltonian. Hence the resulting Bose-Hubbard Hamiltonian reads

$$\hat{\mathcal{H}}_{\text{BH}} = - \sum_{\langle i'j', ij \rangle} t^{(0)} (\hat{b}_{i,j}^\dagger \hat{b}_{i',j'} + \hat{b}_{i',j'}^\dagger \hat{b}_{i,j}) + \frac{U}{2} \sum_{i,j} \hat{n}_{i,j} (\hat{n}_{i,j} - 1) + \sum_{i,j} \hat{\epsilon}_{i,j} \hat{n}_{i,j} \quad (4.34)$$

where the  $\langle i'j', ij \rangle$  in the sum denotes the nearest neighbors of the corresponding lattice site. The onsite energy is defined as

$$\hat{\epsilon}_{i,j} = \epsilon^{(0)} + \delta\hat{\epsilon}_{i,j}, \quad (4.35)$$

which the sum of a constant term  $\epsilon^{(0)}$ , and of a term which depends on the

lattice site and is due to the cavity field. In detail, the constant terms read

$$\begin{aligned}\epsilon^{(0)} &= E_0 + V_0 X_0, \\ t^{(0)} &= -E_1 - V_0 X_1.\end{aligned}$$

The terms with  $E_s$  and  $X_s$  given in Eqs. (4.19) are due to the dynamics in absence of the cavity field. The first term in the right-hand side (RHS) of (4.31) is due to the standing wave of the classical transverse pump. The other terms on the RHS of Eq. (4.31) are due to the cavity field, while

$$\hat{\delta}_{\text{eff}} = \delta_c - u_0 \sum_{i,j} Y_0^{(i,j)} \hat{n}_{i,j} / K \quad (4.36)$$

is an operator, whose mean value gives the shift of the cavity resonance due to the atomic distribution [93, 94]. All these terms are multiplied by the operator  $\hat{\Phi}$  defined in (4.33) which is the sum of the atomic density over the lattice mediated by the Raman scattering amplitude.

#### 4.2.5 Discussion

The Hamiltonian we have derived reduces, when the pump is off,  $\Omega = 0$ , to the typical Bose-Hubbard Hamiltonian. The latter exhibits a SF-MI quantum phase transition which is either controlled by changing the potential depth  $V_0$ , and hence the hopping coefficient  $t$ , or the onsite interaction strength  $U$  [122, 124]. In this thesis we assume  $U$  to be constant so that  $t$  is varied by varying the potential depth  $V_0$ .

When the transverse laser drives the cavity field by means of elastic scattering processes, the Hamiltonian depends on the nonlocal operator (4.33), which originates from the long-range interaction between the atoms mediated by the cavity field. The physical observable which is associated with this operator is the cavity field amplitude,

$$\hat{a}_{\text{st}} \approx \frac{S_0 K \hat{\Phi}}{\hat{\delta}_{\text{eff}} + i\kappa}, \quad (4.37)$$

as is visible by using Eq. (4.33) in Eq. (4.14), and after discarding the noise term, assuming this is small. It can be measured by homodyne detection of the field at the cavity output [135]. The intracavity photon number,

$\hat{n}_{\text{cav}} = \hat{a}_{\text{st}}^\dagger \hat{a}_{\text{st}}$ , reads

$$\hat{n}_{\text{cav}} \approx \frac{S_0^2 K^2}{\hat{\delta}_{\text{eff}}^2 + \kappa^2} \hat{\Phi}^2 \equiv K \frac{s_0^2}{\hat{\delta}_{\text{eff}}^2 + \kappa^2} \hat{\Phi}^2, \quad (4.38)$$

and the intensity of the field at the cavity output provides a measurement of operator  $\hat{\Phi}^2$ , where the second expression on the RHS uses the chosen scaling of the cavity parameters with the number of sites. The intracavity photon number vanishes when the atomic gas forms a MI state: In this case  $\langle \hat{\Phi}^2 \rangle_{\text{MI}} \propto (\sum_{i,j} Z_{0,0}^{(i,j)})^2 = 0$ , since there is no coherent scattering into the cavity mode. Also deep in the SF phase  $\langle \hat{\Phi} \rangle_{\text{SF}} \rightarrow 0$ .

It is interesting to note that, using definitions (4.33) and (4.36), Hamiltonian (4.34) can be cast in the form

$$\begin{aligned} \hat{\mathcal{H}}_{\text{BH}} = & - \sum_{\langle i'j', ij \rangle} t (\hat{b}_{i,j}^\dagger \hat{b}_{i',j'} + \hat{b}_{i',j'}^\dagger \hat{b}_{i,j}) + \frac{U}{2} \sum_{i,j} \hat{n}_{i,j} (\hat{n}_{i,j} - 1) \\ & + \sum_{i,j} \epsilon^{(0)} \hat{n}_{i,j} - V_1 \sum_{i,j} J_0^{(i,j)} \hat{n}_{i,j} + \frac{\hbar s_0^2 \delta_c}{\hat{\delta}_{\text{eff}}^2 + \kappa^2} K \hat{\Phi}^2, \end{aligned} \quad (4.39)$$

where we have neglected the site-dependence of the tunneling parameter,  $t \approx t^{(0)}$ , which is a negligible correction. In this form the Bose-Hubbard Hamiltonian depends explicitly on the operator corresponding to the number of intracavity photons, see Eq. (4.38), showing the long-range interacting potential due to the cavity field. This potential either decreases or increases the total energy depending on the sign of  $\delta_c$ : Its sign hence critically determines whether "disordered" (i.e., aperiodic) density distributions are energetically favourable. In particular, when  $\delta_c < 0$ , disordered density distributions are expected when the density is not an integer number. The dependence of the chemical potential on operator  $\hat{\Phi}$  is a peculiar property of our model, that makes it differ from the case of a bichromatic optical lattice [45, 136], in which the strength of the incommensurate potential is an external parameter, independent of the phase of the ultracold atomic gas.

### 4.3 Results

The Bose-Hubbard model of Eq. (4.34) is at the basis of the results of this section. We first consider a one-dimensional lattice along the cavity axis by

taking the aspect ratio  $\beta \gg 1$  in  $V_{cl}(\mathbf{r})$  and briefly discuss the phase diagram which has been evaluated by means of quantum Monte Carlo simulation by André Winter [137]. We then analyse the situation where the atoms are ordered in a two-dimensional optical lattice inside the cavity and determine the phase diagram by using a mean-field approach. In both cases, the phase diagram is found by evaluating the ground state  $|\phi_G\rangle$  of the free-energy, such that it fulfills the relation

$$\min \left\{ \langle \phi_G | \hat{\mathcal{H}}_{\text{BH}} - \mu \hat{N} | \phi_G \rangle \right\}, \quad (4.40)$$

where  $\mu$  is the chemical potential.

In the following the ratio between the typical interparticle distance  $d_0$  and the wave length of the cavity is chosen to be  $d_0/\lambda = 83/157$ , which is close to  $1/2$ . Although this ratio is a rational number, nevertheless, for sufficiently small system sizes (here between 100 and 300 sites per axis) the emerging dynamics simulates the incommensurate behaviour. We remark that, for the chosen number of sites, the number of intracavity photon is zero for pointlike scatterers when the density is uniform. We refer the reader to Refs. [48, 49], where the phase diagram of bichromatic potentials in systems of finite-size is discussed.

The parameters for the cavity field, which determine the coefficients of the Bose-Hubbard Hamiltonian in Eq. (4.34), are extracted from the experimental values  $g_0/2\pi = 14.1$  MHz,  $\kappa/2\pi = 1.3$  MHz, and  $\gamma/2\pi = 3$  MHz for  $^{87}\text{Rb}$  atoms [33, 138]. From these values, after fixing the size of the lattice, we get  $u_0$  and the range of parameters within which we vary the rescaled pump strength  $s_0$ . Finally, the onsite interaction in the one-dimensional case is  $U/\hbar \sim 50$  Hz ( $U_{11}/\hbar = 6.4 \times 10^{-6}$  Hz m) and has been taken from Ref. [139]. For the two-dimensional optical lattice,  $U/\hbar$  varies between 1 and 3 kHz ( $U_{11}/\hbar = 5.5 \times 10^{-11}$  Hz m<sup>2</sup>), see Ref. [140]. A detailed discussion on the validity of Eq. (4.34) for this choice of parameters is reported in Sec. 4.4.

### 4.3.1 One-dimensional lattice

We focus here on atoms confined in the lowest band of a one-dimensional lattice along the cavity axis. For this geometry the first term of the RHS of Eq. (4.31) is a constant energy shift along the cavity axis and can be reabsorbed in the chemical potential. The one-dimensional Hamiltonian can

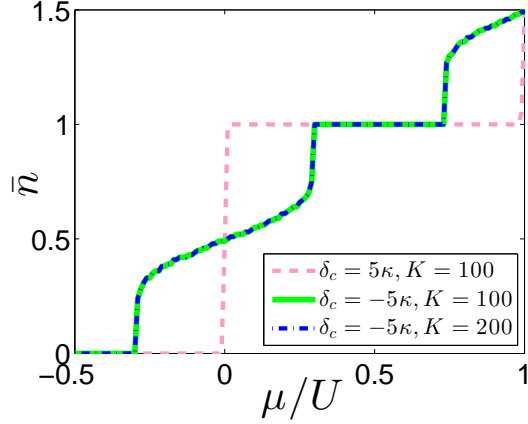


Figure 4.5: Mean density  $\bar{n}$  as a function of the chemical  $\mu$  (in units of  $U$ ) at  $t = 0$  in a one-dimensional lattice. The curves have been obtained by a diagonalization of Hamiltonian (4.41) for (dashed line)  $\delta_c = 5\kappa$  and (solid line)  $\delta_c = -5\kappa$ , both for  $K = 100$ . The diagonalization, is based on the iterative calculation of the evaluating the value of  $\hat{\Phi}$ , which has been treated in a mean-field way, i.e.,  $\hat{\Phi}^2 \approx \langle \hat{\Phi}^2 \rangle + 2\langle \hat{\Phi} \rangle \hat{\Phi}$ . The other parameters are  $s_0 = 0.006\kappa$  (with  $\kappa = 2\pi \times 1.3$  MHz),  $u_0 = 0.8\kappa$ , and  $U/\hbar = 50$  Hz. Here, the chemical potential is reported without the constant shift  $\epsilon^{(0)}$ ,  $\mu \rightarrow \mu - \epsilon^{(0)}$ . The dash-dotted line has been evaluated for the same parameters of the solid line, except with  $K = 200$ . It shows that the results remain invariant as the system size is scaled up.

be thus written as

$$\begin{aligned} \hat{\mathcal{H}}_{\text{BH}}^{(1D)} &= - \sum_{\langle i', i \rangle} t (\hat{b}_i^\dagger \hat{b}_{i'} + \hat{b}_{i'}^\dagger \hat{b}_i) + \frac{U}{2} \sum_i \hat{n}_i (\hat{n}_i - 1) \\ &\quad + (\epsilon^{(0)} - V_1 J_0) \sum_i \hat{n}_i + \frac{\hbar s_0^2 \delta_c}{\hat{\delta}_{\text{eff}}^2 + \kappa^2} K \hat{\Phi}^2, \end{aligned} \quad (4.41)$$

where  $i$  labels the lattice site along the lattice and  $J_0$  is the value of integral (4.23) at the position of one-dimensional lattice. Here, the onsite energy term depends on the sites only through cavity QED effects.

#### 4.3.1.1 Tunneling coefficient $t \rightarrow 0$

We first analyse the case in which the tunneling  $t \rightarrow 0$ , where the atoms are classical pointlike particles localized at the minima of the external potential. We determine the mean density  $\bar{n} = \sum_{i=1}^K \langle \hat{n}_i \rangle / K$  as a function of the chemical potential  $\mu$  by diagonalizing the Hamiltonian (4.41) setting  $t = 0$ . The

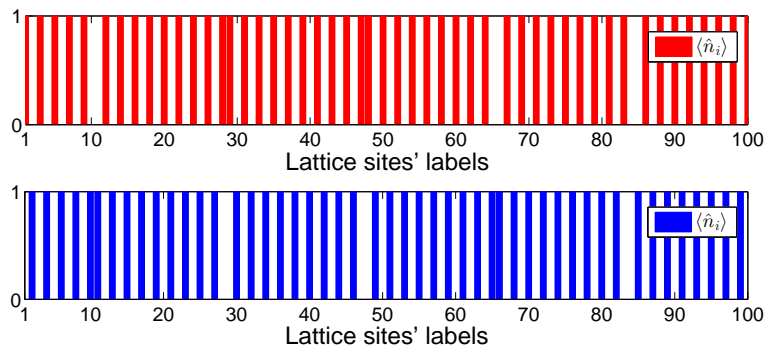


Figure 4.6: Mean density per site,  $\langle \hat{n}_i \rangle$ , as a function of the site  $i$  for the two distributions corresponding to  $\delta_c = -5\kappa$  here for  $\mu = 0$ . The other parameters are the same as in Fig. 4.5. The filled stripes correspond to  $\langle \hat{n}_i \rangle = 1$ , the white stripes to  $\langle \hat{n}_i \rangle = 0$ .

curves for different parameters are shown in Fig. 4.5. The derivative of the curve gives the compressibility  $\chi = \partial \bar{n} / \partial \mu$ .

The two curves in Fig. 4.5 correspond to two behaviours that are determined by the sign of  $\delta_c$  in Eq. (4.41), namely, on whether the laser frequency is tuned to the red or of the blue of the cavity frequency (the parameter choice is discussed in Sec. 4.4). When  $\delta_c > 0$ , for a finite intracavity photon number the cavity-induced interaction energy is positive. Hence, the configurations minimizing the energy are thus the ones with  $\langle \hat{n}_{\text{cav}} \rangle = 0$ , for which Hamiltonian (4.41) reduces to the Bose-Hubbard model for atoms in a periodic potential.

For  $\delta_c < 0$ , on the other hand, the cavity-induced interaction energy is negative. In this case it is energetically favourable that the atomic density organize so to maximize the intracavity field. The interval of values of the incompressible phase at  $\bar{n} = 1$  is reduced, while for fractional densities the compressibility is different from zero and the intracavity field is significantly different from zero. For incommensurate densities, in particular, the quantum ground state is doubly-degenerate. Figure 4.6 displays the density as a function of the lattice site for the case  $\delta_c < 0$  and  $\mu = 0$ , for which  $\bar{n} < 1$ . Each configuration corresponds to either particle occupation at the lattice sites with  $Z_0^{(i,j)} > 0$  (hence  $\langle \hat{\Phi} \rangle > 0$ ) or with  $Z_0^{(i,j)} < 0$  (hence  $\langle \hat{\Phi} \rangle < 0$ ). The two configurations correspond to two phases of the cavity field which differ by  $\pi$ . This behaviour is analogous to the one encountered in selforganization

of ultracold atoms in optical potentials [32,39]. We remark that, while in the system of Ref. [39] the atomic patterns are periodic and maximize scattering into the resonator, here scattering into the cavity is maximized by aperiodic density distributions.

It is interesting to draw a comparison between the results found in our model and the curves predicted for a one-dimensional bichromatic lattice with incommensurate wave lengths [48,49]. For this purpose we display the curves of the density as a function of the chemical potential by substituting the operator  $\hat{\Phi}$  with a scalar in Eq. (4.41) taking the value  $\hat{\Phi} \rightarrow 1/4$ . This choice is made in order to obtain similar curves at commensurate densities  $\bar{n} = 0, 1, 2$  for  $s_0 = 0.004\kappa$ . Figure 4.7(a) displays the corresponding density as a function of the chemical potential for different strengths of the cavity field and  $\delta_c < 0$ . For this case we observe that, by increasing  $s_0$  in the "classical model" (where  $\hat{\Phi}$  is a scalar) the parameter regions for which the gas is incompressible rapidly shrink<sup>2</sup>. This trend is significantly slower for the case in which cavity backaction is taken into account, as can be observed in Fig. 4.7(b). In addition, when cavity backaction is considered, discontinuities in the values of the compressibility are encountered and seem to correspond to the first order phase transition. This behaviour qualitatively differs from the one encountered in Fig. 4.7(a) in which the cavity backaction is artificially removed. For the largest value of the laser intensity here considered,  $s_0 = 0.008\kappa$ , the incompressible phases disappear.

#### 4.3.1.2 Phase diagram for $t > 0$

The results obtained at  $t > 0$  for the one-dimensional lattice are evaluated using a quantum Monte Carlo (QMC) approach [141–143] by André Winter [137]. Here, for the sake of completeness, we mention the main QMC results for a one-dimensional lattice.

In the QMC approach, the phase diagram is extrapolated by tracking the behavior of the density  $\bar{n}$  versus the chemical potential for different tunneling values. Figure 4.8(a) displays the resulting phase diagram in the  $\mu - t$  parameter plane. The grey regions indicate the MI states at densities

---

<sup>2</sup>In Fig. 4.6(a) we do not observe the plateaus with fractional filling, which were instead found in Roux *et al.* [48], which is justified since our parameter regime is different from the one considered in Ref. [48]. We have verified that these plateaus are found in our model by increasing  $s_0 \rightarrow 10s_0$  and  $U \rightarrow 100U$ .

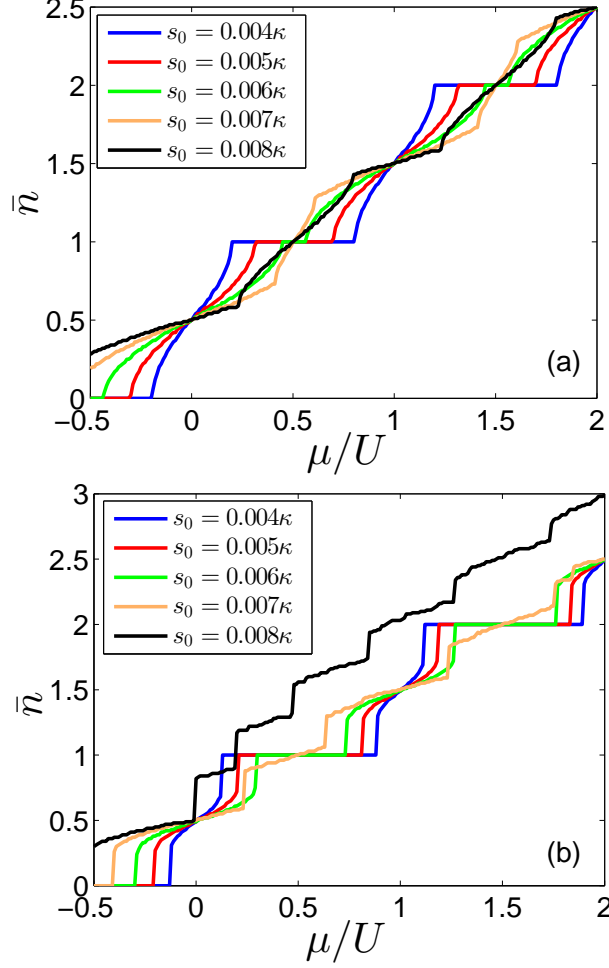


Figure 4.7: Mean density  $\bar{n}$  as a function of  $\mu$  (in units of  $\mu$  for a one-dimensional lattice of  $K = 100$  sites for  $t = 0$ ,  $\delta_c = -5\kappa$ ,  $u_0 = 0.8\kappa$ ,  $U/\hbar = 50$  Hz (with  $\kappa/2\pi = 1.3$  MHz), while the values of  $s_0$  are reported in the legend. The curves in (a) are evaluated by diagonalizing Eq. (4.41) after setting  $\langle \hat{\Phi} \rangle = 1/4$  (i.e., by artificially removing cavity backaction). The curves in (b) are found for the corresponding parameters by diagonalizing the full quantum model of Eq. (4.41). The other parameters are as described in Fig. 4.5.

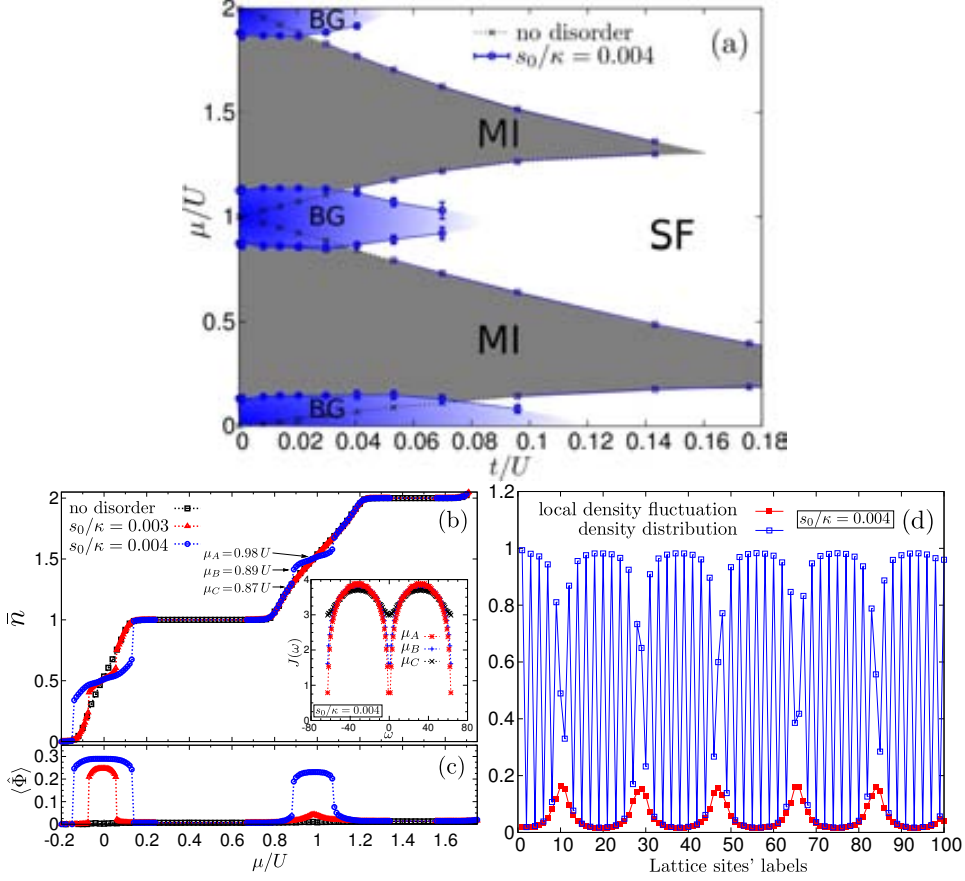


Figure 4.8: Results of QMC simulations for a one-dimensional lattice ( $\beta \gg 1$ ) with 100 sites and periodic boundary conditions. (a) The phase diagram is obtained by QMC calculation for a one-dimensional lattice with 100 sites for  $s_0 = 0.004\kappa$ . The results are compared with the pure case (dotted curves). (b) Linear density  $\bar{n}$  and (c)  $\langle \hat{\Phi} \rangle$  as a function of  $\mu$  for  $t = 0.053U$  and  $s_0/\kappa = 0.003$  (triangles),  $s_0/\kappa = 0.004$  (circles), and  $s_0 = 0$  (squares): The number of photons is different from zero for the parameters corresponding to the blue regions in (a). The inset of (b) displays the Fourier transform of the pseudo current-current correlation function  $J(\omega)$  [141–143] for the parameters indicated by the arrows in the curve of (b): the extrapolated value at zero frequency is proportional to the SF density. (d) Local density distribution  $\langle \hat{n}_i \rangle$  (empty points joined by the blue curve) and local density fluctuations  $\langle \hat{n}_i^2 \rangle - \langle \hat{n}_i \rangle^2$  (filled points joined by the red curve) as a function of the site for  $\mu = 0$  and  $s_0 = 0.004\kappa$ . The other parameters are as in Fig. 4.5.

$\bar{n} = 1, 2$ , the blue regions the compressible phase with vanishing SF density, where the number of intracavity photon is large, while outside these shaded region the phase is SF. The effect of cavity backaction is evident at low tunneling, where  $\langle \hat{\Phi} \rangle > 0$ : Here the size of the MI regions is reduced and one observes a direct transition between MI and BG phase. At larger tunneling a direct MI-SF transition occurs and the MI-SF phase boundary merges with the one found for  $s_0 = 0$ : In fact, for larger quantum fluctuations  $\langle \hat{\Phi} \rangle \rightarrow 0$  in the thermodynamic limit. This feature is strikingly different from the situation in which the incommensurate potential is classical [48, 49]: There, the MI lobes shrink at all values of  $t$  with respect to the pure case. The SF density is obtained by extrapolating the Fourier transform of the pseudo current-current correlation function  $J(\omega)$  [141–143] to zero frequency (see inset of panel (b)). The atomic density and corresponding value of  $\langle \hat{\Phi} \rangle$  are displayed in Fig. 4.8(b) and (c) as a function of  $\mu$  for different values of the transverse laser intensity (thus  $s_0$ ): The incommensurate potential builds in the blue region of the diagram, which we label by BG, where the number of intracavity photons does not vanish. Panel (d) displays the local density distribution  $\langle \hat{n}_i \rangle$  and the local density fluctuations in the BG region: the density oscillates in a quasi-periodic way over clusters in which the atoms scatter in phase into the cavity mode. The fluctuations are larger at the points where  $Z_0^{(i)}$ , which oscillates at the cavity mode wave length, becomes out of phase with the trapping potential. In this way the density distribution maximizes scattering into the cavity mode. This distribution is reminiscent of a density-wave<sup>3</sup> [48], which is characterized by zero order parameter and non-vanishing compressibility. We denote the corresponding region by BG, which stands for Bose glass, using the terminology applied in Refs. [48, 49] to similar density distributions found in the bichromatic Bose-Hubbard model.

### 4.3.2 Two-dimensional lattice

We now analyze the phase diagram of a two-dimensional lattice, of which one axis coincide with the cavity axis while in the perpendicular direction the atoms are pumped by the standing wave laser which is quasi resonant with the cavity field. In this situation, hence, the site-dependent term proportional to the laser intensity ( $V_1$ ) in Eq. (4.31) is relevant and significantly

<sup>3</sup>A density-wave phase is an insulating phase which is gapped in the excitation spectrum, that makes it distinguished from a BG phase.

affects the phase diagram, such that even in the absence of the cavity field, the effects due to this classical field, with wavelength incommensurate with the confining optical lattice, modify the properties of the ground state.

Before we discuss the results, some consideration on the parameters is in order. The size of the lattice is fixed to vary about the value  $K \sim 100 \times 100$ , then for the parameters we choose the expectation value of operator  $\hat{\delta}_{\text{eff}}$  in Eq. (4.36) is such that the operator can be approximated by

$$\hat{\delta}_{\text{eff}} \sim -u_0 \sum_{i,j} Y_0^{(i,j)} \hat{n}_{i,j} / K.$$

A check of the parameter shows, moreover, that the effect of the classical incommensurate potential proportional to  $V_1$  dominates over the cavity incommensurate field in determining the value of the onsite energy, Eq. (4.31), whose sign is determined by  $\Delta_a$ .

We first analyse the behaviour of the mean density as a function of the chemical potential when  $t \rightarrow 0$  for opposite signs of  $\Delta_a$ , which is found by diagonalizing the two-dimensional Hamiltonian in Eq (4.39) after setting the tunneling coefficient  $t = 0$ . The corresponding curves are displayed in Fig. 4.9. For the considered set of parameters the appearance of incompressible phases is observed. To a very good approximation they are in the interval of values determined by the classical incommensurate potential  $V_1$ , which takes either positive or negative values depending on whether  $\Delta_a$  is positive or negative. For commensurate density  $\bar{n} = 1$  and  $\Delta_a < 0$ , for instance, an incompressible phase is found in the interval  $0 < \mu \leq \mu_1 < U$ , where  $\mu_1$  depends on  $V_1$ . For  $\Delta_a > 0$ , instead, the incompressible phase is in the interval  $0 < \mu_1 \leq \mu < 1$ . Different from the one-dimensional case, we do not observe shrinking on both sides of the incommensurate phase since for  $t \rightarrow 0$  the cavity potential is a small correction to the term due to the classical pump (i.e., for  $\Delta_a > 0$  in Fig. 4.9 we have  $\delta\epsilon_{i,j} > 0, \forall i, j$ ). The dominant effect of the classical field is also visible when analysing the curve in the parameter regime where the phase is compressible: The inset shows a zoom of the curve for  $\Delta_a > 0$ , which exhibits various discontinuities in the compressibility. The finite compressibility is here due to the classical field. However, the jump visible for  $\mu'$ , with  $0 < \mu' < 0.5$  is due to the cavity quantum potential. For  $0 < \mu < \mu'$ , in particular, the intracavity photon number vanishes.

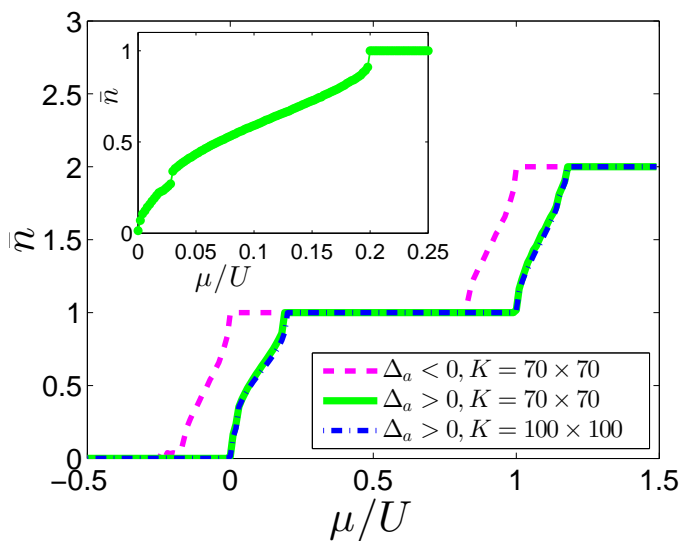


Figure 4.9: Mean density  $\bar{n}$  versus  $\mu$  (in units of  $U$ ) for a two-dimensional lattice. The curves are evaluated by a diagonalization of Hamiltonian (4.39) for  $t = 0$ , in the mean-field approximation when  $\hat{\Phi}^2 \approx \langle \hat{\Phi}^2 \rangle + 2\langle \hat{\Phi} \rangle \hat{\Phi}$ , when  $K = 70 \times 70$  and  $\Delta_a < 0$  (dashed line), and  $K = 70 \times 70$  and  $\Delta_a > 0$  (solid line). The parameters are  $|\Delta_a| = 2\pi \times 58GHz$ ,  $s_0 = 0.15\kappa$ ,  $\delta_c = -5\kappa$ ,  $u_0 = 237\kappa$  ( $\kappa = 2\pi \times 1.3$  MHz). Inset: Zoom of the curve at  $K = 70 \times 70$  and  $\Delta_a > 0$  in the compressible phase. The dashed-dotted line for  $K = 100 \times 100$  and  $\Delta_a > 0$  shows, when compared with the solid line, that the qualitative behaviour of the curves remain invariant as the system size is scaled up.

We now determine the behaviour at finite  $t$  for the two-dimensional lattice taking  $\Delta_a > 0$  by means of a local mean-field calculation. This is performed by setting  $\hat{b}_{i,j} = \psi_{i,j} + \delta\hat{b}_{i,j}$  where  $\psi_{i,j} = \langle \hat{b}_{i,j} \rangle$  is a scalar giving the local SF order parameter and  $\delta\hat{b}_{i,j}$  are the fluctuations with zero mean value. The new form is substituted in Eq. (4.34) and the second order fluctuations of the hopping term, namely, the terms  $\delta\hat{b}_{i,j} \delta\hat{b}_{i',j'}$ , are discarded [144]. The resulting Bose-Hubbard Hamiltonian in the mean-field approximation takes the form  $\hat{\mathcal{H}}_{\text{BH}}^{(MF)} = \sum_{i,j} \hat{\mathcal{H}}_{i,j}$ , where

$$\hat{\mathcal{H}}_{i,j} = \left\{ -t\eta_{i,j} \left( \hat{b}_{i,j}^\dagger - \frac{\psi_{i,j}^*}{2} \right) + \text{H.c.} \right\} + \frac{U}{2} \hat{n}_{i,j} (\hat{n}_{i,j} - 1) + \hat{\epsilon}_{i,j} \hat{n}_{i,j}, \quad (4.42)$$

and  $\eta_{i,j} = \psi_{i+1,j} + \psi_{i-1,j} + \psi_{i,j+1} + \psi_{i,j-1}$  is the sum of the local SF parameters of the neighbouring sites. We remark that cavity backaction makes Hamiltonian  $\hat{\mathcal{H}}_{i,j}$  in (4.42) non-local in the density, since it depends on the collective operator  $\hat{\Phi}$  appearing in  $\hat{\epsilon}_{i,j}$ . The local SF order parameters  $\psi_{i,j}$  are found by solving the coupled set of self-consistency equations  $\psi_{i,j} = \langle \phi_G^{(MF)} | \hat{b}_{i,j} | \phi_G^{(MF)} \rangle$ , where  $|\phi_G^{(MF)}\rangle = \otimes_{j=1}^K |\phi_j\rangle$  is the ground state in the mean-field approximation, and is thus the direct product of the single-site states  $|\phi_j\rangle$ . In our numerical implementation the evaluation of ground state is repeated till the averaged SF order parameter  $\psi = \sum_{i,j} \psi_{i,j} / K$  converges up to a tolerance of 0.005. The recursive calculation of the ground states of the self-consistent Hamiltonian  $\hat{\mathcal{H}}_{\text{BH}}^{(MF)}$  is terminated once the value of  $\bar{n}$  converges with an accuracy of  $2 \times 10^{-4}$ .

Figure 4.10 displays the mean density as a function of the chemical potential for the same parameters of the solid curve in Fig. 4.9 but for  $t = 0.01U$ . The curve has been determined by means of the local mean-field approach. The zoom on the region of parameters where the compressibility is different from zero shows that also at finite  $t$  the curve is discontinuous. The jumps indicate the interval of values in which there is an intracavity field (see green crosses in Figure 4.10). The inset displays the corresponding curve when the pump is far detuned from the cavity field: the compressibility does not present jumps in the compressible phase and the mean intracavity field is at least 3 orders of magnitude smaller.

Figure 4.11(a) displays the mean SF order parameter in the  $\mu - t$  plane and for density  $\bar{n} \leq 1$ . Here, the dotted lines identify the regions where the order parameter takes values below 0.02. The solid curve indicates where

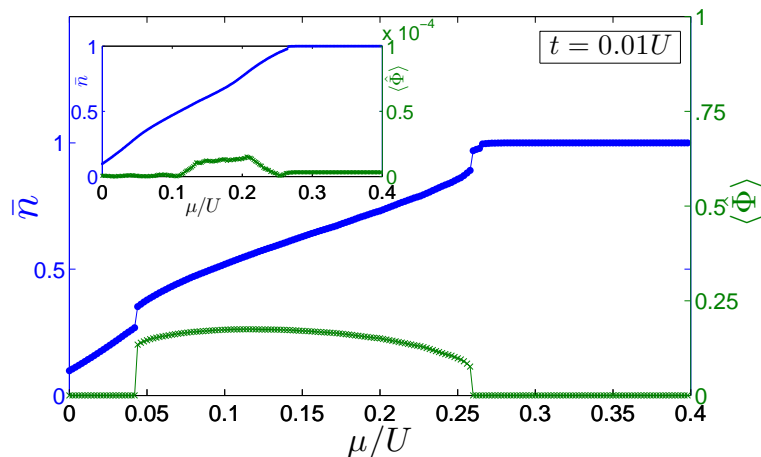


Figure 4.10: Mean density  $\bar{n}$  (blue line) and  $\langle \hat{\Phi} \rangle$  (green line with crosses) versus  $\mu$  (in units of  $U$ ) for a two-dimensional lattice. The curves are evaluated using local mean-field for  $t = 0.01U$  and  $K = 70 \times 70$ . The parameters are  $\Delta_a = 2\pi \times 58\text{GHz}$ ,  $s_0 = 0.15\kappa$ ,  $\delta_c = -5\kappa$ ,  $u_0 = 237\kappa$  ( $\kappa = 2\pi \times 1.3$  MHz). Inset: Same curves but for  $\delta_c = -300\kappa$ . Note that the maximum value of  $\langle \hat{\Phi} \rangle$  is 3 orders of magnitude smaller than for  $\delta_c = -5\kappa$ .

the gap in the spectrum is different from zero, corresponding to vanishing density fluctuations  $\Delta\rho = (\overline{n^2} - \bar{n}^2)^{1/2}$  where  $\bar{n} = \sum_{i,j} \langle \hat{n}_{i,j} \rangle / K$  and  $\overline{n^2} = \sum_{i,j} \langle \hat{n}_{i,j}^2 \rangle / K$  (the threshold is set at 0.02). For comparison, Fig. 4.11(b) displays the corresponding diagram when the cavity is pumped far from resonance, so that the effect of cavity back action is very small and practically negligible. We note that the curve delimiting the MI phase has a very similar behaviour in presence and in absence of cavity backaction, showing that for the considered parameters the existence of incompressible phases is determined by the transverse optical lattice. The behaviour of the compressible phase with vanishing order parameter, which we here denote by BG phase, varies instead significantly in presence of the cavity potential, as one can observe by comparing Fig. 4.11(a) and (b). We finally point out the region delimited by the dashed line, which appears only in the subplot (a): This indicates the parameters for which the mean value of  $\hat{\Phi}$  is at least two orders of magnitude larger than outside. In this region there is an intracavity field, which is constructed and supported by the scattering of the atoms.

The typical onsite density encountered in this parameter region, and in particular for the parameters indicated by the squared point in (a), is shown

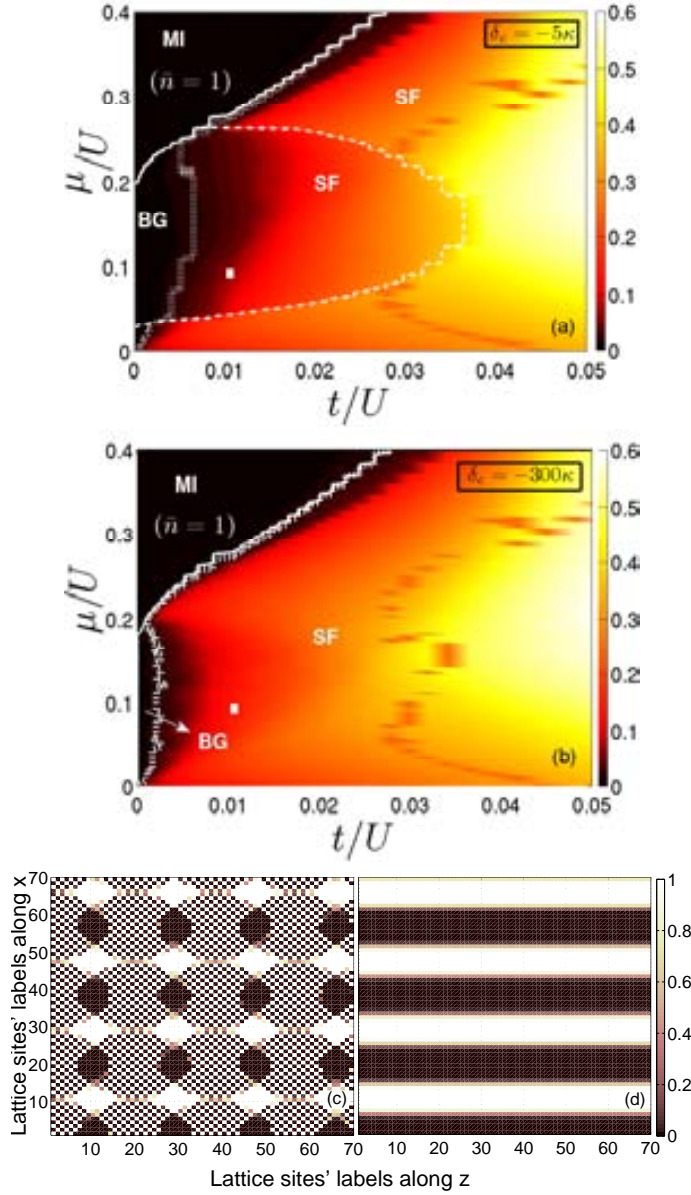


Figure 4.11: (a), (b) Order parameters in  $\mu$ - $t$  plane (in units of  $U$ ) obtained by the mean-field calculation for a  $70 \times 70$  lattice with periodic boundary conditions. The dotted lines separate the region with vanishing order parameters, while the solid line identifies the border for the incompressible MI state at density  $\bar{n}$ . The regions with finite compressibility and vanishing order parameters correspond to BG phases. The dashed line separates the region where the photon number is 2 order of magnitude larger than outside. The parameters are  $s_0 = 0.15\kappa$ ,  $u_0 = 237\kappa$ ,  $\Delta_a = 2\pi \times 58$  GHz, whereas (a)  $\delta_c = -5\kappa$  and (b)  $\delta_c = -300\kappa$ . In the latter case the effect of the cavity potential is expected to be small. The local densities  $\langle \hat{n}_{i,j} \rangle$  of the phase diagram at  $\mu = 0.092U$  and  $t = 0.01\kappa$  are shown in (c) for  $\delta_c = -5\kappa$  and  $\bar{n} = 0.5$  (squared point in (a)) and in (d) for  $\delta_c = -300\kappa$  and  $\bar{n} = 0.446$  (squared point in (b)).

in subplot (c). It is first instructive to consider the case without cavity backaction: the density corresponding to the squared point in (b) is displayed in subplot (d). Here, one observes dark stripes along the vertical direction at which the density is minimum. The stripes are almost regularly distributed and are due to the classical incommensurate potential along the  $x$  axis. When cavity back action becomes relevant, an incommensurate potential also appears along the  $z$  direction. This intracavity potential is associated with the appearance of clusters within which the density exhibit a checkerboard distribution, as shown in Fig. 4.11(c). These clusters are the two-dimensional analogy of the density-wave like behaviour observed in a one-dimensional lattice [48]: they maximize scattering into the cavity field and their size is determined by the length due to the beating between the lattice wave length and the incommensurate cavity potential.

We now analyse the signal at the cavity output which can be observed as a function of the tunneling coefficient at fixed incommensurate density. The corresponding intensity is evaluated by calculating  $n_{\text{out}} = \langle \hat{a}_{\text{out}}^\dagger \hat{a}_{\text{out}} \rangle$ , where  $\hat{a}_{\text{out}}$  is given in Eq. (4.15) where  $\hat{a}$  is a function of the quantum gas, see Eq. (4.14). The intensity as a function of the tunneling coefficient  $t$  is reported in Fig. 4.12(a): By increasing the trapping potential depth  $V_0$  (decreasing the tunneling) a sudden increase of the cavity photon number is observed. This corresponds to the transition to density distributions according to checkerboard clusters, as the subplots (b) and (d) show in detail. Before this sudden increase the density distribution is almost flat along the cavity axis: the atoms delocalize over the lattice sites and there is no coherent scattering of photons into the resonator.

## 4.4 Experimental Parameters

The Bose-Hubbard Hamiltonian in Eq. (4.34) has been derived by performing a series of approximations which have been discussed in detail in the previous section. In this section we show that existing experimental setups, like the one of Ref. [33, 138] can observe the phases predicted by Eq. (4.34). Moreover, we identify here the parameters which are then used in the numerical plots presented in Sec. 4.3.

The parameters for the cavity field, which determine the coefficients of the Bose-Hubbard Hamiltonian in Eq. (4.34), are extracted from the exper-

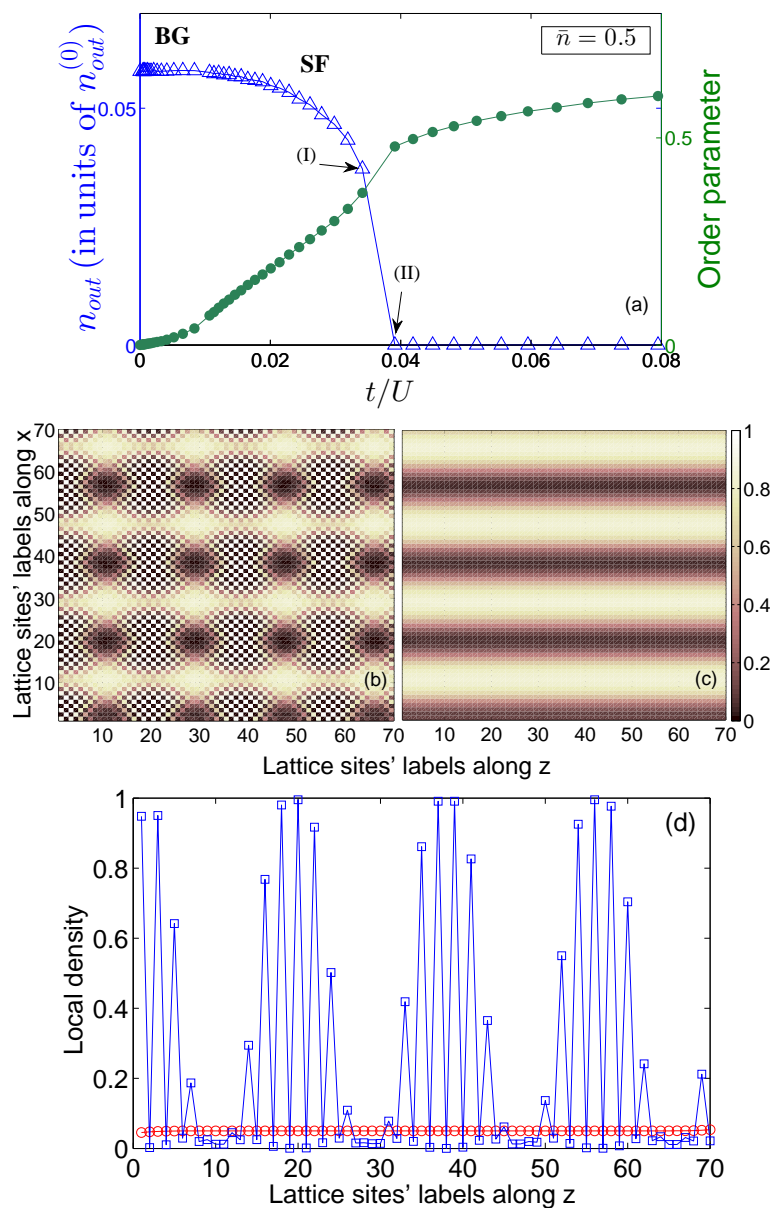


Figure 4.12: (a) Intensity at the cavity output,  $n_{out} = \langle \hat{a}_{out}^\dagger \hat{a}_{out} \rangle$  as a function of  $t$  (in units of  $U$ ) for the parameters of Fig. 4.11(a) and by fixing  $\bar{n} = 0.5$ . Here,  $n_{out}$  is in units of  $n_{out}^{(0)} = \kappa n_{cav}^{(max)}$  where  $n_{cav}^{(max)} = s_0^2 K / (\delta_{eff}^2 + \kappa^2)$  is the maximum number of intracavity photons, obtained when all atoms scatter in phase into the cavity mode. The curve with circles (right  $y$ -axis) gives the corresponding order parameter. Subplot (b) displays the contour plot of the local density distributions at point (I) in panel (a), where  $t = 0.034U$ ,  $\mu = 0.106U$ ,  $\langle \hat{\Phi} \rangle = 0.136$ . Subplot (c) displays the local density distributions at point (II) in panel (a), where  $t = 0.039U$ ,  $\mu = 0.122U$ , while  $\langle \hat{\Phi} \rangle \simeq 0$ . Subplot (d) displays the local density  $\langle \hat{n}_{i,j} \rangle$  as a function of the site numbers along  $z$  for the lattice site 20 along  $x$ . The blue squares (red circles) correspond to the parameters of panel (b) (panel (c), respectively).

imental values  $g_0/2\pi = 14.1$  MHz,  $\kappa/2\pi = 1.3$  MHz, and  $\gamma/2\pi = 3$  MHz for  $^{87}\text{Rb}$  atoms [33, 138]. The detuning between atoms and the cavity mode at wavelength  $\lambda = 785$  nm is about  $\Delta_a/2\pi = 58$  GHz. For these parameters  $U_0/\pi \approx 3.4$  kHz. The corresponding value of  $S_0$  depends on the Rabi frequency of the transverse laser. For instance, for  $\Omega/2\pi = 3.08$  MHz then  $S_0/2\pi = 0.74$  kHz. An external optical lattice trapping the atoms such that the ratio  $d_0/\lambda \simeq 83/157$  is realized can be made by pumping the mode at wave length 830 nm.

*Parameters.* We now check that these values are consistent with the approximations we made in deriving Eq. (4.34). For this purpose we must fix the number of sites, and thus the number of atoms  $N$ , since the total shift and the total scattering amplitude must be properly rescaled by  $N$ . For densities  $\bar{n} = 1$  the number of sites is equal to the number of atoms. For a one-dimensional lattice with  $K \simeq 300$  sites one finds  $u_0/2\pi = U_0K/2\pi \approx 1.02$  MHz and  $s_0/2\pi = S_0\sqrt{K}/2\pi \approx 0.013$  kHz, or alternatively  $u_0 \simeq 0.8\kappa$  and  $s_0 = 0.01\kappa$ . Other values are obtained by accordingly changing the Rabi frequency  $\Omega$ . We set  $|\delta_c| = 5\kappa$  and observe that for this value  $|\delta_c - u_0| \approx |\delta_c|$ . We shall now check the order of magnitude of the coefficients of the Bose-Hubbard model for these parameters. Here,  $s_0^2K|\delta_c|/(\delta_c^2 + \kappa^2) \simeq 0.004\kappa \simeq 2\pi \times 5.75\text{kHz}$ . For these parameters the onsite energy due to the cavity field exceeds the MI gap when  $\langle \hat{\Phi}^2 \rangle \geq 10^{-3}$ . For a two-dimensional lattice with  $K = 300 \times 300$  sites then  $u_0 = U_0K \simeq 2\pi \times 308.5$  MHz or alternatively  $u_0 = 237\kappa$ . For  $\Omega/2\pi = 2.6$  MHz, for instance, then  $s_0 = S_0\sqrt{K} \simeq 0.15\kappa$  and  $V_1 = \Omega^2/\Delta_a \simeq 0.78$  kHz. For these parameters, typical values of the density distribution give  $|\delta_{\text{eff}}| \simeq 88\kappa \gg \kappa$ , such that  $s_0^2K\delta_{\text{eff}}/(\delta_{\text{eff}}^2 + \kappa^2) \simeq 1.3\kappa$ . Here, already for  $\langle \hat{\Phi}^2 \rangle \geq 10^{-4}$  cavity backaction has a significant effect.

*Spontaneous emission rate.* Both in the one-dimensional and two-dimensional cases, the parameters give a very small occupation of the excited state: The probability that an atom is excited scales with  $P_{\text{exc}} \sim K \max(g_0^2 n_{\text{cav}}, \Omega^2)/\Delta_a^2$ , where  $n_{\text{cav}}$  is the mean intracavity photon number. For the considered parameters  $P_{\text{exc}} \lesssim 10^{-3} \ll 1$ . The corresponding spontaneous emission rate following an excitation due to the cavity field reads  $\gamma'_c = \gamma g_0^2 n_{\text{cav}}/\Delta_a^2 \simeq 2\pi \times 0.17 n_{\text{cav}}$  Hz, while the spontaneous decay rate of an excitation due to the transverse laser scales with  $\gamma'_L = \gamma \Omega^2/\Delta_a^2 \simeq 2\pi \times 0.08$  Hz.

*Adiabatic elimination of the cavity mode.* We now check the conditions for the adiabatic elimination of the cavity mode for a one-dimensional lat-

tice with 300 sites. The adiabatic elimination of the cavity field from the atomic equations of motion requires that one neglects the coupling with the atoms over the time-scale over which the cavity reaches a “stationary” value which depends on the instantaneous density distribution. This introduces a time-scale  $\Delta t = 1/|\delta_c + i\kappa|$ , for which the following inequalities shall be fulfilled:  $S_0\sqrt{n_{\text{cav}}}\Delta t \ll 1$  and  $U_0n_{\text{cav}}\Delta t \ll 1$ . These relations are satisfied for the typical numbers of intracavity photons we encounter. In addition, since the atoms must move slowly over this time-scale, their kinetic energy (temperature) must be such that  $k_B T \ll \hbar/\Delta t$ , where  $k_B$  is the Boltzmann constant. This latter condition is satisfied for atoms at  $T \simeq 1\mu\text{K}$ , which is achieved in Bose-Einstein condensates.

*Neglecting quantum noise.* Quantum noise in Eq. (4.14) can be neglected when  $Ks_0^2\langle\hat{\Phi}^2\rangle \gg \kappa^2$ , which corresponds to a depth of the lattice created by photon scattering which is much larger than single photon fluctuations. For the parameters here discussed one needs a lattice with sites  $K \gg 10^4$ , which corresponds to the two-dimensional situation we analyse. The one-dimensional lattice we numerically consider contains  $K \simeq 100$  sites, however the scaling of the behaviour with the number of particles show that our predictions remain valid for larger numbers, where one can discard fluctuations in the intracavity photon number.

*Single-band approximation.* In the derivation of the Bose-Hubbard Hamiltonian in Eq. (4.34) we have performed an expansion of the field operator (4.16) into Wannier functions of the lowest band of the external lattice. Discarding the higher bands is correct as long as the energy gap between a lowest and a first excited Bloch band  $\Delta E = \sqrt{4E_R|V_0|}$  is much larger than the interaction energy  $V_{\text{int}}$ , which is here  $V_{\text{int}} = U + \max|\delta\epsilon_{i,j}|$  between the particles [122], where  $E_R = \hbar^2k_0^2/2m$  is the recoil energy. Figure 4.13 displays the ratio  $\Delta E/V_{\text{int}}$  in the limit of zero tunneling  $t \rightarrow 0$ . We have checked that this ratio remains smaller than unity for the parameters here chosen. Increasing the laser amplitude  $\Omega$ , i.e., increasing of  $s_0$  (and hence  $\delta\epsilon$ ) leads to an increase of  $V_{\text{int}}$  and thus forces one to take into account higher Bloch bands.

Finally, at the remaining of this Chapter we discuss the ground state of the one-dimensional Hamiltonian in (4.41) when the short-range contact interaction  $U$  is absent. We show that for a sufficiently large amplitude of disorder, a localized state of matter in a cavity can be realized which is an

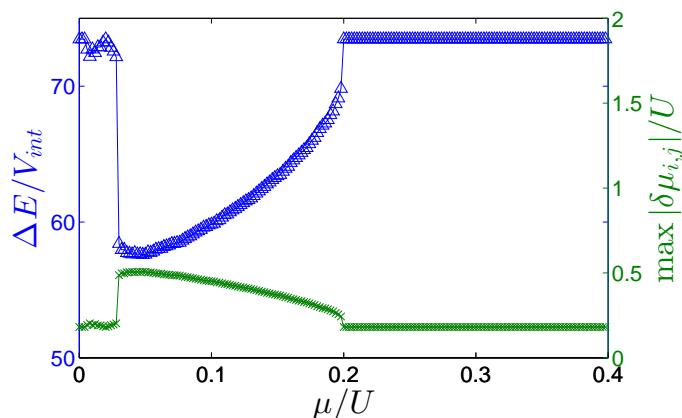


Figure 4.13: Ratio between the energy gap between the two Bloch bands,  $\Delta E = \sqrt{4E_R|V_0|}$ , and the interaction energy,  $V_{\text{int}} = U + \max |\delta\epsilon_{i,j}|$ , as a function of the chemical potential  $\mu$  (in units of  $U$ ) and at zero tunneling. The single-band approximation is valid  $\Delta E/V_{\text{int}} \gg 1$ . The green curve with crosses shows the maximum values of  $\langle \delta\hat{\epsilon}_{i,j} \rangle$  at the corresponding values of  $\mu/U$ . The parameters are as same as in Fig. 4.11(a).

analogous to Anderson localization in a disordered systems.

## 4.5 Anderson glass

Localization of electrons in a disordered potential of a crystal was initially proposed by Anderson for weakly-interacting bosonic systems [145]. It has been shown that for a two-dimensional lattice, when the disorder amplitude reaches a critical value, the state of matter localizes in space. Afterwards, a localization of matter for non-interacting bosons in incommensurate bichromatic potentials has been observed experimentally [146–148] in a one-dimensional tight-binding André-Aubry model [149]. The André-Aubry model is a single-particle (non-interacting) model which exhibits a localization transition in one dimension. In this Chapter we discuss the one-dimensional case of the system of ultracold atoms inside a cavity, in which the short-range  $s$ -wave scattering strength  $\mathcal{G}_s$  is tuned to zero by means of the Feshbach resonance. Therefore the Hamiltonian (4.41) reduces to

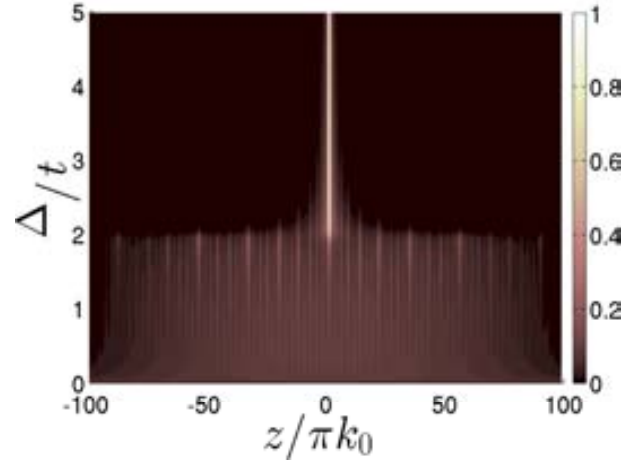
$$\hat{H} = \sum_i \hat{\epsilon}_i \hat{n}_i - t \sum_{\langle i,j \rangle} (\hat{b}_i^\dagger \hat{b}_j + \text{H.c.}). \quad (4.43)$$

In Eq. (4.43) as a result of the collective scattering effect, the onsite energy  $\hat{\epsilon}_i$  depends on the atomic density distribution which differs from the André-Aubry model. In the André-Aubry model because of the absence of the onsite interaction, the ground state for a single particle and for  $N$  particles are the same. When the parameters  $\epsilon_i$  are density-independent, the Hamiltonian is quadratic and can be diagonalized exactly. In the presence of cavity backaction and for a density-dependent  $\hat{\epsilon}_i$ , here we study the single-atom case. Similar to the BG phases due to the cavity backaction, the particles accumulate at lattice sites such that scattering into the cavity is enhanced.

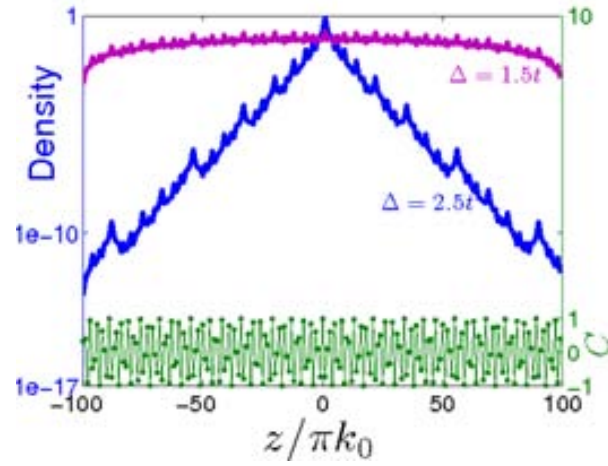
It has been shown that for the one-dimensional André-Aubry model, in contrary to the random disordered cases, when the disorder amplitude  $\Delta$  is above the critical value, i.e.,  $\Delta > 2t$ , there is a phase transition from an extended-state to a localized-state [146–149]. This behaviour is shown in Fig. 4.14. In presence of the cavity backaction, we observe quite different behavior for the phase transition. In Fig. 4.15 we show how by increasing the amplitude of the transverse pump (or  $s_0$ ) we encounter a phase transition from an extended state to a localized state. In the presence of the cavity backaction, as the laser amplitude  $\Omega$  increases, in the vicinity of the critical value of the transition from extended to localized state, the system encounters a discontinuity in the disorder amplitude  $\Delta$ . This is due to the fact that near the phase transition, photon scattering into the cavity is enhanced and the cavity backaction is more pronounced, and hence the critical value for the transition does not exist. This shows the fact that similar to the Anderson glass in a random disordered potential in one-dimensional lattice, there is no critical value for extended-localized phases in the presence of the cavity backaction for quasi-periodic bichromatic lattices.

## 4.6 Summary and outlook

In this Chapter we have studied the quantum ground state when the cavity mode has wave length which is incommensurate with the interparticle distance  $d_0$  due to the external lattice. Ultracold atoms confined in tight classical lattices and strongly coupled with a standing-wave cavity mode selforganize in order to maximize the number of intracavity photons. This selforganization takes place when the atoms are driven by a transverse laser field which is quasi-resonant with the cavity mode and whose intensity ex-

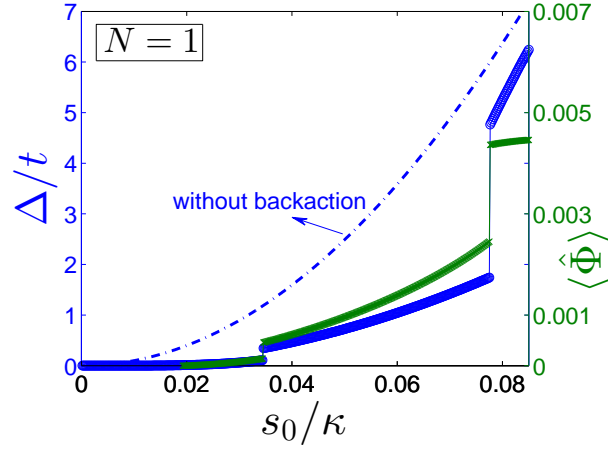


(a)

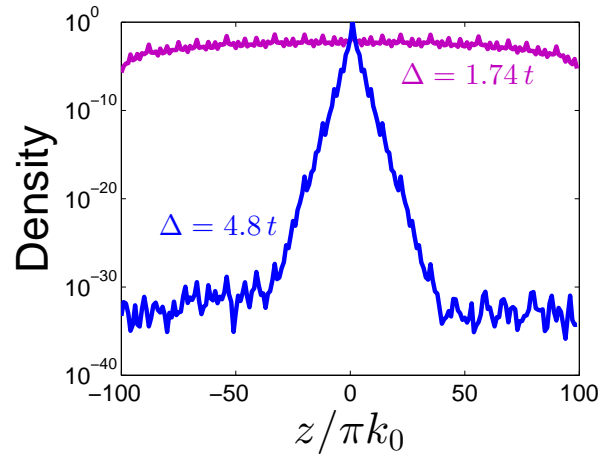


(b)

Figure 4.14: Anderson localization in absence of cavity backaction. (a) Plot of local densities  $\langle \hat{n}_i \rangle$  as a function of  $\Delta = \max |\delta \epsilon_i|$  and position  $z$  for a one-dimensional lattice for  $0 \leq s_0 \leq 0.005\kappa$ . (b) Local densities are plotted for a localized state when  $\Delta = 2.5t$  (blue curve) and for an extended state when  $\Delta = 1.5t$  (purple curve) on the left  $y$ -axis, as well the value of  $C = \cos(kz)$  where  $k = \tilde{\beta}k_0$  and  $\tilde{\beta} = \sqrt{5} - 1$  is taken from Ref. [146]. We chose  $u_0 = 0$  and  $\hat{\Phi} = 1$ . The other parameters are as in Fig. 4.5 for  $\delta_c = -5\kappa$ .



(a)



(b)

Figure 4.15: (a) The maximum amplitude of disorder  $\Delta = \max |\delta \epsilon_i|$  (in units of  $t$ ) in the presence of cavity backaction is plotted as a function of the laser amplitude which is proportional to  $s_0$  (in units of  $\kappa$ ). The right  $y$ -axis shows the corresponding value of  $\langle \hat{\Phi} \rangle$ . The dashed line shows the disorder amplitude in the absence of backaction when we artificially set  $u_0 = 0$  and  $\langle \hat{\Phi} \rangle = 1/K$ . (b) Plot of the local densities as for two values of disorder amplitude  $\Delta = 1.74t$  (extended state) and  $\Delta = 4.8t$  (localized state) which is varied for  $0 \leq s_0 \leq 0.085\kappa$ . Here  $k/k_0 = 785/830$ ,  $\delta_c = -5\kappa$  and the other parameters are as in Fig. 4.5.

ceeds a threshold value. We have shown that the atomic density forms clusters, within which the atoms form density-waves that locally maximize scattering into the cavity mode. The clusters have mean size corresponding with the beating wave length between the two overlapping field and are phase locked with one another, so that the intracavity field is maximum. These quantum phases are often characterized by vanishing order parameter and finite compressibility, so that they share several analogies with a BG phase.

In our theoretical model, the atomic dynamics are described by a Bose-Hubbard type Hamiltonian, where the effect of the cavity field enters by means of a non-local term, which depends on the density at all sites. This term is the cavity-mediated potential, which depends on the atomic distribution and whose sign is determined by the detuning between atoms and fields, which thus controls whether self-organized structures are energetically favourable. When the sign of the detuning is appropriately chosen, the cavity field gives rise to a long-range interaction between the atoms and to new phases, where the atomic density selforganize in order to maximize the intracavity photon number. Our calculations show that in absence of short-range interaction, the ground state of the system has properties similar to the Anderson glass. Future investigations shall identify the properties of the light at the cavity output.



---

## Concluding remarks

---

In this thesis we studied CQED effect for ultracold atoms confined by an optical lattice potential. The atoms are strongly coupled with a single-mode cavity and driven by a transverse laser. In the MI phase for which the spatial degrees of freedom for the atoms are frozen, the cavity backaction is negligible and the atoms are considered as pointlike scatterers. When the ratio between the cavity mode and optical lattice wavelengths are such that the von-Laue condition is not fulfilled, the coherent scattering from the atoms into the cavity is suppressed and photons are pumped into the cavity only through inelastic scattering processes. In this regime, we studied the quantum properties of light at the cavity output which can be either squeezed or antibunched. Moreover we have shown that the cavity mode and a collective excitation of the atomic array can be entangled at steady state of the dynamics.

We then considered the case when the atoms can self-organize themselves due to the cavity backaction. We found quantum ground state properties of the system when the cavity wavelength is incommensurate with the optical lattice periodicity. In this case, the ground state is not necessarily MI. We discussed the resulting phase supported by the cavity backaction on the state of the matter, which self-organizes the matter in checkerboard clusters. The formation of these clusters enhance photons scattered by the atoms into the cavity mode. These ground states lack superfluidity and possess finite compressibility, typical of a Bose-glass phase. We proposed how to measure non-destructively these states of the matter emitted outside the cavity.

At the end of this thesis, we provide some general outlooks to the works of this thesis. An interesting perspective that trapped ultracold atoms inside a cavity may open is an enhancement of antibunching of light by chang-

---

ing the geometry of the setup. This may be achieved when the photon mediated atom-atom interaction is involved, which can be controlled to be repulsive, in analogy with antibunching realized in strongly interacting Rydberg atoms [150–152]. Another interesting question which one can address is studying quantum ground state properties of ultracold atoms, when the atoms are trapped by the cavity potential generated by themselves, as discussed in Ref. [40] but rather outside MI regions. For a situation in which the atoms are driven by a laser with a tilted angle with respect to the cavity axis, one can realize a disordered self-induced cavity potential. In this case, one may expect a new exotic quantum phase, appearing in the phase diagram, due to the long-range cavity mediated interaction. As a further outlook, one can investigate whether it is possible to non-destructively monitor Anderson localization of a single atom induced by the cavity backaction by measuring the light emitted outside the cavity. Moreover, the behaviour of localized state of matter can be explored when the number of atoms increases, and hence the infinitely-ranged cavity-mediated interaction becomes more relevant.

# Appendices



---

A

## Derivation of the effective Hamiltonian (2.40)

---

From the general form of the Hamiltonian in Eq. (2.20) for the case in which there is no coherent scattering ( $Q' \neq \pm Q$ ), in the weak excitation limit one can obtain the effective dynamics for the polariton described by  $\gamma_1$ . We focus on the regime in which  $\Omega\sqrt{N} \ll |\omega_z|$ . As we are interested in the dynamics of the mode  $b_{Q_s}$  and of the cavity mode  $a$ , the relevant terms determining their dynamics are given in lowest order by

$$\mathcal{H}_{\text{eff}} = H_{\text{pump}} + \hbar\omega_{Q'}b_{Q'}^\dagger b_{Q'} + \hbar \sum_{\sigma=1,2} \omega_\sigma \gamma_\sigma^\dagger \gamma_\sigma + \mathcal{H}' \tag{A.1}$$

with

$$\begin{aligned}
\mathcal{H}' &= -\frac{\hbar g}{4\sqrt{N}} \left\{ b_{Q'}^\dagger b_{Q'}^\dagger (b_{-Q} e^{i\varphi} + b_Q e^{-i\varphi}) \delta_{Q', G/2} \right. \\
&+ 2b_{Q'}^\dagger (b_Q^\dagger e^{i\varphi} + b_{-Q}^\dagger e^{-i\varphi}) b_{Q'} \\
&+ (b_Q^\dagger b_Q^\dagger b_Q e^{i\varphi} + b_{-Q}^\dagger b_{-Q}^\dagger b_{-Q} e^{-i\varphi}) \\
&+ (1 - \delta_{k, G/2}) \left[ 2b_Q^\dagger b_{-Q}^\dagger b_{-Q} + \delta_{Q, \pm G_0/4} b_{-Q}^\dagger b_{-Q}^\dagger b_Q \right. \\
&+ 2\delta_{3Q, Q'} b_{-Q}^\dagger b_{Q'}^\dagger b_Q + \delta_{-3Q, Q'} b_{-Q}^\dagger b_{-Q}^\dagger b_{Q'} \\
&+ \left. \delta_{Q', Q+G/2} b_{Q'}^\dagger b_{Q'}^\dagger b_Q \right] e^{i\varphi} \\
&+ (1 - \delta_{k, G/2}) \left[ 2b_Q^\dagger b_{-Q}^\dagger b_Q + \delta_{Q, \pm G_0/4} b_Q^\dagger b_Q^\dagger b_{-Q} \right. \\
&+ 2\delta_{-3Q, Q'} b_Q^\dagger b_{Q'}^\dagger b_{-Q} + \delta_{3Q, Q'} b_Q^\dagger b_Q^\dagger b_{Q'} \\
&+ \left. \delta_{Q', -Q+G/2} b_{Q'}^\dagger b_{Q'}^\dagger b_{-Q} \right] e^{-i\varphi} \left. \right\} a \\
&- i \frac{\hbar \Omega}{2\sqrt{N}} e^{-i\phi_L} \left\{ 2b_{Q'}^\dagger b_Q^\dagger b_Q + 2(1 - \delta_{k, G/2}) b_{-Q}^\dagger b_{Q'}^\dagger b_{-Q} \right. \\
&+ \delta_{Q', G/2} b_Q^\dagger b_{-Q}^\dagger b_{Q'} \left[ 1 + (1 - \delta_{k, G/2}) \right] \\
&+ (1 - \delta_{k, G/2}) \left[ \delta_{3Q, Q'} b_Q^\dagger b_Q^\dagger b_{-Q} + \delta_{-3Q, Q'} b_{-Q}^\dagger b_{-Q}^\dagger b_Q \right. \\
&+ \left. \delta_{Q', Q+G/2} b_Q^\dagger b_Q^\dagger b_{Q'} + \delta_{Q', -Q+G/2} b_{-Q}^\dagger b_{-Q}^\dagger b_{Q'} \right] \left. \right\} \\
&+ \text{H.C.} .
\end{aligned}$$

By substituting  $b_{Q'}$  with its mean value in Eq. (2.39), which corresponds to neglect the backaction on the mode  $Q'$  due to the nonlinear coupling, one obtains closed equations of motion for the modes  $b_{Q_s}$  and  $a$  (where we thereby discard the effect of the nonlinear coupling with the other modes, which are initially empty and which gives rise to higher order corrections). In this limit the effective Hamiltonian (2.40) for the polariton  $\gamma_1$  is derived provided that the detuning of the laser from the polariton  $\gamma_2$  is much larger than the strength of the nonlinear coupling with polariton  $\gamma_1$ .

---

## B

# Positivity

---

For bipartite systems, a density matrix  $\rho$  is separable if there exist  $p_i \geq 0$  such that

$$\rho = \sum_i p_i \rho_i^{(A)} \otimes \rho_i^{(B)} \quad (\text{B.1})$$

with  $\sum_i p_i = 1$  where  $\rho_i^{(A)}$  and  $\rho_i^{(B)}$  are density matrices of subsystems  $A$  and  $B$ , respectively.  $\rho$  is entangled if it cannot be written as a convex sum in the form of (B.1). Peres [153] and Horodeckis [154] showed that for  $2 \times 2$  (two qubits) and  $2 \times 3$  (one qubit and one qutrit) systems the positive partial transposition is a necessary and sufficient criterion for separability. The partial transpose of a general bipartite density matrix  $\rho = \sum_{i,j,k,l} w_{ij}^{kl} |i\rangle_A \langle j| \otimes |k\rangle_B \langle l|$  with respect to the subsystem  $A$  is defined by

$$\rho^{T_A} = \sum_{i,j,k,l} w_{ij}^{kl} \left( |i\rangle_A \langle j| \right)^T \otimes |k\rangle_B \langle l| = \sum_{i,j,k,l} w_{ij}^{kl} |j^*\rangle_A \langle i^*| \otimes |k\rangle_B \langle l|, \quad (\text{B.2})$$

where here  $w_{ij}^{kl}$ 's are not necessarily non-negative and  $\sum_{i,k} w_{ii}^{kk} = 1$ . This concept has been used by Vidal and Werner for introducing the logarithmic negativity [114].

---

## C

# Gaussian dynamics

---

When the four-wave mixing term in the Hamiltonian (3.7) is negligible ( $\chi = 0$ ), then the effective Hamiltonian is quadratic, and the corresponding dynamics is Gaussian. Hence, complete information about the system is contained in the equations for the averages and for the correlations of the field operators. We introduce the vector of operators  $\mathbf{a} = (a, b_Q, a^\dagger, b_Q^\dagger)^T$ , and the correlation matrix  $\mathcal{A} = \langle \mathbf{a} \mathbf{a}^T \rangle$  whose elements are  $\mathcal{A}_{j,k} = \langle \mathbf{a}_j \mathbf{a}_k \rangle$ , then the corresponding equations take the form

$$\begin{aligned} \langle \dot{\mathbf{a}} \rangle &= \mathcal{Z} \langle \mathbf{a} \rangle, \\ \dot{\mathcal{A}} &= \mathcal{Z} \mathcal{A} + \mathcal{A} \mathcal{Z}^T + \mathcal{N}, \end{aligned} \quad (\text{C.1})$$

where

$$\mathcal{Z} = -i \begin{pmatrix} \delta_c - i\kappa & \alpha_{\text{BS}} & 0 & \alpha_{Q,a} \\ \alpha_{\text{BS}} & \delta_b - i\Gamma & \alpha_{Q,a} & 2\alpha_Q \\ 0 & -\alpha_{Q,a} & -\delta_c - i\kappa & -\alpha_{\text{BS}} \\ -\alpha_{Q,a} & -2\alpha_Q & -\alpha_{\text{BS}} & -\delta_b - i\Gamma \end{pmatrix} \quad (\text{C.2})$$

and

$$\mathcal{N} = \begin{pmatrix} 0 & 0 & 2\kappa & 0 \\ 0 & 0 & 0 & 2\Gamma \\ 0 & 0 & 0 & 0 \\ 0 & 0 & 0 & 0 \end{pmatrix}. \quad (\text{C.3})$$

If the initial state is Gaussian, then these equations fully describe the system dynamics and are equivalent to the master equation in Eq. (3.10) when  $\chi = 0$ .

The normal modes of the systems are defined by the eigenvectors of the matrix  $\mathcal{Z}|_{\kappa=0, \Gamma=0}$  at zero dissipation rates. The corresponding eigenvalues

are

$$\begin{aligned}\lambda_{1\pm} &= \mp i\sqrt{X + \sqrt{Y}}, \\ \lambda_{2\pm} &= \mp i\sqrt{X - \sqrt{Y}},\end{aligned}\tag{C.4}$$

with

$$\begin{aligned}X &= \frac{\delta_c^2 + \delta_b^2}{2} + \alpha_{BS}^2 - \alpha_{Q,a}^2 - 2\alpha_Q^2, \\ Y &= 4 \left[ \left( \alpha_Q^2 + \frac{\delta_c^2 - \delta_b^2}{4} \right)^2 - 2\alpha_{BS}\alpha_{Q,a}\alpha_Q\delta_c \right. \\ &\quad \left. + \alpha_{Q,a}^2 \left( \alpha_Q^2 - \frac{(\delta_c - \delta_b)^2}{4} \right) - \alpha_{BS}^2 \left( \alpha_Q^2 - \frac{(\delta_c + \delta_b)^2}{4} \right) \right].\end{aligned}\tag{C.5}$$

It is possible to distinguish two regimes in the dynamics of the system: If the eigenvalues are imaginary then the populations of the two modes oscillate, in time, and remain finite. If on the other hand, the eigenvalues have a finite real part, then the population of the two modes explode with time. Moreover, if initially  $\langle \mathbf{a} \rangle_j = 0 \forall j$ , then it remains zero at all times; if, on the other hand, initially the field is not zero then it is amplified with time when the eigenvalues have a finite real part.

In our system the energies  $\delta_c$  and  $\delta_b$  are the largest parameters; in particular they have opposite sign and similar amplitude, hence  $X > 0$ . Under these conditions, the eigenvalues have a finite real part when  $Y < 0$ .

If we introduce the detunings sum and difference  $d_{\pm} = \delta_b \pm \delta_c$  then, at lowest relevant order in  $1/d_{\pm}$ , we find

$$\begin{aligned}\lambda_{1\pm} &= \mp \frac{i}{2} \left[ d_{\pm} + \sqrt{d_{\pm}^2 - 4\alpha_{Q,a}^2} \right] + \mathcal{O}(1/d_{\pm}), \\ \lambda_{2\pm} &= \mp \frac{i}{2} \left[ d_{\pm} - \sqrt{d_{\pm}^2 - 4\alpha_{Q,a}^2} \right] + \mathcal{O}(1/d_{\pm}),\end{aligned}\tag{C.6}$$

and the eigenvalues have a finite real part when  $|\delta_b + \delta_c| < 2|\alpha_{Q,a}|$ . In particular this is true when the two-mode squeezing term of the Hamiltonian is resonant.

---

D

## Covariance matrix and logarithmic negativity

---

The logarithmic negativity  $E_N$  in (3.4) can be expressed in terms of the covariance matrix of the system [113],  $\mathcal{C} = [\langle \mathbf{x}\mathbf{x}^T \rangle + \langle \mathbf{x}\mathbf{x}^T \rangle^T] / 2 - \langle \mathbf{x} \rangle \langle \mathbf{x} \rangle^T$ , where  $\mathbf{x}$  is the vector of quadrature operators, which in our case is given by  $\mathbf{x} = (x_a, p_a, x_b, p_b)^T = \Pi \mathbf{a}$  with  $\mathbf{a}$  introduced in App. C, and

$$\Pi = \begin{pmatrix} 1 & 0 & 1 & 0 \\ -i & 0 & i & 0 \\ 0 & 1 & 0 & 1 \\ 0 & -i & 0 & i \end{pmatrix} \quad (\text{D.1})$$

In the case of Gaussian states,

$$\mathcal{C} = \Pi \frac{\mathcal{A} + \mathcal{A}^T}{2} \Pi^T - \Pi \langle \mathbf{a} \rangle \langle \mathbf{a} \rangle^T \Pi^T. \quad (\text{D.2})$$

The logarithmic negativity for bipartite Gaussian states is then defined as

$$E_N = \max\{0, -\log_2(\nu_-)\} \quad (\text{D.3})$$

where  $\nu_-$  is the smallest symplectic eigenvalue of the partially transposed covariance matrix  $\tilde{\mathcal{C}} = \mathcal{T}\mathcal{C}\mathcal{T}$ . Here the matrix

$$\mathcal{T} = \begin{pmatrix} 1 & 0 & 0 & 0 \\ 0 & -1 & 0 & 0 \\ 0 & 0 & 1 & 0 \\ 0 & 0 & 0 & 1 \end{pmatrix}. \quad (\text{D.4})$$

performs the partial transposition. The system is entangled when  $E_N$  is non-zero ( $\nu_- < 1$ ).

The expression in Eq. (D.3) has been applied to the the covariance matrix of the system, which has been computed using the solution of Eq. (C.1), in order to compute the logarithmic negativity for the results in which we have neglected the non-quadratic term of Eq. (3.7).

---

E

# Two-mode squeezing spectrum of the emitted field

---

The field emitted by the cavity and scattered by the atoms can be described using the input-output formalism [13] which connect the output field to the system and input noise operators

$$\begin{aligned} a_{\text{out}}(t) &= \sqrt{2\kappa} a(t) - a_{\text{in}}(t), \\ b_{\text{out}}(t) &= \sqrt{2\Gamma} b_Q(t) - b_{\text{in}}(t), \end{aligned} \quad (\text{E.1})$$

where the input field operators  $a_{\text{in}}$  and  $b_{\text{in}}$  are decorrelated from each other, have zero average values and the only non zero correlations are  $\langle a_{\text{in}}(t), a_{\text{in}}^\dagger(t') \rangle = \langle b_{\text{in}}(t), b_{\text{in}}^\dagger(t') \rangle = \delta(t - t')$ . The system operators satisfy the quantum Langevin equations  $\dot{\mathbf{a}}(t) = \mathcal{Z} \mathbf{a}(t) + \mathcal{Q} \mathbf{a}^{\text{in}}(t)$ , where we have introduced the vectors of operators  $\mathbf{a}^{\text{out}}(t) = (a_{\text{out}}(t), b_{\text{out}}(t), a_{\text{out}}^\dagger(t), b_{\text{out}}^\dagger(t))^T$  and similar for the input noise, and where  $\mathcal{Z}$  is defined in Eq. (C.2) and  $\mathcal{Q}$  is a diagonal matrix whose diagonal elements are  $(\sqrt{2\kappa}, \sqrt{2\Gamma}, \sqrt{2\kappa}, \sqrt{2\Gamma})$ .

## E.1 Spectral properties of the emitted field

In Fourier space defined by  $\mathbf{a}(\omega) = (a(\omega), b(\omega), a^\dagger(\omega), b^\dagger(\omega))^T = \frac{1}{\sqrt{2\pi}} \int dt e^{i\omega t} \mathbf{a}(t)$  and similar for the input and output operators, the input operators satisfy  $\langle a_{\text{in}}(\omega), a_{\text{in}}^\dagger(\omega') \rangle = \langle b_{\text{in}}(\omega), b_{\text{in}}^\dagger(\omega') \rangle = \delta(\omega + \omega')$  and

$$\mathbf{a}^{\text{out}}(\omega) = \mathcal{Q} \mathbf{a}(\omega) - \mathbf{a}^{\text{in}}(\omega), \quad (\text{E.2})$$

$$-i\omega \mathbf{a}(\omega) = \mathcal{Z} \mathbf{a}(\omega) + \mathcal{Q} \mathbf{a}^{\text{in}}(\omega). \quad (\text{E.3})$$

Form these equations we find  $\mathbf{a}^{\text{out}}(\omega) = -\mathcal{W}(\omega) \mathbf{a}^{\text{in}}(\omega)$ , with

$$\mathcal{W}(\omega) = \mathcal{Q}(\mathcal{Z} + i\omega)^{-1} \mathcal{Q} + \mathbb{1}. \quad (\text{E.4})$$

Therefore the spectrum of the correlation matrix of the output field, whose elements are  $\mathcal{A}_{j,k}(\omega, \omega') = \langle \mathbf{a}_j^{\text{out}}(\omega) \mathbf{a}_k^{\text{out}}(\omega') \rangle$ , is

$$\mathcal{A}(\omega, \omega') = \langle \mathbf{a}^{\text{out}}(\omega) \mathbf{a}^{\text{out}}(\omega')^T \rangle = \delta(\omega + \omega') \mathcal{A}_0(\omega) \quad (\text{E.5})$$

where

$$\mathcal{A}_0(\omega) = \mathcal{W}(\omega) \mathcal{G} \mathcal{W}^T(-\omega) \quad (\text{E.6})$$

with

$$\mathcal{G} = \begin{pmatrix} 0 & \mathbf{1} \\ 0 & 0 \end{pmatrix}. \quad (\text{E.7})$$

We are interested in the correlations between different spectral components of the output field. We consider two modes of the output field at frequency  $\omega_a$  and  $\omega_b$ , such that the first corresponds to one mode coupled to the cavity and the other to one coupled to the atoms. The corresponding annihilation and creation operators are  $a_{\text{out}}(\omega_a)$ ,  $a_{\text{out}}^\dagger(-\omega_a)$  and  $b_{\text{out}}(\omega_b)$ ,  $b_{\text{out}}^\dagger(-\omega_b)$ . We define the vector of operators

$$\mathbf{c}(\omega_a, \omega_b) = \left( a_{\text{out}}(\omega_a), b_{\text{out}}(\omega_b), a_{\text{out}}^\dagger(-\omega_a), b_{\text{out}}^\dagger(-\omega_b) \right)^T,$$

and the vectors  $\mathbf{\Omega} = (\omega_a, \omega_b, -\omega_a, -\omega_b)$  and  $\mathbf{\Omega}' = (\omega'_a, \omega'_b, -\omega'_a, -\omega'_b)$ , then the corresponding correlation matrix can be written in terms of Eq. (E.5) as

$$\mathcal{C}_{j,k}[\mathbf{\Omega}, \mathbf{\Omega}'] = \langle \mathbf{c}_j(\omega_a, \omega_b) \mathbf{c}_k(\omega'_a, \omega'_b) \rangle = \delta(\mathbf{\Omega}_j + \mathbf{\Omega}'_k) \mathcal{A}_{0j,k}(\mathbf{\Omega}_j). \quad (\text{E.8})$$

This matrix can be used to determine the entanglement between the two modes, by calculating, for example, the logarithmic negativity (See. App. D).

It can be also used to determine the variance of a composite quadrature

$$\begin{aligned} X^{(\theta_a, \theta_b)}(\omega_a, \omega_b) &= \frac{1}{\sqrt{2}} \left[ a_{\text{out}}(\omega_a) e^{i\theta_a} + a_{\text{out}}^\dagger(-\omega_a) e^{-i\theta_a} \right. \\ &\quad \left. + b_{\text{out}}(\omega_b) e^{i\theta_b} + a_{\text{out}}^\dagger(-\omega_b) e^{-i\theta_b} \right] \\ &\equiv \mathbf{u}^T(\theta_a, \theta_b) \mathbf{c}(\omega_a, \omega_b) \end{aligned} \quad (\text{E.9})$$

with  $\mathbf{u}(\theta_a, \theta_b) = \frac{1}{\sqrt{2}} (e^{i\theta_a}, e^{i\theta_b}, e^{-i\theta_a}, e^{-i\theta_b})^T$ . Therefore, the corresponding variance is

$$\begin{aligned} \Delta X^{(\theta_a, \theta_b)}(\omega_a, \omega_b, \omega'_a, \omega'_b) &= \left\langle X^{\theta_a, \theta_b}(\omega_a, \omega_b) X^{\theta_a, \theta_b}(\omega'_a, \omega'_b) \right\rangle \\ &\quad - \left\langle X^{\theta_a, \theta_b}(\omega_a, \omega_b) \right\rangle^2. \end{aligned} \quad (\text{E.10})$$

In the case in which the average of the quadrature is zero  $\langle X^{\theta_a, \theta_b}(\omega_a, \omega_b) \rangle = 0$ , which is the relevant case for our work, we find

$$\Delta X^{(\theta_a, \theta_b)}(\omega_a, \omega_b, \omega'_a, \omega'_b) = \mathbf{u}^T(\theta_a, \theta_b) \mathcal{C}(\boldsymbol{\Omega}, \boldsymbol{\Omega}') \mathbf{u}(\theta_a, \theta_b). \quad (\text{E.11})$$

## E.2 Measurement of the squeezing spectrum

The spectral properties of the emitted field can be measured by homodyne detection with two local oscillator, at frequencies  $\omega_{LOa}$  and  $\omega_{LOB}$  respectively, used to independently homodyne-detect the field lost by the cavity and the field scattered by the atoms in a set-up similar to the one discussed in [18, 19]. By this means it is possible to measure the composite quadrature

$$\begin{aligned} \tilde{X}^{(\theta_a, \theta_b)}(\omega) &= \frac{1 - \delta_{\omega, 0}}{\sqrt{2}} \left[ X^{(\theta_a, \theta_b)}(\omega + \Delta_a, \omega + \Delta_b) \right. \\ &\quad \left. + X^{(\theta_a, \theta_b)}(-\omega + \Delta_a, -\omega + \Delta_b) \right] \\ &\quad + \delta_{\omega, 0} X^{(\theta_a, \theta_b)}(\Delta_a, \Delta_b) \end{aligned} \quad (\text{E.12})$$

where  $\Delta_a = \omega_{LOa} - \omega_p$  and  $\Delta_b = \omega_{LOB} - \omega_p$  indicate the frequencies of the local oscillators relative to the driving laser frequency. The corresponding

variance can be expressed in terms of the correlation matrix

$$\begin{aligned} \widetilde{\mathcal{C}}^{(\Delta_a, \Delta_b)}(\omega, \omega') &= \frac{1 - \delta_{\omega, 0}}{2} \times \\ &\quad \left\{ \mathcal{C} [\boldsymbol{\Omega}_\Delta(\omega), \boldsymbol{\Omega}_\Delta(\omega')] + \mathcal{C} [\boldsymbol{\Omega}_\Delta(-\omega), \boldsymbol{\Omega}_\Delta(\omega')] \right. \\ &\quad \left. + \mathcal{C} [\boldsymbol{\Omega}_\Delta(\omega), \boldsymbol{\Omega}_\Delta(-\omega')] + \mathcal{C} [\boldsymbol{\Omega}_\Delta(-\omega), \boldsymbol{\Omega}_\Delta(-\omega')] \right\} \\ &\quad + \delta_{\omega, 0} \mathcal{C} [\boldsymbol{\Omega}_\Delta(0), \boldsymbol{\Omega}_\Delta(0)] \end{aligned} \quad (\text{E.13})$$

where we have introduced the vector function

$$\boldsymbol{\Omega}_\Delta(\omega) = (\omega + \Delta_a, \omega + \Delta_b, -\omega - \Delta_a, -\omega - \Delta_b),$$

and  $\mathcal{C} [\boldsymbol{\Omega}_\Delta(\omega), \boldsymbol{\Omega}_\Delta(\omega')]$  is defined in Eq. (E.8). Hence the variance takes the form

$$\widetilde{\Delta X}^{(\theta_a, \theta_b)}(\omega, \omega') = \mathbf{u}^T(\theta_a, \theta_b) \widetilde{\mathcal{C}}^{(\Delta_a, \Delta_b)}(\omega, \omega') \mathbf{u}(\theta_a, \theta_b). \quad (\text{E.14})$$

The corresponding spectral density, i.e. the two-mode squeezing spectrum, is obtained by integrating Eq. (E.14) over a small range of frequency  $\omega'$  around  $-\omega$

$$S(\theta_a, \theta_b, \omega) = \lim_{\delta_\omega \rightarrow 0} \int_{-\omega - \delta_\omega/2}^{-\omega + \delta_\omega/2} d\omega' \widetilde{\Delta X}^{(\theta_a, \theta_b)}(\omega, \omega'). \quad (\text{E.15})$$

If we introduce the quantities

$$S_{j,k}(\omega) = \mathbf{u}_j(\theta_a, \theta_b) \mathcal{A}_{0j,k}(\omega) \mathbf{u}_k(\theta_a, \theta_b) \quad (\text{E.16})$$

with  $\mathcal{A}_0(\omega)$  defined in Eq. (E.6), then

$$S(\theta_a, \theta_b, \omega) = \frac{1}{2} \left[ \widetilde{S}(\omega) + \widetilde{S}(-\omega) \right] \quad (\text{E.17})$$

where

$$\begin{aligned}
\tilde{S}(\omega) = & S_{1,3}(\omega + \Delta_a) + S_{3,1}(-\omega - \Delta_a) \\
& + S_{2,4}(\omega + \Delta_b) + S_{4,2}(-\omega - \Delta_b) \\
& + \delta_{\Delta_a, -\Delta_b} [S_{1,2}(\omega + \Delta_a) + S_{3,4}(-\omega - \Delta_a)] \\
& + S_{2,1}(\omega + \Delta_b) + S_{4,3}(-\omega - \Delta_b) \\
& + \delta_{\Delta_a, 0} [S_{1,1}(\omega + \Delta_a) + S_{3,3}(-\omega - \Delta_a)] \\
& + \delta_{\Delta_b, 0} [S_{2,2}(\omega + \Delta_b) + S_{4,4}(-\omega - \Delta_b)] \\
& + \delta_{\Delta_a, \Delta_b} [S_{1,4}(\omega + \Delta_a) + S_{3,2}(-\omega - \Delta_a) \\
& + S_{2,3}(\omega + \Delta_b) + S_{4,1}(-\omega - \Delta_b)].
\end{aligned}$$

In the case in which only a fraction of the emitted field is detected, with a detection efficiencies  $\eta_a$  and  $\eta_b \in [0, 1]$  for the measurement of the field lost by the cavity and the field emitted by the spins respectively, then the Eqs. (E.2) and (E.3) become

$$\mathbf{a}_d^{\text{out}}(\omega) = \mathcal{Q}' \mathbf{a}(\omega) - \mathbf{a}_d^{\text{in}}(\omega), \quad (\text{E.18})$$

$$-i\omega \mathbf{a}(\omega) = \mathcal{Z} \mathbf{a}(\omega) + \mathcal{Q}' \mathbf{a}_d^{\text{in}}(\omega) + \mathcal{Q}'' \mathbf{a}_{nd}^{\text{in}}(\omega), \quad (\text{E.19})$$

where the labels  $d$  and  $nd$  indicate the external modes which are detected and that which are not detected respectively. The matrix  $\mathcal{Q}'$  is diagonal and its diagonal elements are  $(\sqrt{2\eta_a\kappa}, \sqrt{2\eta_b\Gamma}, \sqrt{2\eta_a\kappa}, \sqrt{2\eta_b\Gamma})$ , and  $\mathcal{Q}'' = \sqrt{\mathcal{Q}^2 - \mathcal{Q}'^2}$ . In this way  $\mathbf{a}_d^{\text{out}}(\omega) = -\mathcal{W}'(\omega) \mathbf{a}_d^{\text{in}}(\omega) - \mathcal{W}''(\omega) \mathbf{a}_{nd}^{\text{in}}(\omega)$ , with

$$\begin{aligned}
\mathcal{W}'(\omega) &= \mathcal{Q}' (\mathcal{Z} + i\omega)^{-1} \mathcal{Q}' + \mathbb{1}, \\
\mathcal{W}''(\omega) &= \mathcal{Q}' (\mathcal{Z} + i\omega)^{-1} \mathcal{Q}'',
\end{aligned} \quad (\text{E.20})$$

and correspondingly Eq. (E.6) becomes

$$\mathcal{A}_0(\omega) = \mathcal{W}'(\omega) \mathcal{G} \mathcal{W}'^T(-\omega) + \mathcal{W}''(\omega) \mathcal{G} \mathcal{W}''^T(-\omega), \quad (\text{E.21})$$

where we have used the fact that the modes  $\mathbf{a}_d^{\text{in}}(\omega)$  and  $\mathbf{a}_{nd}^{\text{in}}(\omega)$  are decorrelated.

---

## F

# Wannier function for a periodic potential

---

Here we discuss a derivation of a localized Wannier function for a single atom in a periodic optical lattice potential.

According to the Bloch's theorem [5, 155] the eigenstates of a single particle Hamiltonian

$$\hat{H}_1 = \frac{\hat{p}^2}{2m} + V(z) \quad (\text{F.1})$$

with a mass  $m$  confined in a periodic one-dimensional trapping potential  $V(z) = V_0 \cos^2(k_0 z)$ , can be described by a plane-wave times a function which has a periodicity of the lattice, i.e.,

$$\psi_{n,q}(z) = e^{iqz} u_{n,q}(z) \quad (\text{F.2})$$

where  $u_{n,q}(z) = u_{n,q}(z + R)$  for a Bravais lattice vector  $R = n_i \frac{\pi}{k_0}$  ( $n_i \in \mathbb{Z}$ ) and a Bloch band  $n$ . Hence we get

$$\psi_{n,q}(z + R) = e^{iqR} \psi_{n,q}(z). \quad (\text{F.3})$$

On the other hand the boundary condition  $\psi_{n,q}(z + R) = \psi_{n,q}(z)$  (so-called Born-von Karman boundary condition) allows the certain values for  $q$  such that

$$e^{iqR} = 1 \quad \longrightarrow \quad q = \frac{m_i}{n_i} k_0 \quad (\text{F.4})$$

for  $m_i \in \mathbb{Z}$ . The solution of the Schrödinger equation  $\hat{H}_1 \phi_n(z) = E_n \phi_n(z)$

is the set of all plane-waves which satisfy Eq. (F.4) and has the form

$$\phi_n(z) = \sum_q \phi_{n,q}(z) = \sum_q c_{n,q} e^{iqz} \quad (\text{F.5})$$

in which  $c_{n,q}$ 's form orthonormal bases. An equivalent set of functions are Wannier functions

$$w_n(z - R) = \frac{1}{\sqrt{K}} \sum_{q \in BZ} \phi_{n,q}(z) e^{iqR} \quad (\text{F.6})$$

defined at a lattice position  $R$  for a Bloch band  $n$ . The Wannier functions in (F.6) are the discrete Fourier transform of the Bloch functions. The sum in (F.6) is taken over the first Brillouin zone (BZ) which contains the values of the quasi-momentum  $q \in [-\frac{G_0}{2}, \frac{G_0}{2})$  for a primitive reciprocal lattice vector  $G_0 = 2\pi/d$  where  $d = \pi/k_0$  is a lattice constant, and  $K$  is the number of primitive cells in the lattice. The localized Wannier functions  $w_n(z - R)$  in (F.6) at different lattice site position  $R$  are equivalent.

To obtain the Bloch functions  $\phi_{n,q}$  one can evaluate the coefficients  $c_{n,q}$  in the following way. Consider the Schrödinger equation of motion

$$\left( -\frac{\hbar^2}{2m} \nabla_z^2 + V(z) \right) \phi_n(z) = E \phi_n(z). \quad (\text{F.7})$$

Substituting  $\phi_n(z)$  of (F.5) in Eq. (F.7) and expanding the potential in reciprocal space as

$$V(z) = \sum_G V_G e^{iGz} \quad (\text{F.8})$$

for a reciprocal lattice vector  $G = nG_0$ , we get the central equation relation

$$\left( \frac{\hbar^2}{2m} q^2 - E_n \right) c_{n,q} + \sum_G V_G c_{n,q-G} = 0 \quad (\text{F.9})$$

where

$$V_G = \frac{1}{d} \int_{-d/2}^{d/2} dz V(z) e^{-iGz} \quad (\text{F.10})$$

and  $V_G = V_{-G}$ . Hence, for Eq. (F.9) one obtains the eigenenergies  $E_n$

---

corresponding to the eigenvectors

$$\mathbf{c}_n = \begin{pmatrix} c_{n,q-NG_0} \\ \vdots \\ c_{n,q} \\ \vdots \\ c_{n,q+NG_0} \end{pmatrix}. \quad (\text{F.11})$$

Due to the fact that in this thesis, we work in the energy-scale well-below the energy gap between the first and the second Bloch bands, we focus on the Wannier function of the first Bloch band, that is when  $n = 1$ , and we show that this assumption is consistent in the purpose of our studies.



# Bibliography

---

- [1] P. Berman, editor. *Cavity Quantum Electrodynamics (Advances in Atomic, Molecular and Optical Physics)*. Academic Press, January 1994.
- [2] Herbert Walther, Benjamin T H Varcoe, Berthold-Georg Englert, and Thomas Becker. Cavity quantum electrodynamics. *Reports on Progress in Physics*, 69(5):1325, 2006.
- [3] Helmut Ritsch, Peter Domokos, Ferdinand Brennecke, and Tilman Esslinger. Cold atoms in cavity-generated dynamical optical potentials. *Rev. Mod. Phys.*, 85:553–601, Apr 2013.
- [4] Igor B. Mekhov, Christoph Maschler, and Helmut Ritsch. Cavity-enhanced light scattering in optical lattices to probe atomic quantum statistics. *Phys. Rev. Lett.*, 98:100402, Mar 2007.
- [5] N. W. Ashcroft and N. D. Mermin. *Solid State Physics*. Harcourt College, Orlando, 1976.
- [6] Ron Lifshitz. What is a crystal? *Zeitschrift für Kristallographie - Crystalline Materials*, 222(6):313–317, June 2007.
- [7] L. Mandel. Photon interference and correlation effects produced by independent quantum sources. *Phys. Rev. A*, 28:929–943, Aug 1983.
- [8] C. Skornia, J. von Zanthier, G. S. Agarwal, E. Werner, and H. Walther. Nonclassical interference effects in the radiation from coherently driven uncorrelated atoms. *Phys. Rev. A*, 64:063801, Nov 2001.
- [9] G. S. Agarwal, J. von Zanthier, C. Skornia, and H. Walther. Intensity-intensity correlations as a probe of interferences under conditions of noninterference in the intensity. *Phys. Rev. A*, 65:053826, May 2002.

- 
- [10] W. Vogel and D. G. Welsch. Squeezing pattern in resonance fluorescence from a regular  $n$ -atom system. *Phys. Rev. Lett.*, 54:1802–1805, Apr 1985.
- [11] S. Fernández-Vidal, S. Zippilli, and G. Morigi. Nonlinear optics with two trapped atoms. *Phys. Rev. A*, 76:053829, Nov 2007.
- [12] L. L. Jin, M. Macovei, S. Q. Gong, C. H. Keitel, and J. Evers. Squeezing in strong light scattered by a regular structure of atoms. *Optics Communications*, 283(5):790 – 794, 2010. <ce:title>Quo vadis Quantum Optics?</ce:title>.
- [13] D.F. Walls and G.J. Milburn. *Quantum Optics*. Springer, Berlin, 1994.
- [14] A. Kubanek, A. Ourjoumtsev, I. Schuster, M. Koch, P. W. H. Pinkse, K. Murr, and G. Rempe. Two-photon gateway in one-atom cavity quantum electrodynamics. *Phys. Rev. Lett.*, 101:203602, Nov 2008.
- [15] A. Einstein, B. Podolsky, and N. Rosen. Can quantum-mechanical description of physical reality be considered complete? *Phys. Rev.*, 47:777–780, May 1935.
- [16] E. Schrödinger. Die gegenwärtige situation in der quantenmechanik. *Naturwissenschaften*, 23:807–812, 1935.
- [17] E. Schrödinger. Discussion of probability relations between separated systems. *Mathematical Proceedings of the Cambridge Philosophical Society*, 31:555–563.
- [18] M. D. Reid. Demonstration of the einstein-podolsky-rosen paradox using nondegenerate parametric amplification. *Phys. Rev. A*, 40:913–923, Jul 1989.
- [19] P. D. Drummond and M. D. Reid. Correlations in nondegenerate parametric oscillation. ii. below threshold results. *Phys. Rev. A*, 41:3930–3949, Apr 1990.
- [20] M. D. Reid, P. D. Drummond, W. P. Bowen, E. G. Cavalcanti, P. K. Lam, H. A. Bachor, U. L. Andersen, and G. Leuchs. *Colloquium* : The einstein-podolsky-rosen paradox: From concepts to applications. *Rev. Mod. Phys.*, 81:1727–1751, Dec 2009.

- 
- [21] Z. Y. Ou, S. F. Pereira, H. J. Kimble, and K. C. Peng. Realization of the einstein-podolsky-rosen paradox for continuous variables. *Phys. Rev. Lett.*, 68:3663–3666, Jun 1992.
- [22] Klemens Hammerer, Anders S. Sørensen, and Eugene S. Polzik. Quantum interface between light and atomic ensembles. *Rev. Mod. Phys.*, 82:1041–1093, Apr 2010.
- [23] Jacob F. Sherson, Hanna Krauter, Rasmus K. Olsson, Brian Julsgaard, Klemens Hammerer, Ignacio Cirac, and Eugene S. Polzik. Quantum teleportation between light and matter. *Nature*, 443(7111):557–560, October 2006.
- [24] Monika H. Schleier-Smith, Ian D. Leroux, and Vladan Vuletić. Squeezing the collective spin of a dilute atomic ensemble by cavity feedback. *Phys. Rev. A*, 81:021804, Feb 2010.
- [25] Monika H. Schleier-Smith, Ian D. Leroux, and Vladan Vuletić. States of an ensemble of two-level atoms with reduced quantum uncertainty. *Phys. Rev. Lett.*, 104:073604, Feb 2010.
- [26] Ian D. Leroux, Monika H. Schleier-Smith, and Vladan Vuletić. Implementation of cavity squeezing of a collective atomic spin. *Phys. Rev. Lett.*, 104:073602, Feb 2010.
- [27] Emanuele G. Dalla Torre, Johannes Otterbach, Eugene Demler, Vladan Vuletic, and Mikhail D. Lukin. Dissipative preparation of spin squeezed atomic ensembles in a steady state. *Phys. Rev. Lett.*, 110:120402, Mar 2013.
- [28] Peter Domokos and Helmut Ritsch. Collective cooling and self-organization of atoms in a cavity. *Phys. Rev. Lett.*, 89:253003, Dec 2002.
- [29] J. K. Asbóth, P. Domokos, H. Ritsch, and A. Vukics. Self-organization of atoms in a cavity field: Threshold, bistability, and scaling laws. *Phys. Rev. A*, 72(5):053417, Nov 2005.
- [30] C. Nagy, G. Szirmai, and P. Domokos. Self-organization of a bose-einstein condensate in an optical cavity. *Eur. Phys. J. D*, 48:127, 2008.

- 
- [31] Hilton W. Chan, Adam T. Black, and Vladan Vuletić. Observation of collective-emission-induced cooling of atoms in an optical cavity. *Phys. Rev. Lett.*, 90:063003, Feb 2003.
- [32] Adam T. Black, Hilton W. Chan, and Vladan Vuletić. Observation of collective friction forces due to spatial self-organization of atoms: From rayleigh to bragg scattering. *Phys. Rev. Lett.*, 91:203001, Nov 2003.
- [33] K. Baumann, C. Guerlin, F. Brennecke, and T. Esslinger. Dicke quantum phase transition with a superfluid gas in an optical cavity. *Nature*, 464:1301–1306, Feb 2010.
- [34] J. Keeling, M. J. Bhaseen, and B. D. Simons. Collective dynamics of bose-einstein condensates in optical cavities. *Phys. Rev. Lett.*, 105:043001, Jul 2010.
- [35] K. Baumann, R. Mottl, F. Brennecke, and T. Esslinger. Exploring symmetry breaking at the dicke quantum phase transition. *Phys. Rev. Lett.*, 107:140402, Sep 2011.
- [36] K. J. Arnold, M. P. Baden, and M. D. Barrett. Self-organization threshold scaling for thermal atoms coupled to a cavity. *Phys. Rev. Lett.*, 109:153002, Oct 2012.
- [37] R. H. Dicke. Coherence in spontaneous radiation processes. *Phys. Rev.*, 93:99–110, Jan 1954.
- [38] D. Nagy, G. Kónya, G. Szirmai, and P. Domokos. Dicke-model phase transition in the quantum motion of a bose-einstein condensate in an optical cavity. *Phys. Rev. Lett.*, 104:130401, Apr 2010.
- [39] R. Mottl, F. Brennecke, K. Baumann, R. Landig, T. Donner, and T. Esslinger. Roton-type mode softening in a quantum gas with cavity-mediated long-range interactions. *Science*, 336(6088):1570–1573, June 2012.
- [40] Sonia Fernández-Vidal, Gabriele De Chiara, Jonas Larson, and Giovanna Morigi. Quantum ground state of self-organized atomic crystals in optical resonators. *Phys. Rev. A*, 81:043407, Apr 2010.

- 
- [41] Sarang Gopalakrishnan, Benjamin L. Lev, and Paul M. Goldbart. Emergent crystallinity and frustration with bose-einstein condensates in multimode cavities. *Nat Phys*, 5(11):845–850, November 2009.
- [42] S. Gopalakrishnan, B. L. Lev, and P. M. Goldbart. Atom-light crystallization of bose-einstein condensates in multimode cavities: Nonequilibrium classical and quantum phase transitions, emergent lattices, supersolidity, and frustration. *Phys. Rev. A*, 82:043612, Oct 2010.
- [43] Sarang Gopalakrishnan, Benjamin L. Lev, and Paul M. Goldbart. Frustration and glassiness in spin models with cavity-mediated interactions. *Phys. Rev. Lett.*, 107:277201, Dec 2011.
- [44] Philipp Strack and Subir Sachdev. Dicke quantum spin glass of atoms and photons. *Phys. Rev. Lett.*, 107:277202, Dec 2011.
- [45] B. Damski, J. Zakrzewski, L. Santos, P. Zoller, and M. Lewenstein. Atomic bose and anderson glasses in optical lattices. *Phys. Rev. Lett.*, 91:080403, Aug 2003.
- [46] L. Fallani, J. E. Lye, V. Guarrera, C. Fort, and M. Inguscio. Ultracold atoms in a disordered crystal of light: Towards a bose glass. *Phys. Rev. Lett.*, 98:130404, Mar 2007.
- [47] Leonardo Fallani, Chiara Fort, and Massimo Inguscio. Bose-einstein condensates in disordered potentials. 56:119 – 160, 2008.
- [48] G. Roux, T. Barthel, I. P. McCulloch, C. Kollath, U. Schollwöck, and T. Giamarchi. Quasiperiodic bose-hubbard model and localization in one-dimensional cold atomic gases. *Phys. Rev. A*, 78:023628, Aug 2008.
- [49] Xiaolong Deng, R. Citro, A. Minguzzi, and E. Orignac. Phase diagram and momentum distribution of an interacting bose gas in a bichromatic lattice. *Phys. Rev. A*, 78:013625, Jul 2008.
- [50] Serge Haroche and Jean-Michel Raimond. *Exploring the Quantum: Atoms, Cavities, and Photons (Oxford Graduate Texts)*. Oxford University Press, USA, 1st ed edition, October 2006.
- [51] J. M. Raimond, M. Brune, and S. Haroche. Manipulating quantum entanglement with atoms and photons in a cavity. *Rev. Mod. Phys.*, 73:565–582, Aug 2001.

- [52] R Miller, T E Northup, K M Birnbaum, A Boca, A D Boozer, and H J Kimble. Trapped atoms in cavity qed: coupling quantized light and matter. *Journal of Physics B: Atomic, Molecular and Optical Physics*, 38(9):S551, 2005.
- [53] Gerd Leuchs and Thomas Beth (edited). *Quantum Information Processing*. Wiley-VCH Verlag GmbH & Co. KGaA, 2005.
- [54] S.J. van Enk, H.J. Kimble, and H. Mabuchi. Quantum information processing in cavity-qed. *Quantum Information Processing*, 3(1-5):75–90, 2004.
- [55] F. Brennecke, T. Donner, S. Ritter, T. Bourdel, M. Kohl, and T. Esslinger. Cavity qed with a bose-einstein condensate. *Nature*, 450:268–271, Nov 2007.
- [56] C. Cohen-Tannoudji, J. Dupont-Roc, and G. Grynberg. *Photons and atoms: Introduction to quantum electrodynamics*. Wiley, New York, 1989.
- [57] J. J. Sanchez-Mondragon, N. B. Narozhny, and J. H. Eberly. Theory of spontaneous-emission line shape in an ideal cavity. *Phys. Rev. Lett.*, 51:550–553, Aug 1983.
- [58] G. S. Agarwal. Vacuum-field rabi splittings in microwave absorption by rydberg atoms in a cavity. *Phys. Rev. Lett.*, 53:1732–1734, Oct 1984.
- [59] E.T. Jaynes and F. W. Cummings. Comparison of quantum and semiclassical radiation theories with application to the beam maser. *Proc. IEEE*, 51(1):89, Jan 1963.
- [60] H. J. Carmichael. *An Open System Approach to Quantum Optics*. Springer Verlag, Berlin Heidelberg, 1993.
- [61] C. W. Gardiner and P. Zoller. *Quantum Noise. A Handbook of Markovian and Non-Markovian Quantum Stochastic Methods with Applications to Quantum Optics*. Springer Verlag, Berlin Heidelberg, 1993.
- [62] H J Kimble. Strong interactions of single atoms and photons in cavity qed. *Physica Scripta*, 1998(T76):127, 1998.

- [63] Luigi A. Lugiato. {II} theory of optical bistability. volume 21 of *Progress in Optics*, pages 69 – 216. Elsevier, 1984.
- [64] J. McKeever, J. R. Buck, A. D. Boozer, A. Kuzmich, H.-C. Nägerl, D. M. Stamper-Kurn, and H. J. Kimble. State-insensitive cooling and trapping of single atoms in an optical cavity. *Phys. Rev. Lett.*, 90:133602, Apr 2003.
- [65] D. F. Walls and P. Zoller. Reduced quantum fluctuations in resonance fluorescence. *Phys. Rev. Lett.*, 47:709–711, Sep 1981.
- [66] L. Mandel and E. Wolf. *Optical Coherence and Quantum Optics*. Cambridge University, Cambridge, UK, 1995.
- [67] M. Hennrich, A. Kuhn, and G. Rempe. Transition from antibunching to bunching in cavity qed. *Phys. Rev. Lett.*, 94:053604, Feb 2005.
- [68] S. Zippilli, G. Morigi, and H. Ritsch. Suppression of bragg scattering by collective interference of spatially ordered atoms with a high- $q$  cavity mode. *Phys. Rev. Lett.*, 93:123002, Sep 2004.
- [69] S. Slama, C. von Cube, M. Kohler, C. Zimmermann, and Ph. W. Courteille. Multiple reflections and diffuse scattering in bragg scattering at optical lattices. *Phys. Rev. A*, 73:023424, Feb 2006.
- [70] W. Vogel and D.G. Welsch. *Quantum Optics*. Wiley, 2006.
- [71] Rodney Loudon. *The Quantum Theory of Light (Oxford Science Publications)*. Oxford University Press, USA, 3 edition, nov 2000.
- [72] H. J. Kimble, M. Dagenais, and L. Mandel. Photon antibunching in resonance fluorescence. *Phys. Rev. Lett.*, 39:691–695, Sep 1977.
- [73] R.W. Boyd. *Nonlinear Optics*. Electronics & Electrical. Acad. Press, 2003.
- [74] T. Holstein and H. Primakoff. Field dependence of the intrinsic domain magnetization of a ferromagnet. *Phys. Rev.*, 58:1098–1113, Dec 1940.
- [75] Julian Klinner, Malik Lindholdt, Boris Nagorny, and Andreas Hemmerich. Normal mode splitting and mechanical effects of an optical lattice in a ring cavity. *Phys. Rev. Lett.*, 96:023002, Jan 2006.

- 
- [76] A. Dantan, M. Albert, J. P. Marler, P. F. Herskind, and M. Drewsen. Large ion coulomb crystals: A near-ideal medium for coupling optical cavity modes to matter. *Phys. Rev. A*, 80:041802, Oct 2009.
- [77] A. Dantan, J. P. Marler, M. Albert, D. Guénot, and M. Drewsen. Non-invasive vibrational mode spectroscopy of ion coulomb crystals through resonant collective coupling to an optical cavity field. *Phys. Rev. Lett.*, 105:103001, Aug 2010.
- [78] Giovanna Morigi, Jürgen Eschner, Stefano Mancini, and David Vitali. Coherent generation of epr-entangled light pulses mediated by a single trapped atom. *Phys. Rev. A*, 73:033822, Mar 2006.
- [79] David Vitali, Giovanna Morigi, and Jürgen Eschner. Single cold atom as efficient stationary source of epr-entangled light. *Phys. Rev. A*, 74:053814, Nov 2006.
- [80] H. J. Kimble. *in Cavity Quantum Electrodynamics*. edited by P. R. Berman, Academic Press, page 203, New York, 1994.
- [81] A. K. Tuchman, R. Long, G. Vrijsen, J. Boudet, J. Lee, and M. A. Kasevich. Normal-mode splitting with large collective cooperativity. *Phys. Rev. A*, 74:053821, Nov 2006.
- [82] M. Hafezi, D. E. Chang, V. Gritsev, E. A. Demler, and M. D. Lukin. Photonic quantum transport in a nonlinear optical fiber. *EPL (Europhysics Letters)*, 94(5):54006, 2011.
- [83] A. Imamog̃lu, H. Schmidt, G. Woods, and M. Deutsch. Strongly interacting photons in a nonlinear cavity. *Phys. Rev. Lett.*, 79:1467–1470, Aug 1997.
- [84] Philippe Grangier, Daniel F. Walls, and Klaus M. Gheri. Comment on “strongly interacting photons in a nonlinear cavity”. *Phys. Rev. Lett.*, 81:2833–2833, Sep 1998.
- [85] A. Imamog̃lu, H. Schmidt, G. Woods, and M. Deutsch. Erratum: Strongly interacting photons in a nonlinear cavity [phys. rev. lett. 79, 1467 (1997)]. *Phys. Rev. Lett.*, 81:2836–2836, Sep 1998.

- 
- [86] Y. Colombe, T. Steinmetz, G. Dubois, F. Linke, D. Hunger, and J. Riechel. Strong atom-field coupling for bose-einstein condensates in an optical cavity on a chip. *Nature*, 450:272–276, Nov 2007.
- [87] D. Hunger, T. Steinmetz, Y. Colombe, C. Deutsch, Hänsch T.W., and Riechel J. A fiber fabry-perot cavity with high finesse. *New Journal of Physics*, 12:065038, June 2010.
- [88] S. Zippilli, G. Morigi, and H. Ritsch. Collective effects in the dynamics of driven atoms in a high- $q$  resonator. *The European Physical Journal D - Atomic, Molecular, Optical and Plasma Physics*, 31:507–518, 2004.
- [89] D. Kruse, C. von Cube, C. Zimmermann, and Ph. W. Courteille. Observation of lasing mediated by collective atomic recoil. *Phys. Rev. Lett.*, 91:183601, Oct 2003.
- [90] D. Kruse, M. Ruder, J. Benhelm, C. von Cube, C. Zimmermann, Ph. W. Courteille, Th. Elsässer, B. Nagorny, and A. Hemmerich. Cold atoms in a high- $q$  ring cavity. *Phys. Rev. A*, 67:051802, May 2003.
- [91] S. Slama, S. Bux, G. Krenz, C. Zimmermann, and Ph. W. Courteille. Superradiant rayleigh scattering and collective atomic recoil lasing in a ring cavity. *Phys. Rev. Lett.*, 98:053603, Feb 2007.
- [92] Stefan Rist, Patrizia Vignolo, and Giovanna Morigi. Photonic spectrum of bichromatic optical lattices. *Phys. Rev. A*, 79:053822, May 2009.
- [93] Jonas Larson, Bogdan Damski, Giovanna Morigi, and Maciej Lewenstein. Mott-insulator states of ultracold atoms in optical resonators. *Phys. Rev. Lett.*, 100:050401, Feb 2008.
- [94] Jonas Larson, Sonia Fernández-Vidal, Giovanna Morigi, and Maciej Lewenstein. Quantum stability of mott-insulator states of ultracold atoms in optical resonators. *New Journal of Physics*, 10(4):045002, 2008.
- [95] A. S. Parkins, P. Marte, P. Zoller, and H. J. Kimble. Synthesis of arbitrary quantum states via adiabatic transfer of zeeman coherence. *Phys. Rev. Lett.*, 71:3095–3098, Nov 1993.

- 
- [96] J. I. Cirac, P. Zoller, H. J. Kimble, and H. Mabuchi. Quantum state transfer and entanglement distribution among distant nodes in a quantum network. *Phys. Rev. Lett.*, 78:3221–3224, Apr 1997.
- [97] A. D. Boozer, A. Boca, R. Miller, T. E. Northup, and H. J. Kimble. Reversible state transfer between light and a single trapped atom. *Phys. Rev. Lett.*, 98:193601, May 2007.
- [98] H. J. Kimble. The quantum internet. *Nature*, 453(7198):1023–1030, June 2008.
- [99] Tatjana Wilk, Simon C. Webster, Axel Kuhn, and Gerhard Rempe. Single-atom single-photon quantum interface. *Science*, 317(5837):488–490, 2007.
- [100] Holger P. Specht, Christian Nolleke, Andreas Reiserer, Manuel Uphoff, Eden Figueroa, Stephan Ritter, and Gerhard Rempe. A single-atom quantum memory. *Nature*, 473(7346):190–193, May 2011.
- [101] Stephan Ritter, Christian Nolleke, Carolin Hahn, Andreas Reiserer, Andreas Neuzner, Manuel Uphoff, Martin Mücke, Eden Figueroa, Jörg Bochmann, and Gerhard Rempe. An elementary quantum network of single atoms in optical cavities. *Nature*, 484(7393):195–200, April 2012.
- [102] C. Nölleke, A. Neuzner, A. Reiserer, C. Hahn, G. Rempe, and S. Ritter. Efficient teleportation between remote single-atom quantum memories. *ArXiv e-prints*, December 2012.
- [103] Tobias Kampschulte, Wolfgang Alt, Stefan Brakhane, Martin Eckstein, René Reimann, Artur Widera, and Dieter Meschede. Optical control of the refractive index of a single atom. *Phys. Rev. Lett.*, 105:153603, Oct 2010.
- [104] Ian D. Leroux, Monika H. Schleier-Smith, and Vladan Vuletić. Orientation-dependent entanglement lifetime in a squeezed atomic clock. *Phys. Rev. Lett.*, 104:250801, Jun 2010.
- [105] Vladan Vuletić, Ian D. Leroux, and Monika H. Schleier-Smith. *Microchip-Based Trapped-Atom Clocks*. Wiley-VCH Verlag GmbH & Co. KGaA, 2011.

- 
- [106] P. Grünwald and W. Vogel. Entanglement in atomic resonance fluorescence. *Phys. Rev. Lett.*, 104:233602, Jun 2010.
- [107] Werner Vogel. Nonclassical correlation properties of radiation fields. *Phys. Rev. Lett.*, 100:013605, Jan 2008.
- [108] Christine A. Muschik, Eugene S. Polzik, and J. Ignacio Cirac. Dissipatively driven entanglement of two macroscopic atomic ensembles. *Phys. Rev. A*, 83:052312, May 2011.
- [109] M. D. Reid and P. D. Drummond. Quantum correlations of phase in nondegenerate parametric oscillation. *Phys. Rev. Lett.*, 60:2731–2733, Jun 1988.
- [110] Lu-Ming Duan, G. Giedke, J. I. Cirac, and P. Zoller. Inseparability criterion for continuous variable systems. *Phys. Rev. Lett.*, 84:2722–2725, Mar 2000.
- [111] S.L. edited by Braunstein and A.K. Pati. *Quantum Information with Continuous Variables*. Kluwer, Dordrecht, Springer-Verlag Berlin Heidelberg, 2003.
- [112] Samuel L. Braunstein and Peter van Loock. Quantum information with continuous variables. *Rev. Mod. Phys.*, 77:513–577, Jun 2005.
- [113] Gerardo Adesso and Fabrizio Illuminati. Entanglement in continuous-variable systems: recent advances and current perspectives. *Journal of Physics A: Mathematical and Theoretical*, 40(28):7821, 2007.
- [114] G. Vidal and R. F. Werner. Computable measure of entanglement. *Phys. Rev. A*, 65:032314, Feb 2002.
- [115] R. F. Werner and M. M. Wolf. Bound entangled gaussian states. *Phys. Rev. Lett.*, 86:3658–3661, Apr 2001.
- [116] Hanna Krauter, Christine A. Muschik, Kasper Jensen, Wojciech Wasilewski, Jonas M. Petersen, J. Ignacio Cirac, and Eugene S. Polzik. Entanglement generated by dissipation and steady state entanglement of two macroscopic objects. *Phys. Rev. Lett.*, 107:080503, Aug 2011.

- 
- [117] G. Birkl, M. Gatzke, I. H. Deutsch, S. L. Rolston, and W. D. Phillips. Bragg scattering from atoms in optical lattices. *Phys. Rev. Lett.*, 75(15):2823–2826, Oct 1995.
- [118] M. Weidemüller, A. Hemmerich, A. Görlitz, T. Esslinger, and T. W. Hänsch. Bragg diffraction in an atomic lattice bound by light. *Phys. Rev. Lett.*, 75(25):4583–4586, Dec 1995.
- [119] Matthias Weidemüller, Axel Görlitz, Theodor W. Hänsch, and Andreas Hemmerich. Local and global properties of light-bound atomic lattices investigated by bragg diffraction. *Phys. Rev. A*, 58:4647–4661, Dec 1998.
- [120] S. Slama, C. von Cube, B. Deh, A. Ludewig, C. Zimmermann, and Ph. W. Courteille. Phase-sensitive detection of bragg scattering at 1d optical lattices. *Phys. Rev. Lett.*, 94:193901, May 2005.
- [121] Christof Weitenberg, Peter Schauß, Takeshi Fukuhara, Marc Cheneau, Manuel Endres, Immanuel Bloch, and Stefan Kuhr. Coherent light scattering from a two-dimensional mott insulator. *Phys. Rev. Lett.*, 106:215301, May 2011.
- [122] D. Jaksch, C. Bruder, J. I. Cirac, C. W. Gardiner, and P. Zoller. Cold bosonic atoms in optical lattices. *Phys. Rev. Lett.*, 81:3108–3111, Oct 1998.
- [123] Maciej Lewenstein, Anna Sanpera, and Veronica Ahufinger. *Ultracold Atoms in Optical Lattices: Simulating quantum many-body systems*. OUP Oxford, Oxford, 2012.
- [124] Immanuel Bloch, Jean Dalibard, and Wilhelm Zwerger. Many-body physics with ultracold gases. *Rev. Mod. Phys.*, 80:885–964, Jul 2008.
- [125] Matthew P. A. Fisher, Peter B. Weichman, G. Grinstein, and Daniel S. Fisher. Boson localization and the superfluid-insulator transition. *Phys. Rev. B*, 40:546–570, Jul 1989.
- [126] Markus Greiner, Olaf Mandel, Tilman Esslinger, Theodor W. Hansch, and Immanuel Bloch. Quantum phase transition from a superfluid to a mott insulator in a gas of ultracold atoms. *Nature*, 415(6867):39–44, January 2002.

- [127] Thilo Stöferle, Henning Moritz, Christian Schori, Michael Köhl, and Tilman Esslinger. Transition from a strongly interacting 1d superfluid to a mott insulator. *Phys. Rev. Lett.*, 92:130403, Mar 2004.
- [128] J. K. Freericks and H. Monien. Phase diagram of the bose-hubbard model. *EPL (Europhysics Letters)*, 26(7):545, 1994.
- [129] L. Pollet, N. V. Prokof'ev, B. V. Svistunov, and M. Troyer. Absence of a direct superfluid to mott insulator transition in disordered bose systems. *Phys. Rev. Lett.*, 103:140402, Sep 2009.
- [130] D. Boiron, C. Mennerat-Robilliard, J.-M. Fournier, L. Guidoni, C. Salomon, and G. Grynberg. Trapping and cooling cesium atoms in a speckle field. *The European Physical Journal D - Atomic, Molecular, Optical and Plasma Physics*, 7:373–377, 1999.
- [131] U. Bissbort and W. Hofstetter. Stochastic mean-field theory for the disordered bose-hubbard model. *EPL (Europhysics Letters)*, 86(5):50007, 2009.
- [132] Ulf Bissbort, Ronny Thomale, and Walter Hofstetter. Stochastic mean-field theory: Method and application to the disordered bose-hubbard model at finite temperature and speckle disorder. *Phys. Rev. A*, 81:063643, Jun 2010.
- [133] F. Igloi, D. Karevski, and H. Rieger. Random and aperiodic quantum spin chains: A comparative study. *The European Physical Journal B - Condensed Matter and Complex Systems*, 1(4):513–517, 1998.
- [134] Christoph Maschler and Helmut Ritsch. Cold atom dynamics in a quantum optical lattice potential. *Phys. Rev. Lett.*, 95:260401, Dec 2005.
- [135] Dirk-Gunnar Welsch, Werner Vogel, and Tomas Opatrny. Li homodyne detection and quantum-state reconstruction. volume 39 of *Progress in Optics*, pages 63 – 211. Elsevier, 1999.
- [136] B. Deissler, M. Zaccanti, G. Roati, C. D'Errico, M. Fattori, M. Modugno, G. Modugno, and M. Inguscio. Delocalization of a disordered bosonic system by repulsive interactions. *Nat Phys*, 6(5):354–358, May 2010.

- 
- [137] Hessam Habibian, André Winter, Simone Paganelli, Heiko Rieger, and Giovanna Morigi. Bose-glass phases of ultracold atoms due to cavity backaction. *Phys. Rev. Lett.*, 110:075304, Feb 2013.
- [138] S. Ritter, F. Brennecke, K. Baumann, T. Donner, C. Guerlin, and T. Esslinger. Dynamical coupling between a boseinstein condensate and a cavity optical lattice. *Applied Physics B*, 95(2):213–218, May.
- [139] Thomas Volz, Stephan Dürr, Sebastian Ernst, Andreas Marte, and Gerhard Rempe. Characterization of elastic scattering near a feshbach resonance in  $^{87}\text{Rb}$ . *Phys. Rev. A*, 68:010702, Jul 2003.
- [140] Peter Krüger, Zoran Hadzibabic, and Jean Dalibard. Critical point of an interacting two-dimensional atomic bose gas. *Phys. Rev. Lett.*, 99:040402, Jul 2007.
- [141] Ghassan George Batrouni, Richard T. Scalettar, and Gergely T. Zimanyi. Quantum critical phenomena in one-dimensional bose systems. *Phys. Rev. Lett.*, 65:1765–1768, Oct 1990.
- [142] Ghassan George Batrouni and Richard T. Scalettar. World-line quantum monte carlo algorithm for a one-dimensional bose model. *Phys. Rev. B*, 46:9051–9062, Oct 1992.
- [143] Parhat Niyaz, R. T. Scalettar, C. Y. Fong, and G. G. Batrouni. Phase transitions in an interacting boson model with near-neighbor repulsion. *Phys. Rev. B*, 50:362–373, Jul 1994.
- [144] K. Sheshadri, H. R. Krishnamurthy, R. Pandit, and T. V. Ramakrishnan. Superfluid and insulating phases in an interacting-boson model: Mean-field theory and the rpa. *EPL (Europhysics Letters)*, 22(4):257, 1993.
- [145] P. W. Anderson. Absence of diffusion in certain random lattices. *Phys. Rev.*, 109:1492–1505, Mar 1958.
- [146] Giacomo Roati, Chiara D’Errico, Leonardo Fallani, Marco Fattori, Chiara Fort, Matteo Zaccanti, Giovanni Modugno, Michele Modugno, and Massimo Inguscio. Anderson localization of a non-interacting bose-einstein condensate. *Nature*, 453(7197):895–898, June 2008.

- 
- [147] Michele Modugno. Exponential localization in one-dimensional quasi-periodic optical lattices. *New Journal of Physics*, 11(3):033023, 2009.
- [148] Giovanni Modugno. Anderson localization in bose-einstein condensates. *Reports on Progress in Physics*, 73(10):102401, 2010.
- [149] S. Aubry and G. André. Analyticity breaking and anderson localization in incommensurate lattices. *Annals of the Israel Physical Society*, 3:133–164, 1980.
- [150] M. Saffman, T. G. Walker, and K. Mølmer. Quantum information with rydberg atoms. *Rev. Mod. Phys.*, 82:2313–2363, Aug 2010.
- [151] E. Urban, T. A. Johnson, T. Henage, L. Isenhower, D. D. Yavuz, T. G. Walker, and M. Saffman. Observation of Rydberg blockade between two atoms. *Nat Phys*, 5(2):110–114, January 2009.
- [152] Thibault Peyronel, Ofer Firstenberg, Qi-Yu Liang, Sebastian Hofferberth, Alexey V. Gorshkov, Thomas Pohl, Mikhail D. Lukin, and Vladan Vuletic. Quantum nonlinear optics with single photons enabled by strongly interacting atoms. *Nature*, 488(7409):57–60, August 2012.
- [153] Asher Peres. Separability criterion for density matrices. *Phys. Rev. Lett.*, 77:1413–1415, Aug 1996.
- [154] Michał Horodecki, Paweł Horodecki, and Ryszard Horodecki. Mixed-state entanglement and distillation: Is there a “bound” entanglement in nature? *Phys. Rev. Lett.*, 80:5239–5242, Jun 1998.
- [155] C. Kittel. *Introduction to Solid State Physics*. John Wiley and sons, Hoboken, 2005.



# Acknowledgements

---

At this point I would like to thank firstly my advisor, Giovanna Morigi, from whom I have learned a lot, beside physics, kindness and self-devotion. I acknowledge all the people who have provided me their experiences and knowledges during my Ph.D. studies, specially Stefano Zippilli: such a fantastic and distinguished person I had a chance to work with to improve my abilities. I am grateful to all my colleagues, both in Barcelona and Saarbrücken, namely Jens Baltrusch with whom I spent 4 unforgettable years, Marc Bienert with whom I shared the office for about 3 years, Stefan Schütz for collaboration and training in Saarbrücken football team, and Mauricio Torres for bringing a unique latin american friendship to the office during the last year of my studies. I am also grateful to James Douglas for reading my thesis. I would like to thank Ramón Corbalán as my co-advisor at UAB, as well as Gaspar Orriols and Jordi Mompart who helped me a lot regarding administrative formalities. Finally, I would like to thank for the patience of my wife, Naeimeh Behbood, during the time I was away from Barcelona.



# Publications

---

This thesis is based on the following publications:

## Part I

- *Quantum light by atomic arrays in optical resonators*,  
H. Habibian, S. Zippilli, and G. Morigi,  
Phys. Rev. A. **84**, 033829 (2011).
- *Stationary light-matter entanglement by atomic arrays in optical resonators*,  
H. Habibian, S. Zippilli, F. Illuminati, and G. Morigi,  
in preparation.

## Part II

- *Bose-glass phases of ultracold atoms due to cavity backaction*,  
H. Habibian, A. Winter, S. Paganelli, H. Rieger, and G. Morigi,  
Phys. Rev. Lett. **110**, 075304 (2013).
- *Quantum phases of incommensurate optical lattices due to cavity backaction*,  
H. Habibian, A. Winter, S. Paganelli, H. Rieger, and G. Morigi,  
in preparation.

The following articles have been published during and before my PhD studies although they are not discussed along this thesis:

- *Greenberger-Horne-Zeilinger and W entanglement witnesses for the non-interacting Fermi gas*,  
H. Habibian, J. W. Clark, N. Behbood, and K. Hingerl,  
Phys. Rev. A **81**, 032302 (2010).
- *Aspects of Entanglement in Quantum Many-Body Systems*,  
J. W. Clark, H. Habibian, A. D. Mandilara, and M. L. Ristig,  
Foundation of Physics **40**, 1200-1220 (2010).
- *Coupled Cavities Polaritons for Switching and Slow-light Applications*,  
G. Manzacca, H. Habibian, K. Hingerl, and G. Cincotti,  
Photonics and Nanostructures-Fundamental and Application **7**, 39-46  
(2008).
- *Multi-qubit Stabilizer and Cluster Entanglement Witnesses*,  
M. A. Jafarizadeh, G. Najarbashi, Y. Akbari, and H. Habibian,  
Eur. Phys. Jour. D **47**, 233-255 (2008).
- *Manipulating Multi-qudit Entanglement Witnesses by Using Linear Programming*,  
M. A. Jafarizadeh, G. Najarbashi, and H. Habibian,  
Phys. Rev. A **75**, 052326 (2007).

# Curriculum Vitae

---

Name: Hessam Habibian  
Address: Nooalam, Poortaghi alley 30, Babol, IRAN  
Date of Birth: 30 July 1982  
Place of Birth: Babol  
Nationality: Iranian

- **Ph.D. candidate in Quantum Optics**  
since October 2008,  
Joint co-tutelle program between Universitat Autònoma de Barcelona, Spain and Universität des Saarlandes, Germany.  
Thesis title: *Cavity Quantum Electrodynamics with Ultracold Atoms.*
- **Postgraduate fellowship**  
October 2007 till September 2008,  
Christian Doppler Lab., Johannes Kepler Universität Linz, Austria.  
Project: *Switching and Slow-light Applications.*
- **M.Sc. in Theoretical Physics (Quantum Information)**  
October 2004 till February 2007,  
Tabriz University, Tabriz, Iran.  
Thesis title: *Investigation of Entanglement Witnesses and Stabilizer Operators.*
- **B.Sc. in Solid State Physics**  
October 2000 till July 2004,  
University of Mazandaran, Babolsar, Iran.
- **Diploma / High School**  
October 1996 till June 1999, Alborz high school, Tehran, Iran.  
October 1999 till June 2000, Kharazmi Pre-university, Tehran, Iran.